ISSN: 2642-9020

Research Article

Journal of Marine Science Research and Oceanography

Evidence for a recent (0.65 Ma) formation of the Isthmus of Panama

Leonidas Brikiatis

Unaffiliated, 17564, Palaeo Faliro, Greece

*Corresponding Author

Leonidas Brikiatis, Unaffiliated, 17564, Palaeo Faliro, Greece

Submitted: 02 Feb 2023; **Accepted:** 20 Feb 2023 **Published:** 03 Mar 2023

Citation: Brikiatis, L. (2023). Evidence for a recent (0.65 Ma) formation of the Isthmus of Panama. *J Mari Scie Res Ocean*, 6(2), 25-68.

Abstract

The exact age of the final formation of the Isthmus of Panama is a critical reference point for oceanographic, climatic, biogeographic, and evolutionary hypotheses. The prevailing interpretation of geotectonic evidence is that the isthmus was completed between 12 Ma and 3 Ma, and an age of 3–4 Ma has been used as a benchmark in hundreds of studies over the past 30 years. Phylogeographic data indicate the existence of marine connections across the isthmus much more recently, however. Here, using the most updated data available, I reconsider the geological arguments invoked to conclude the age of 3–4 Ma and show that, in fact, this age is not supported by the current geological knowledge. Rather, recent geotectonic evidence, in conjunction with multiple lines of indirect phylogeographic, biostratigraphic, oceanographic, and paleoclimatic indications, suggests that as many as four transisthmian seaways persisted until as recently as the onset of the Middle Pleistocene (~0.65 Ma). The concurrence of the final formation of the Isthmus of Panama with the mid-Pleistocene Transition of glacial/interglacial periodicity suggests a tight relationship between these events. Unusual and contrasting climate phenomena, including the "900-Ka (cold) event" and the "greening" of South Greenland during the MIS 22 glacial maximum, can be explained by this palaeogeographical and palaeoceonographical scenario.

Keywords: 900-Ka event; Atrato Seaway; Bering Strait closure; Mid-Pleistocene Transition; Nicaraguan Seaway; Panama Isthmus Formation

Introduction

The most recent exposure of the Isthmus of Panama is one of the most significant events in the recent geological history of the Earth [1-3], because it resulted in the closure of the Central American Seaway (CAS), which along with its precursor the Hispanic Corridor, connected the Pacific and Atlantic Oceans since the Late Jurassic (160 Ma) [4-5] (Figure 1A). Different ages have been proposed for the event, including the very ancient Miocene (23 Ma [1] or 14 Ma [6]) and the more recent Late Pliocene (3.5 Ma or 2.8 Ma [7-8]). Some authors have questioned these dates by highlighting the persistence in more recent times of marine paleontological evidence indicating shallow-water faunal exchanges from the Early Pleistocene (Gelasian) until about 2–1.8 Ma [9-11]. Here, I define the formation of the isthmus as the complete interruption of any interoceanic communication.

Although the various proposed ages probably correspond to distinct ephemeral exposures [1], the most recent exposure (which I will call "final" for simplicity) is the most important, because it modulated the modern oceanographic, climatic, and biogeographic configuration of the Earth. By influencing the Gulf Stream intensity and, in turn, the configuration of the Atlantic meridional overturning circulation (AMOC), the final formation of the isthmus modulated the modern European and global climates ([12-13] and references therein). Moreover, the operation of the isthmus as a barrier to marine dispersals and a corridor for terrestrial dispersals affected the diversity and geographic distributions of the biota of North and South America [1-2, 14]. Therefore, the age and regime of the final formation of the Isthmus of Panama have important implications to oceanographic and climatic models, biogeographic hypothesis, and the calibration of evolutionary rates [1-3]. For example, in the absence of relevant paleontological records, hundreds of molecular dating studies of transisthmian "geminate" species have calibrated their molecular clocks using a ~3–4 Ma age of the final formation of the Isthmus of Panama as a benchmark [1-2]. This age is widely accepted at present and is based on interpretation of the available geological evidence, which is summarised in the Late Pliocene (3 Ma) palaeogeographical reconstruction of Coates & Obando [8] (Figure 1C) and reproduced in more recent biogeographical analyses (e.g. [15]).

Here, I review the geological arguments invoked to support the concept of the latest Pliocene (~3 Ma) age of the isthmus formation and show that the current geotectonic evidence, in agreement

with multiple sources of phylogeographic, biostratigraphic, oceanographic, and paleoclimatic data, suggest that the complete and final closure of the Isthmus of Panama occurred much more recently than was previously believed. I then discuss how the scenario of the recent formation of the Isthmus of Panama can be related to the occurrence of the great paleoclimatic change known as the (early to) mid-Pleistocene Transition (MPT) [16].

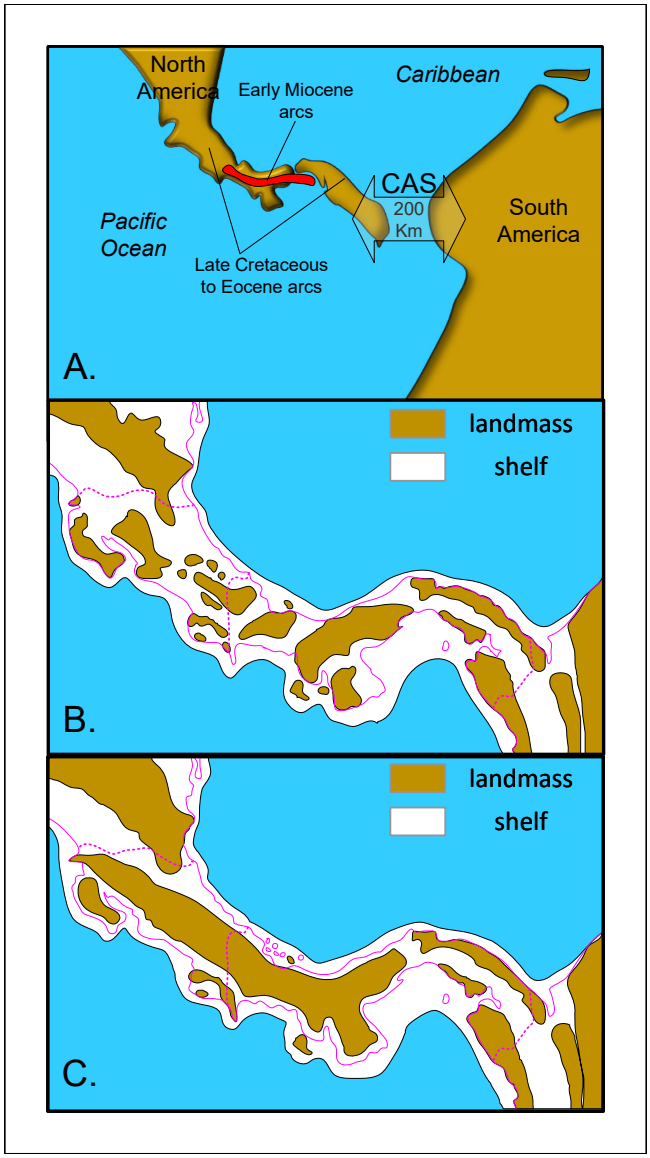

Figure 1: Previous palaeogeographical reconstructions of the Central American Seaway (CAS) and its ruminant straits. A) Early Miocene reconstruction (~20 Ma) [139]; B) Late Miocene reconstruction (~6–7 Ma) [8]; C) Latest Pliocene reconstruction (~3 Ma) [8].

Geotectonic Data

The hypothesis that the final formation of the Isthmus of Panama occurred ~3 Ma is summarized in the latest Neogene-Quaternary palaeogeographical reconstructions of Coates & Coates & Obando [8] (Figure 1B & 1C). According to that scenario, interoceanic marine communication through the isthmus was maintained until the Pliocene via three persistent seaways (Figure 1C): the Nicaraguan Seaway (through the Nicaragua Depression), the Canal Seaway (through the area of the current Panama Canal), and the Atrato Seaway (through the Atrato Basin of Colombia) (see also [17]). . Another seaway, here called the Barú Seaway, although shown in Coates & Obando's Late Miocene (~6 Ma) palaeogeographical reconstruction [6] (Figure 1B), was considered to be subaerially exposed in their 3 Ma reconstruction (Figure 1C). In the following sections, I review the available geotectonic data in order to determine whether recent developments in geoscience support this palaeogeographical scenario.

The Nicaraguan Seaway

The Nicaraguan Depression is a prominent, 40–70 km wide tectonic graben extending ~1000 km from the Caribbean side of Costa Rica in the southeast to the northern Gulf of Fonseca in El Salvador (Figure 2 & 3). The depression has been interpreted as having probably developed since the Pliocene [18-19]. The most recent

structural studies of the El Salvador Fault Zone show that the graben structures are the result of a two-phase evolution starting with an initial extensional phase that occurred between 7.2–6.1 Ma (latest Miocene) and 1.9–0.8 Ma (Early Pleistocene) [20]. At the northwest side of the Nicaraguan Seaway (sensu Coates & Obando [8]), the shallow-water El Salto Formation unconformably overlies older sequences (the Rivas, Brito, Masachapa, and El Fraile Formations) of various ages from Cretaceous to Pliocene [19]. While the fossil sites in Nicaragua have so far produced only land mammals of Late Pleistocene age, a baleen whale was found in the Mine K-11 locality within the El Salto Formation [21]. Pyroclastic-alluvial deposits of the Las Sierras Group succeed the marine deposits of the El Salto Formation, so the age of the El Salto deposition corresponds to the minimum age of the Nicaraguan Seaway at its northwest end. Based on molluscan fossil findings, an Early Pliocene age has long been assigned to the El Salto Formation; however, that age is considered to be poorly constrained ([21] and references therein). Correlation of offshore commercial wells in the Sandino basin and onshore stratigraphic studies showed [22] that although the El Salto. Formation includes the complete Pliocene, its top (sequence 12, SB12) reaches up to the MPT ~0.9 Ma ago. This age is congruent with the end of the second, trans tensional phase of the formation of the Nicaraguan Depression (1.9–0.8 Ma; Early Pleistocene), implying that the associated extensional structures are contemporaneous with, and might have led to, the deposition of the El Salto Formation, which has a thickness of 100 m onshore and up to 1,000 m offshore.

The two large freshwater lakes, Lake Nicaragua and Lake Managua, contained in the Nicaraguan Depression are also considered to have been formatted since the Early Pleistocene [23]. Investigations of whether and when the lakes were last connected to the oceans did not reach a clear conclusion [24]. Nevertheless, the occurrence of marine-like nematodes such as *Theristus setosus* (Btitschli) Filipjev (an inhabitant of marine and brackish environments [25]), *Polygastrophora octobulba* [an inhabitant of marine and freshwater environments [26]), and the endemic *Viscosia nicaraguensis* [considered to originate from the marine *Viscosia papillate* [27]) in the lakes does not exclude the possibility that the lakes were once connected directly to the sea ([24] and references therein).

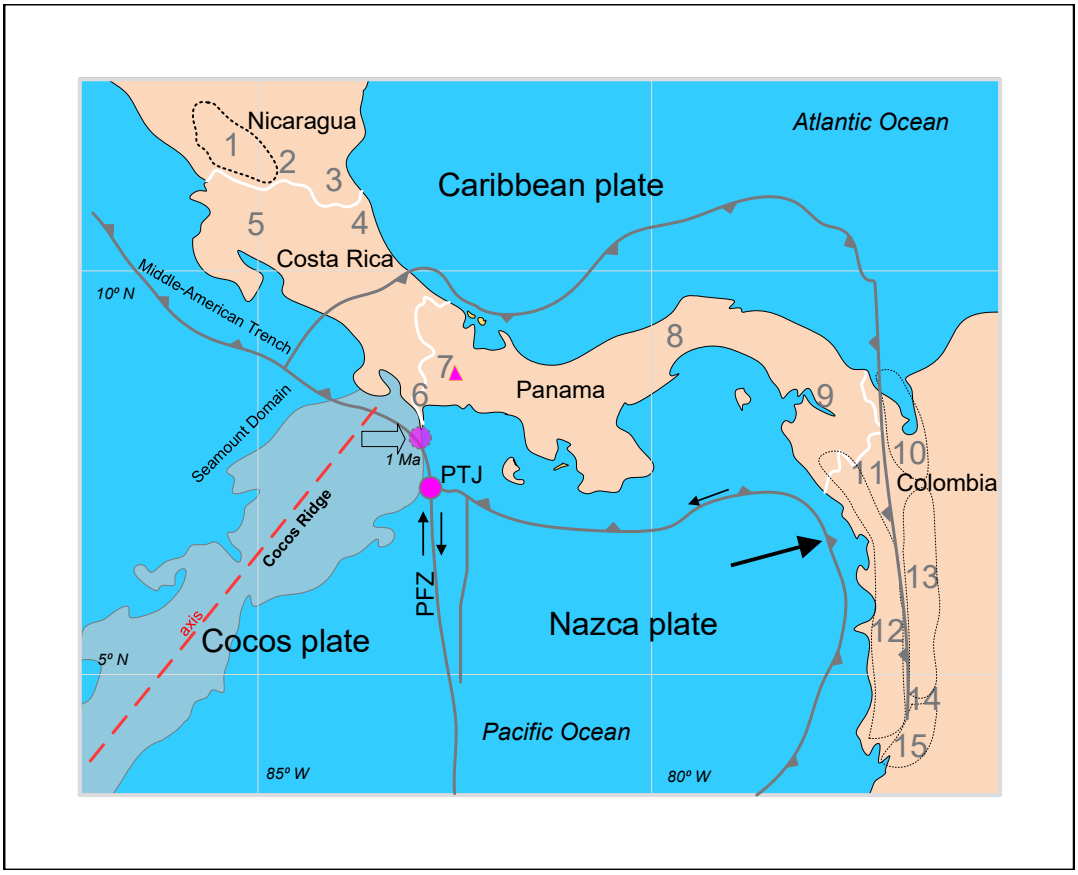

Figure 2: Modern map of the Isthmus of Panama with plate tectonic setting and marked locations of prominent features mentioned in the text. 1) Nicaraguan Depression; 2) San Carlos Basin; 3) Northern Limón Basin; 4) Southern Limón Basin 5) Tempisque Basin; 6) Burica Peninsula; 7) Barú volcano; 8) Panama Canal; 9) Chucunaque Basin; 10) Urabá Basin; 11) Salaquí river; 12) Serranía de Baudó; 13) Atrato Basin; 14) San Juan Paleohigh; 15) San Juan Basin. PFZ= Panama Fracture Zone; PTJ= Panama Triple Junction. Modified from [40].

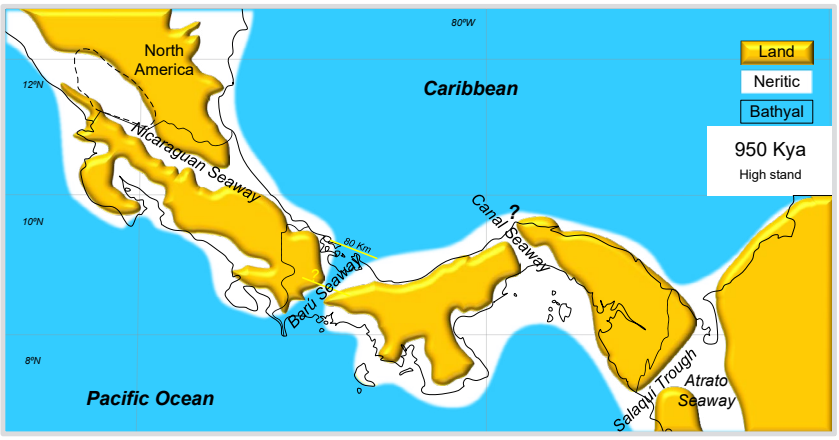

Figure 3: Latest Early Pleistocene palaeogeographical reconstruction of the Isthmus of Panama according to the conclusions of the present study

In any case, Coates & Obando [8] independently showed that the Pacific seashore reached at least the middle of the Nicaraguan Seaway (Venado Formation, San Carlos Basin) during the Early Pleistocene (see also [28]) and maybe had a southward connection via the Tempisque Basin as well (see map in [15], and [29]). They further suggested that thereafter, during the Pliocene, the Nicaraguan Seaway was connected (although somehow restricted by the Sarapiquí Arch) to the Caribbean Sea through the Northern Limón Basin.

The Northern Limón Basin is an undeformed, normal faulted back arc basin that is separated from the Southern Limón Basin by the Moín High, and from the San Carlos Basin to the west by the Sarapiquí Arch [28]. Miocene regional uplifting of the inner arc formed a series of intermountain basins on the western, inland portion and shallow marine conditions on the eastern, Caribbean side. Subsequently, prograded fan deltaic, continental fan deposits, and patch reef development produced bay conditions corresponding to the Plio-Pleistocene Suretka Formation [28]. Such a transition is displayed in the classic stratigraphic scheme of the Limón Basin [30] where the Middle Miocene–Early Pliocene, deltaic shallow marine Río Banano Formation is unconformably succeeded by the shallow marine and continental rocks of the Plio-Pleistocene Suretka Formation (e.g. [31]). According to this very generalised stratigraphical interpretation, the conglomerates of the Suretka Formation demonstrate the southwards exposure limit of the Nicaraguan Seaway toward the Atlantic. This view is reproduced in the palaeogeographical reconstruction of Coates & Obando [8] which is based on a 2.5 Ma estimation for the age of the upper boundary of the Río Banano Formation [8, Formation [32]. That age cannot be assumed for the younger marine depositions in the Northern Limón Basin, however, because it is based entirely on cross-section data from the Southern Limón Basin [32] which experienced a different geodynamic history and deformation than the Northern Limón Basin and is much more poorly studied [28, 31]. For example, although the Northern Limón and San Carlos Basins cover a 12.000 km^2 onshore area, only three deep wells have been drilled on land [28] and outcrops are extremely rare [33]. On the other hand, the age of the Suretka Formation is unapproved, as no index fossil that dates a geological age was ever found [34]. Therefore, the stratigraphical data from the Southern Limón Basin are not representative of the palaeogeography of the Northern Limón Basin.

Recent geological research based on well and seismographic analyses showed that continuous marine Pleistocene deposits can be laterally traced for several tens of kilometres on the northwest-to-southeast coastline northwards of the Moín High [31, 35] and across the whole coast of the Northern Limón Basin (see [28]: fig 10). Therefore, given the potential for extended Pleistocene deposits in the Northern Limón Basin, the most recent age corresponding to the complete transoceanic exposure of the Nicaraguan Seaway is not defined by the conglomerates of the Suretka Formation, but instead by the Early Pleistocene deposits of the Venado Formation in the San Carlos Basin. Today, only 34 m of relief separates Caribbean and Pacific waters in the area of the San Carlos basin [36], and it is likely that the area has been slightly uplifted under the tectonic effect of the Cocos Ridge subduction beneath Costa Rica during the Early Pleistocene [37].

The Barú Seaway

In the Late Miocene (~6 Ma) palaeogeographical reconstruction of Coates & Obando [8] (Figure 1B), the Atlantic Bocas del Toro Basin and the Pacific Burica Basin are connected by a marine trough, which I refer to as the Barú Seaway because of its location where the Barú volcano (3,474m) is today (Figure 2 & 3). Also in the vicinity of the Barú Seaway is the Panama Fracture Zone, an active right lateral-moving transform fault that forms part of the tectonic boundary between the Cocos and Nazca Plates and the larger southeast-moving triple junction between the Cocos, Nazca, and Caribbean Plates [37] (Figure 2). As the oceanic crust of the Cocos Plate moved north eastward, it was partially subducted beneath the

volcanic arc system of Costa Rica and western Panama, causing rapid elevation of the Central American Isthmus from the Arenal volcano in Costa Rica to El Valle in Panama. The result of this orogenic procedure is the mountain range of Cordillera de Talamanca (eastern Costa Rica) and Cordillera Central (western Panama) [37-38], which cuts off the Barú Seaway and other interoceanic basins across the isthmus in the Late Pliocene (~3 Ma) reconstruction of Coates & Obando [8], supporting the view of a complete formation of the Isthmus of Panama around the same time as the rise of the mountain range Therefore, the exact age of the orogenic uplift due to the Cocos Plate collision is fundamental to scenarios of the final formation of the Isthmus of Panama.

The timing of Cocos Ridge subduction is currently one of the most widely discussed debates in Central American tectonics [39-40] with estimates ranging from as old as 8 Ma (e.g. [41]) to as young as 0.5 Ma (e.g. [42]). The youngest estimates for the Cocos Ridge arrival (0.5–3.5 Ma) at the Middle America Trench are derived from onshore rock uplift and subsidence patterns as well as plate reconstructions, whereas the oldest estimates (8–5 Ma) are largely based on the cessation of "normal" (non-adakitic) calc-alkaline volcanism within the Cordillera de Talamanca ([39] and references therein). Recent studies have concluded that the cessation of arc volcanism and the onset of Cocos Ridge collision (<3 Ma) are separate events, however, reflecting recent changes in the configuration of the plate boundary system [39-40]. Hence, scenarios for a young age of Cocos Ridge subduction are increasingly favoured today.

Deposition facies of the Burica Peninsula on the Pacific side of the isthmus have been studied as a proxy for the tectonic movements of the Cocos Plate, because the peninsula is located at the eastern edge and front of the plate (Figure 2). The facies nomenclature used here is based on Morell et al. [43]. The most comprehensive study of the area [44] concluded that the marine faunal evidence contained in the Pliocene to Early Pleistocene (3.5–1.5 Ma) Burica Member of the Charco Azul Formation suggests strong subsidence and a bathyal environment (~2,000 m) in the area during the Early Pliocene, followed by gradual shoaling from 2,000 m to 1,400 m during the Late Pliocene through Early Pleistocene Overlain strata assigned to the lowermost Armuelles Formation (late Early Pleistocene) were found to contain faunas indicative of water depths between 1,200 m and 1,300 m. By contrast, shallow-water molluscs in stratigraphically higher exposures of the Armuelles Formation are indicative of shelf deposits. Therefore, within the deposition interval of the Armuelles Formation, rapid shoaling took place at a time corresponding to the "Early Pleistocene–Late Pleistocene boundary". These findings led Corrigan et al. [44] to conclude that rapid uplift due to Cocos Plate subduction took place after the Early Pleistocene In agreement with that view, Gardner et al. [42] using a radiometrically calibrated geodynamical model, concluded that the collision took place at 0.5 Ma.

In contrast to these views, Collins et al. [38] considered the whole Armuelles Formation to include very shallow-water deposits (<10 m) and proposed that the rapid 2,000 m uplift in the Burica Peninsula falls within the interval of deposition of the underlain Burica Member of the Charco Azul Formation from the Late Pliocene Furthermore, Collins et al. [38] suggested that the subduction of the buoyant Cocos Ridge and the orogeny of the Cordillera de Talamanca began about 3.6 Ma, or 2 to 3 million years earlier than the date proposed by Collins et al. [38] and Gardner et al. [42]. In particular, based on a ~1.6 Ma age for the top of the Moín Formation (i.e. the age of the most recent marine deposits in the Southern Limón Basin at the Atlantic coast to the north), Collins et al. [38] concluded that the subaerial exposure of the Southern Limón Basin was caused by uplift from the delivery of the subducted Cocos Plate Therefore, they placed the whole orogenesis within the interval 3.6–1.6 Myr. However, subsequent studies of the Southern Limón Basin revised the age of the basin uplift to<1 Ma [45], and more recent studies concluded that the whole Colón carbonate platform in the Bocas del Toro region of Panama (south of the Southern Limón Basin) was finally subaerially exposed during a Middle Pleistocene regional uplift [46]. Geological research in the Bocas del Toro region of Panama found that although neritic deposits persisted in the Northern region (Colón platform) until the end of the Early Pleistocene, there was a hiatus in deposition over a distance of ~80 km between Isla Colón and the Escudo de Veraguas Island (yellow line in Figure 3) during the last 3.5 Myr and over an even greater distance within the last 1.8 Myr [47]. Therefore, the available data are not sufficient to refute the existence of a seaway with bathyal property during the hiatus interval.

In the middle of the proposed Barú Seaway, where the Barú volcano (3,474 m) stands today, there is independent evidence that low-elevation relief may have persisted until as recently as the mid-Pleistocene, whereas rapid uplift took place thereafter [48]. Barú and Tisingal Volcanos, both located landward of the Panama Fracture Zone, are the only active volcanoes within a 200-km region directly inboard of the Panama Triple Junction [39]. Moreover, the age of the Barú volcano formation is considered to be ~0.5 My. It is therefore likely that the uplift that closed the Barú Seaway was a recent event that took place around the Early to Middle Pleistocene boundary (1–0.5 Ma). Indeed, most recent geotectonic analyses are congruent with the palaeobythometric interpretation of Corrigan et al. [44] rather than the interpretation of Collins et al. [38] (e.g. [40, 43]), suggesting that neither the Osa Peninsula nor the Burica Peninsula was emergent until at least 1 Ma, when the axis of the Cocos Ridge reached the Middle American Trench [40].

The Canal Seaway

The Canal Basin (in a broad sense) is an elongate, northwest-southeast–trending transisthmian sedimentary trough controlled by a fault system known as the Canal Discontinuity [49] which extends across the isthmus within an 80-km wide zone (Figure 2 & 3) Today, it results in a major topographic discontinuity between high volcanic mountain ranges to the east and west and lowlands

punctuated by small (generally <300 m high) topographic features of unclear tectonic and/or volcanic origins [50]. It remains uncertain whether the topographic highs in the Canal Basin are erosional remnants of Eocene/Miocene volcanic landforms that could have obstructed an interoceanic strait or instead of islands within a more recent than Miocene interoceanic seaway [51].

In the simplest terms, the geology of the Canal Basin consists of a pre-middle Eocene volcanic basement overlain by late Eocene to Late Miocene marine deposits interbedded with volcanic and volcaniclastic rocks [52]. Younger deposits are generally poorly exposed. The relatively recent scenario for the formation of the Isthmus of Panama depicted in the Pliocene palaeogeographical reconstruction of Coates & Obando [8] is based on the assumption of a Pliocene age for the most recent marine deposits in the Canal Basin (i.e. those at the top of the Chagres Sandstone; e.g. [53-54]). In fact, the Chagres Sandstone, which conformably overlays the Late Miocene Gatún Formation, has been dated to be at least as old as the Late Miocene [17] (see also [55]). On the other hand, the only extended marine deposits that provide evidence of an interoceanic communication via the Canal Basin is the Early Miocene ''La Boca Formation'' [more recently re-interpreted as being the lower part of the Culebra Formation [55]. There is, however, certain other geological evidence suggesting that the Canal Basin might have experienced marine transgression episodes much more recently.

The Canal Basin is broken at the point where the isthmus reaches its lowest topographic elevation, originally ~84 m above sea level [36], making it the best location for the construction of the interoceanic Panama Canal and also a possible location for the past exposure of a natural transoceanic seaway [38]. The question is when the current topographical highs in the Canal Basin that currently separate the two oceans emerged. It is known that the Panama Arc began rising around 6 Ma and has continued to rise until the present day. On the other hand, the area maintained a low topography, which was certainly influenced by glacio-eustasy during the Quaternary (e.g. [7]). The detailed chronological sequence of events is not well known, however, because of the complex geological history of the area and the difficulty of making direct geological observations [53].

Within the Canal Zone, the most pronounced expression of low topography in the Canal watershed area is the once-extensive swamp within the broad valley of the Chagres River, which is now covered by the Panama Canal's Gatún lake [56, 57]. The valley penetrated to within 25 km of the Pacific Ocean in central Panama, where the Pacific–Caribbean drainage divide descends to one of its lowest elevations in Central America (<200 m) in the low saddle of the Culebra Cut (also known as the Gaillard Cut) along the Panama Canal [50]. The saddle of the Culebra Cut marks the southern boundary of the Río Chagres basin, the geomorphology of which is the result of four continent-shaping movements that followed the cessation of intense volcanic activity in the Early Miocene and resulted in the erosive and depositional intervals that created the present day land mass [56, 58]. During the first movement, the central portion of the isthmus was elevated above the coastal lines, developing the present morphology of the Central and Pacific portions of the isthmus. The second movement elevated the terrain to more than 90 m in the Atlantic area of the isthmus. Slow settling of the land surface characterised the third movement, during which the lower parts of the isthmus were overtaken by the sea, as evidenced by the layers of marine deposits with strictly fluvial beds in the "Atlantic mud" [58]. The Atlantic mud and "Pacific mud" (also known also as sludges or more generally as Quaternary deposits) are informally known deposits with similar physical properties and appearance that unconformably overlay the Miocene marine formations of the Canal Basin [53]. The age of the muds is considered to be Holocene to Late Pleistocene [53-54) which is supported by radiochronological estimations [59]. The muds are contained in swamp and stream deposits extending as far inland as Gamboa on the Caribbean side of the Canal Zone and as far as the Miraflores Locks on the Pacific side [53], separated by the saddle of the Culebra Cut The muds were deposited upon a stream-eroded topography of considerable relief [56], so that any previous marine deposits in the area were eroded and lost From this view, the uplift of the area around the saddle of the Culebra Cut might correspond to an Early Pleistocene age in which there was a marine connection between the Atlantic and Pacific Oceans through the Canal Basin.

Seismic imaging along the Caribbean coast indicates that faults beneath the Limón Bay may be part of a more extensive set of predominantly north and northeast-trending faults, which are also exposed in the Culebra Cut between Gatún Lake and the Pacific coast [57]. Detailed geologic surveys conducted during the Culebra Cut widening project (1959–1969) revealed over 100 normal, reverse, and strike-slip faults along a single 1.8 km section of the cut. The geologic impression given by the surveys is that the area has been subjected to immense stresses and thoroughly shattered [49] . The faulting in the Canal Zone post-dates Late Miocene strata, and, although the minimum age of displacement is unconstrained, the available data imply a Pliocene or Quaternary age [57]. Indeed, after the cessation of folding in eastern Panama in Plio-Quaternary times, the modern tectonics of the Canal Zone are dominated by strike-slip faults, such as the Río Gatún and Pedro Miguel faults (the latter is near and on the right of the Culebra Cut area), which were modelled by uplift and the emergence of central Panama within the last 3 Myr [60]. Geomorphic analysis suggests that the Pedro Miguel fault continues southward offshore into the Pacific Ocean, where Taboga Island may indicate an uplift at a left step on the fault [61]. In particular, on the basis of the slip-rate (4–7 mm/year) and total displacement (~5–10 km) along the Pedro Miguel fault, Farris et al. [62] concluded that the fault must be younger than 1–3 Ma.

In conclusion, prominent geomorphic lineaments, topographic breaks, and bends in river courses are all consistent with a young, fault-controlled landscape [50]. Therefore, the available data cannot rule out an age <1 Ma for the uplift of the topographical high

separating the low topographies north and south of the Culebra Cut. Such a high could have constituted a terrestrial barrier to a recent interoceanic marine communication through the low topography of the Panama Canal area.

The Atrato Seaway

The Late Pliocene (~3 Ma) reconstruction of Coates & Obando [8] displays another transoceanic seaway through the Atrato and Chucunaque Basins (Figure 1C), the Atrato Seaway, which was originally proposed by Woodring [63]. Recent stratigraphical research showed, however, that the seaway passing through the Chucunaque Basin was subaerially exposed by 5.6 Ma [29] (see also [64]) and therefore no longer in existence during the Late Pliocene (Figure 2 & 3) Based on stratigraphic data from a single well in the Atrato Basin (Opogado-1), Coates et al. [29] postulated that the Atrato trough was also subaerially exposed by 4.8 Ma This age corresponds to the minimum age of the marine deposits at the top of the Munguido Formation in the Opogado-1 well (for detailed biostratigraphy see Duque-Caro [65-66]). Coates & Obando [8] and Coates et al. [29] considered the Mongoido Formation to be the last marine formation in the Atrato Basin, but that assessment now appears to be incorrect The Mongoido Formation is overlain by the Quibdó Formation in wells both north and south of the Opogado-1 well (see [67]: fig. 21), indicating that the stratigraphic scheme of the Opogado-1 well is not representative of the wider Atrato Basin area and therefore cannot be used to infer general palaeogeographical conclusions about the area.

The Quibdó Formation consists of sandstones and occasional conglomerates including marine faunas, and it is overlain by gravels, sands, and sandstones corresponding to alluvial deposits of the Atrato River [68]. On the basis of a Late Pliocene age for the Quibdó Formation, O'Dea et al. [7] argued that the Atrato Seaway persisted until 3.1 Ma and was overlain thereafter by terrestrial sediments. The minimum age of the Quibdó Formation is therefore critical for bracketing the age of the exposure of the Atrato Seaway. Although the age of the Quibdó Formation is uncertain, it has been estimated to be Late Pliocene, but also Pliocene to "Quaternary (?)", with a question mark indicating the possibility that the upper boundary falls within the Quaternary (e.g. [68-69]. Other recent stratigraphical schemes display the minimum age of the Quibdó Formation to be ~1.8 Ma, albeit also accompanied by a question mark indicating that it might be even younger (e.g. [67]: figure. 20; [70]: figure. 17) Stratigraphical schemes in some technical reports show the Quibdó Formation to be Late Pliocene to Middle Pleistocene in (e.g. [71-72]). The confusion over the age of the Quibdó Formation stems from the purely marine biostratigraphic markers that have been recovered from it so far (see [70]: figure. 18). These are the benthic foraminifera *Cassidulinella pliocenica and Ammonia cf. beccarii* and the planktonic foraminifera *Orbulina cf. universa* ([70]: fig. 17). [70]. While the former is congruent with an age as young as the Late Pliocene [73], the latter two are indicators of an age spanning from the Miocene to recent (Paleobiology Database 1; Paleobiology Database 2) [74-75]. In the absence of well biostratigraphic markers, geotectonic data provide additional clues regarding the age of the Quibdó Formation.

The importance of the Quibdó Formation for geologists is not mainly stratigraphical but tectonical, as it is considered to describe the emergence of the Serranía de Baudó area, known as the Baudó Event [67, 70]. The age (usually referred to as "8–4 Ma ?") and the mechanisms responsible for the Baudó Event remain uncertain, because the available data are insufficient to fully explain the kinematics of the Baudó Range emplacement. In any case, the Baudó Event is believed to have led to the formation of the western margin and closure of the Atrato Basin [76] (Figure 2). Thus, while the eastern margin of the Atrato Basin records the shallowing of the basin, large deformations toward the western margin in the Baudó Range can be seen as a result of orogenic activity. A noteworthy example of such a dynamic procedure is printed in the Río Murrí section, where the Eocene Salaquí Formation outcrops in fault contact with the Quibdó Formation [67, 70]. Late Miocene to Pliocene orogeny in the Northern Andes was likely triggered by the onset of a flat-slab subduction of the Nazca plate underneath the northernmost Andes of Colombia [77]. Thus, a Pliocene age of the Quibdó Formation matches well with the latest Neogene tectonic activity in the Northern Andes. It is also evident, however, that orogeny and uplift in the area occurred since the Early Pleistocene (1.8 Ma) until recently [78]. Therefore, the final configuration of the Serranía de Baudó area and subaerial conditions in the Atrato Seaway could be the results of a more recent procedure that occurred in two steps. In this context, the presence of Quibdó Formation deposits in the Salaquí river area may suggest a past westward marine connection of the Atrato Seaway to the Pacific via the northern Baudó mountain range, which was severed during the Early Pleistocene orogeny.

Northwards, a likely connection between the Atrato Seaway and the Atlantic Ocean passes through the Urabá Basin, which is separated from the Atrato Basin by the Mandé magmatic arc [79]. Detailed surveys of the region showed that the sediments in the Atrato Basin extend into the Urabá Basin [7, 79]. In the Urabá Basin, based on the stratigraphic records of the onshore Apartadó-1 and Chigorodó-1 wells, as well as the interpretation of seismic lines, four seismostratigraphic sequences can be defined, ranging from the Lower Miocene to the Pliocene (?) ([70]: fig. 22; the question mark indicates that the data are purely biostratigraphic). Even the lithostratigraphic relations among the drilled units that outcrop on the west and east flanks of the basin are uncertain because of a lack of detailed stratigraphic studies in these areas [69]. Nevertheless, the stratigraphic record of the Necoclí-1 well on the right bank of the Urabá Gulf along with the related seismic line transect (see [70]: figure. 27; [80]: figure. 9;) reveal the geometry of the Urabá Basin and allow a precise biochonostratigraphic estimation for the facies of the whole foredeep basin According to this idealised stratigraphic scheme [80], the oldest recorded sedimentary rocks in the Urabá Basin are Lower Miocene deep-water facies, which grade to Pliocene–Early Pleistocene shallow-water siliciclastic de-

posits and are overlain by more recent alluvial sediments ([80]: figure. 5c). Therefore, an Early Pleistocene exposure of the Atrato Seaway from the Urabá Basin to the Pacific via a marine trough in the northern Baudó mountain range is congruent with the available data. This seaway is not related to the findings of Montes et al. [6] because it was located northwards, not southwards, of the Mandé Batholith (see [6]: figure. 3).

A likely second connection of the Atrato Seaway southwards to the Pacific passes from the adjacent San Juan Basin. There, the Mayorquín Formation can be correlated with the Quibdó Formation on the basis of similarity in (e.g. [70]). However, the Atrato River Valley to the north and the Pacific Plain to the south were separated by the uplift of the "San Juan Paleohigh," resulting in the southernmost extension of the "Istmina Deformation Zone." This uplift was the product of dextral tectonics from the collision of the Panama arch with the Colombia Pacific during the Late Neogene, but the precise age of the event is not well constrained [81].

Phylogeographic Data

Although biogeographical information can be useful in palaeogeography and has often been invoked in the (e.g. [82]), previous efforts to determine the palaeogeography of the Isthmus of Panama (e.g., [1]) did not manage to separate a clear and detailed biogeographical signal In the rest of this section, I reconsider the existing phylogeographical data, focusing on the scenario of a very recent formation of the Isthmus of Panama.

Molecular divergence dates of transisthmian geminate species and populations have been widely used to infer conclusions regarding the formation of the Isthmus of Panama (e.g. [1]). Such divergence dates can be considered reliable only if they are calibrated on independent calibration points rather than on a benchmark date for the formation of the isthmus, because the a priori assumption of a benchmark date for the formation of the isthmus leads to circularity if the goal is to examine the timing of dispersal or vicariance across the isthmus [1]. On the other hand, the characterisation of species or populations as "geminate" is itself subject to limitations and uncertainties, which can influence the phylogeographic conclusions [83]. A proper selection of geminate species should make clear how the invoked speciation is related to the formation of the isthmus, because different forms of life have different capabilities to overpass specific biogeographical barriers, so their biogeographical significance in paleogeographic reconstructions varies accordingly.

In the present work, I categorise the phylogeographical data by qualitatively evaluating its importance and clarity regarding the general concept of a recent isthmus formation as well as the exposure of specific transisthmian seaways. The formation of the Isthmus of Panama is assumed to have predominantly caused vicariant speciation of marine biota and terrestrial biota that dwell exclusively in coastal areas and are unable to cross inland features such as hills, mountains, and forests. Geminate and coastal species of this category (Category A) are currently distributed on either side (Atlantic and Pacific) of the isthmus, because the inland of the isthmus developed a physical barrier to interbreeding between Atlantic and Pacific populations of the common ancestor and thus led to vicariant speciation (see the graphical example in Supplementary Figure 1).

Squirrel monkeys (genus *Saimiri*) currently inhabit each of the areas of vertebrate endemism in the Amazon (i.e. the Atlantic side of South America), but one species, *Saimiri oerstedii*, exists only in a small coastal area on the Pacific side of Central America [82]. The restricted distribution of *S. oerstedii* is accredited to specialisation to a lowland coastal niche, which is thought to have been a characteristic of the last common ancestor of *S. oerstedii* and the other *Saimiri species* [84] The divergence between *S. oerstedii and Saimiri sciureu*s, which is found in the northern Amazon, is estimated to have occurred ~0.95 Ma [84]. Sea birds are another example of coastal organisms for which inland areas present a barrier [85]. The most recent common ancestor of regional populations of masked boobies (*Sula dactylatra*) on either side of the Isthmus of Panama is estimated to have lived ~0.64 Myr ago [86].

Mangrove coastal vegetation is often considered to harbour the signatures of historical vicariance events [87]. It has been argued that because mangrove or coastal habitats were the last to disappear during the final closure of the CAS, the species that inhabited those environments were probably the last to be separated by the closure event [88] (Supplementary Figure 1) Therefore, the divergence times of mangrove species should correspond accurately to the final completion of the isthmus [88]. The Pacific and Atlantic populations of the black mangrove (*Avicennia germinans*) are estimated to have evolved independently since ~0.84 Ma [89]. Equivalent divergence dates have been reported for the mangrove-inhabiting fishes of the transisthmian genera *Dormitator* [90], *Anisotremus, and Mulloidichthys* [1] (Table 1).

With regards to marine biota vicariance, there are several shallow-water fishes, decapoda, arthropods, and bivalves dwelling on either side of the isthmus whose divergence times have been dated close to, or since, 1 Ma using independently calibrated molecular clocks (Table 1). Most of these species are inhabitants of mangrove environments, suggesting a shallow-water property in the last transisthmian seaways. However, the existence of a deep-water species in Category A supports the view that at least one of the seaways maintained a deep sill.

In addition to the examples in Category A, there are many other potential geminate species with molecular divergence dates that are comparable with a <1 Ma age of the formation of the Isthmus of Panama, including plants, insects, reptiles, and birds (e.g. Supplementary Table 8 in [1]). Invocation of these species as direct evidence of the age of the formation of the isthmus would require the exclusion of ecological factors as an alternative explanation, however, as well as composite dispersal scenarios with a substantial degree of uncertainty, so they are counted here just as indications. The most significant of them have been included in a separate Category (Category B) that includes species with distinct (Category B1; Supplementary Table 1) or overlapping (Category B2; Supplementary Table 2) distributions on both sides of the proposed former transisthmian seaways.

Table 1: Molecular divergence dates of transisthmian geminate and coastal, species and divergent populations, supporting a very recent (<1 Ma) exposure of the Isthmus of Panama.

	Type of Life Form	Pacific Coast Variety	Atlantic Coast Variety	Divergence Time (Mya)	Calibration	Reference
1	Fishes	Mulloidichthys dentatus	Mulloidichthys martinicus	0.65	Standard molecular clock rate**	[1]
2	Fishes	Abudefduf concolor	Abudefduf taurus	0.7	Standard molecular clock rate**	[1]
3	Fishes	Anisotremus interruptus	Anisotremus surinamensis	0.8-1.12	1. Standard molecular clock rate**; 2. plus fossils	[1]
4	Fishes	Dormitator latifrons	Dormitator sp.	0.98	Fossils	[90]
5	Fishes*	Anchoa delicatissima	Anchoa parva	0.4-0.75	fossils	[153]
6	Fishes*	Pacific species lineage of Old World Anchovies (genus Engraulis)	Atlantic species lineage of Old World Anchovies (genus Engraulis)	0.67	Mainly on fossils	[154]
7	Fishes*	Lycengraulis poeyi	Lycengraulis grossidens	0.88	Combined, on two fossils and a Panama closure date	[154]
8	Decapoda/Crabs	Eurytium tristani	Eurytium occidentalis	0.63	"Date of Messinian Salinity Crisis"	[83]
9	Arthropoda/ Marine littoral springtails	Psammisotoma dispar	Psammisotoma dispar	1.04	Standard mutation rate**	[155]
10	Marine Bivalves/ Deep-sea clums	Abyssogena novacula+mariana	Abyssogena southwardae	0.95	Fossils	[156]
11	Mammals/ Cetaceans	Fin Whales (Balaenoptera physalus spp.)	"Fin Whales (Balaenoptera physalus spp.)"	0.95-0.99	On fossil-based divergence date	[157]
12	Mammals/ Primates	Saimiri oerstedii	Saimiri saimiri sciureus	0.77-0.95	Fossils-based Saimiri crown age	[1, 84]
13	Birds/Seabirds	Sula dactylatra	Sula dactylatra	0.64	Standard "bird mutation rate"	[86]
14	Plants	Mangrove Avicennia germinans	Mangrove Avicennia germinans	0.84	Standard mutation rate**	[89]
*not considered as geminate species by the original authors						
**stable molecular clock percentage characterizing a specific taxonomic rank						

Detailed palaeo geographical information about the exposures of the transisthmian seaways in specific locations can be extracted from the phylo geography of terrestrial species with limited dispersal, that is, species (mainly endemic) that inhabit the same area for a long time. Accordingly, one can suppose that genetically distinct populations that today inhabit regions on both sides of former seaways will have molecular divergence dates that correspond to the last exposure of the seaways. Species in this category include freshwater dwellers such as fishes and frogs (Supplementary Table 3 and Supplementary Appendix). For example, genetic variants of the freshwater catfish *Pimelodella chagresi* with an estimated divergence time ~0.9 Ma [91] are currently distributed on either side of the ancient locations of the Barú, Canal, and Atrato Seaways (see Supplementary Appendix) In addition, genetic variants of the mosquito *Anopheles albimanus* [92] can be used to help reconstruct the positions of the Early Pleistocene seaways just before the final formation of the Isthmus of Panama The rationale for that approach is that as the relative sea level fell during the formation of the isthmus, saltwater swamps with mangrove vegetation would have developed in the emergent lowlands that were previously occupied by seaways, creating favourable conditions for the saline-tolerant *A. albimanus* to disperse across the isthmus. *A. albimanus* is one of the approximately 5% of mosquito species that live in either brackish or saline water, having adapted a highly developed system to regulate salinity [93]. The continuing sea level fall finally dried the saltwater swamps and separated the ancestral population of *A. albimanus* into isolated regions.

Biostratigraphic Data

Ancient biotic geodispersals are indicative of dispersal routes and provide proxies of ancient paleogeographic configurations (e.g. [82]). Terrestrial migrations across an isthmus provide evidence that the isthmus was exposed as a land bridge at the time of the mi-

gration, whereas the presence of related marine biota on both sides of an isthmus suggests the former presence of a seaway through the isthmus [94]. Evidence from terrestrial biota that might have migrated through a subaerial exposure of the Isthmus of Panama 1–0.89 Ma ago can be found in the concept of the Great American Biotic nterchange [95] and, more specifically, within the third terrestrial migration event (GABI 3) Specifically, the third dispersal event of the Great American Biotic Interchange (GABI 3) between North and South America took place ~0.9 Ma [95], resulting in the presence of opossum *(Didelphis)* in North America ~0.9 Ma (0.8–1.0 Ma) [95] and that of the *jaguarundi Herpailurus*, the cervid Paraceros, the peccary Pecari, and the tayassuid Tayassu in imprecisely dated Bonaerian beds (Middle Pleistocene, ~0.7 Ma) in South America [95-96]. Importantly, the dispersal of *Equus* into South America, which was previously thought to have occurred during the GABI 4 event in the Late Pleistocene (~0.125 Ma), was recently reported to have occurred between ~0.99 Ma and <0.76 Ma, an interval that includes the GABI 3 [97]. Older records of terrestrial immigrants (e.g. GABI 1 and 2) probably correspond to distinct ephemeral exposures of the isthmus.

Evidence of terrestrial migration across the isthmus must be considered indirect evidence because the observed biogeographic patterns might have been influenced by ecological parameters other than the existence of a land bridge. By contrast, the biogeographic distributions of marine biota constitute more direct evidence of the formation of the isthmus, because compared with terrestrial biota, their dispersal depends more on the spread of the medium (sea water) in which they live. In the case of the Isthmus of Panama, biotic extinctions due to ecological change driven by the closure of the CAS have been considered as possible evidence for the timing of the isthmus formation [98]. Major changes in the marine biota of the western Atlantic and the Caribbean region that were expected to coincide with the closure of the CAS at ~3 Ma [99] in fact took place much more recently For example, the intensity of extinctions in coral reefs in the Caribbean region was highest by far in the interval 2–1 Myr ago [100]. In particular, of a total of 133 species reported in the Caribbean Plio-Pleistocene, 77 are currently extinct in the region. Furthermore, all but one of the extinct species (*Pocillopora palmata*) had gone extinct by the Middle Pleistocene, indicating that a major extinction episode occurred during the preceding interval [100]. Similarly, much of the actual turnover in benthic foraminifera has occurred since the Pleistocene, long after the supposed closure of the CAS at ~3 Ma ([99] and references therein) The faunal shift in ostracode assemblages coincides with or slightly precedes the appearance of reefal and carbonate-platform ostracode assemblages in the Early Pleistocene Moín Formation (dated 2 Ma to <1 Ma) [11, 45]. None of the 10 Late Miocene species of *Stylopoma* cheilostome Bryozoans that survived into the Pliocene became extinct afterward, whereas all nine species of *Metrarabdotos* that survived into the Pliocene became extinct by the Early Pleistocene [98]. Likewise, near the end of the Early Pleistocene, "paciphile" taxa disappeared from the Neogene Caribbean marine molluscan assemblages, which prior to that time had been part of a single bioprovince (the Gatunian Province) that spanned both sides of the isthmus [101-102] (Figure 4A). Such a recent resemblance in the molluscan assemblages on either side of the isthmus cannot easily be explained if the final emergence of the isthmus occurred at 3 Ma. Likewise, the occurrence of the atlantiphile tonnoidean gastropod species *Linatella caudata* in the early-to-mid Pleistocene Armuelles Formation [103] in Pacific Panama indicate the existence of shallow-water interoceanic exchange [96] between the Pacific and the Caribbean during the whole Early Pleistocene [94, 101]. Continued Early or Middle Pleistocene connections are also demonstrated by Cymatium cingulatum (now Atlantic) in the Armuelles Formation of Pacific Panama [104].

Stratigraphic and Palaeoceanographic Data

Oceanographic models support the hypothesis that the open CAS permitted relatively fresh and cool Pacific water to flow into the North Atlantic, affecting buoyancy by adding freshwater into the Caribbean and weakening the AMOC (e.g. [105]). For example, a narrow (~100 km) but deep (~2,000 m) transisthmian seaway could exert a profound effect on the global oceanic circulation pattern [105]. The open/close modes of the transisthmian seaway(s) can be traced through changes in ocean salinity and the circulation patterns of ocean surface currents, as well as the circulation of bottom currents and their erosional effect on the ocean floor. Specifically, during periods when the transisthmian seaways were open, low-salinity Pacific waters could penetrate into the high-salinity Caribbean waters, reducing the intensity of the Gulf Stream and the North Atlantic Current on the surface of the Atlantic (Figure 4) and the North Atlantic Deep Water (NADW) formation on the bottom of the Atlantic.

For example, the increasing domination of the Caribbean planktic foraminiferal assemblages by the salinity-tolerant species *Globigerinoides ruber* is considered to reflect increased Atlantic surface-water salinity due to cessation of sustained flow between the Pacific and the Caribbean [9]. The relative abundance of *G. ruber* culminated from 0.9 Ma to 0.6 Ma (Figure 4B).

The dominance of the planktic foraminifera *Globorotalia truncatulinoides* along with the enriched δ13C isotope values of *Neogloboqudrina dutertrei* in ODP Hole 994C, Blake Ridge, NW Atlantic, have been interpreted to indicate the presence of high-salinity, less-productive surface water in the northern Atlantic derived from an intensified Gulf Stream flow due to closure of the CAS [106]. Such changes have been recorded since 0.9 Ma and thereafter, as well as during earlier intervals [104]. The $\delta^{13}C$ of planktonic foraminifera depends on a variety of factors and is therefore not a very good indicator of gyre changes. However, stronger data from the neighbouring ODP Site 1058 also suggest an enhanced subtropical gyre and a pronounced increase in poleward warm water advection since the same interval (MIS22) [107]. This increased poleward warm water advection coincided with increasing benthic foraminiferal $\delta^{13}C$ values, suggesting that it might have contributed to enhanced formation of North Atlantic Deep Water [107]. Estimation of the variation in Northern Component Water (NCW) overflow, the ancient counterpart of the NADW, also highlights a culmination at 0.9 Ma [108] (Figure 4C).

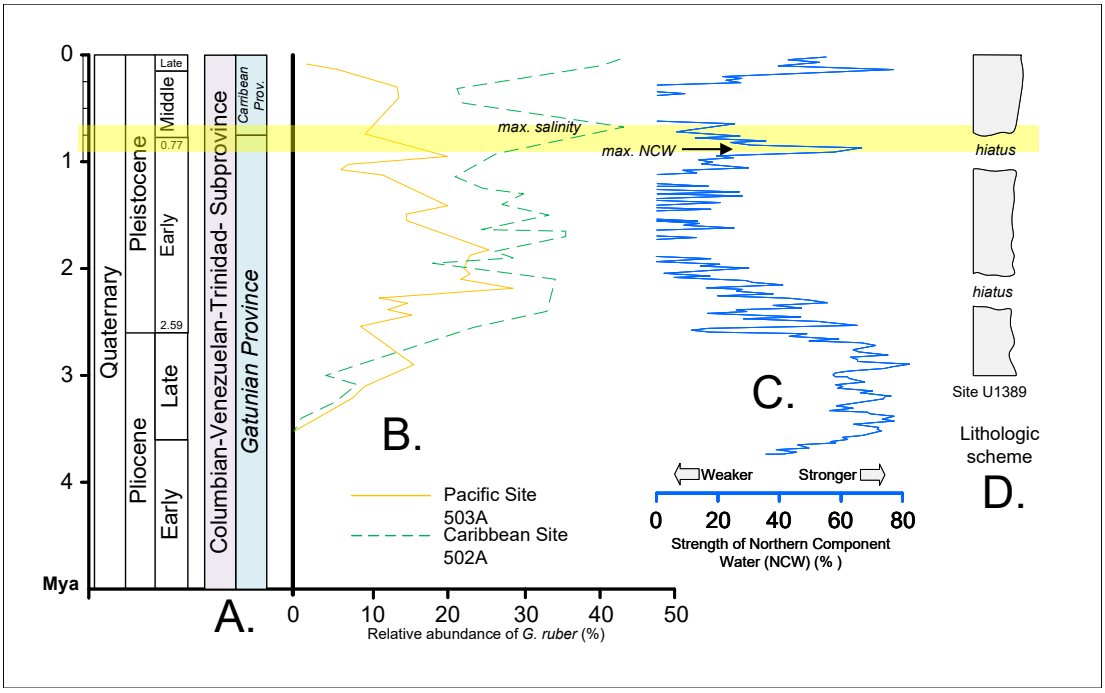

Figure 4: Paleobiogeographic and oceanographic data supporting a major step in the restriction of the transisthmia5n seaways of the Isthmus of Panama, 0.89 Ma and ~0.7 Ma. A) Southern Caribbean Neogene biogeographical units [101]. B) Relative abundance of the high-salinity-tolerant planktic foraminiferal species *Globigerinoides ruber*, as a proxy of surface-water salinity [9]. C) Estimation of the variation in Northern Component Water (NCW) overflow [108]. D) Drill core data of IODP Expedition 339 sites, showing major hiatuses caused by increased saline and warm water transport from the Mediterranean Outflow Water current (MOW) [109-110].

Enhanced Gulf Stream flow is accompanied by increased North Atlantic Deep-Water formation (as part of the AMOC). Periods of increased AMOC strength have been linked to increased salinity and warm water transport from the Mediterranean Outflow Water current (MOW) [109-110] (but see the Discussion). The increased MOW strength is marked by depositional hiatuses on the route of the MOW, indicating erosion by bottom currents due to increased volumes circulating into the North Atlantic. Such hiatuses occurred during three periods, the last of which was from 0.9 Ma to 0.7 Ma [109-110] (Figure 4D).

In contrast to the above indications for increased North Atlantic Deep Water formation, neodymium (Nd) isotope data that have been used as a proxy of the ocean thermohaline circulation show an exceptional weakening of the thermohaline circulation at the end of the MIS 23 interglacial, at ~900 thousand years ago [111]. In the Discussion, I show how this controversial evidence can be explained under the concept of the recent formation of the Isthmus of Panama.

Paleoclimatic data

Climate models developed since the early 1990s have suggested that closure of the CAS would strengthen the production of warm, high-salinity Gulf Stream water, enhancing heat transport to the North Atlantic and the upper NADW formation in the Labrador and Nordic Seas [13; 112 and references therein]. Moreover, as the heat transport through the North Atlantic Current (Figure 5) is accompanied by humidity transport, it has long been argued [113-114], and was recently shown by coupled ocean–atmosphere general circulation models [115-118], that closure of the CAS would result in enhanced precipitation over Greenland. Strati graphical evidence from ODP Site 646 on the continental rise off southern Greenland (58°12.56N, 48°22.15 W) [118] shows that such an event took place in the eye of the glacial maximum of Marine Isotope Stage 22 (MIS22; Supplementary Figure 2). This event is evidenced by increases in pteridophyte and spermatophyte spore and pollen records (Supplementary Figure 2E), respectively, suggesting that south (and probably east) Greenland experienced an unprecedented local climatic optimum characterised by increased vegetation growth. This exceptional event has not been discussed previously and is highlighted here for first time. It was even ignored by the authors who published the original data documenting it [119]. According to these data, the event lasted ~20,000 years, from 0.89 Ma to 0.87 Ma, and can be correlated with an episodic increase of ~4.5°C in SSTs across the track of the North Atlantic Current (Supplementary Figure 2). Two positive SST culminations in the record of ODP Site 980 [120] are particularly well matched with two contemporaneous positive peaks in the spermatophyte pollen record of MIS22 from South Greenland (Figure 6 and Supplementary Figure 2H), suggesting that the intensification of the North Atlantic Current was among the likely reasons for the unprecedented climatic optimum in South Greenland In the Discussion, I provide an alternative oceanographical scenario, implying that all of the previously mentioned palaeoceanographic and pa-

laeoclimatic phenomena are results of effects of the recent Isthmus of Panama formation on the intensity of the cold East Greenland Current rather than on the intensity of the warm North Atlantic Current.

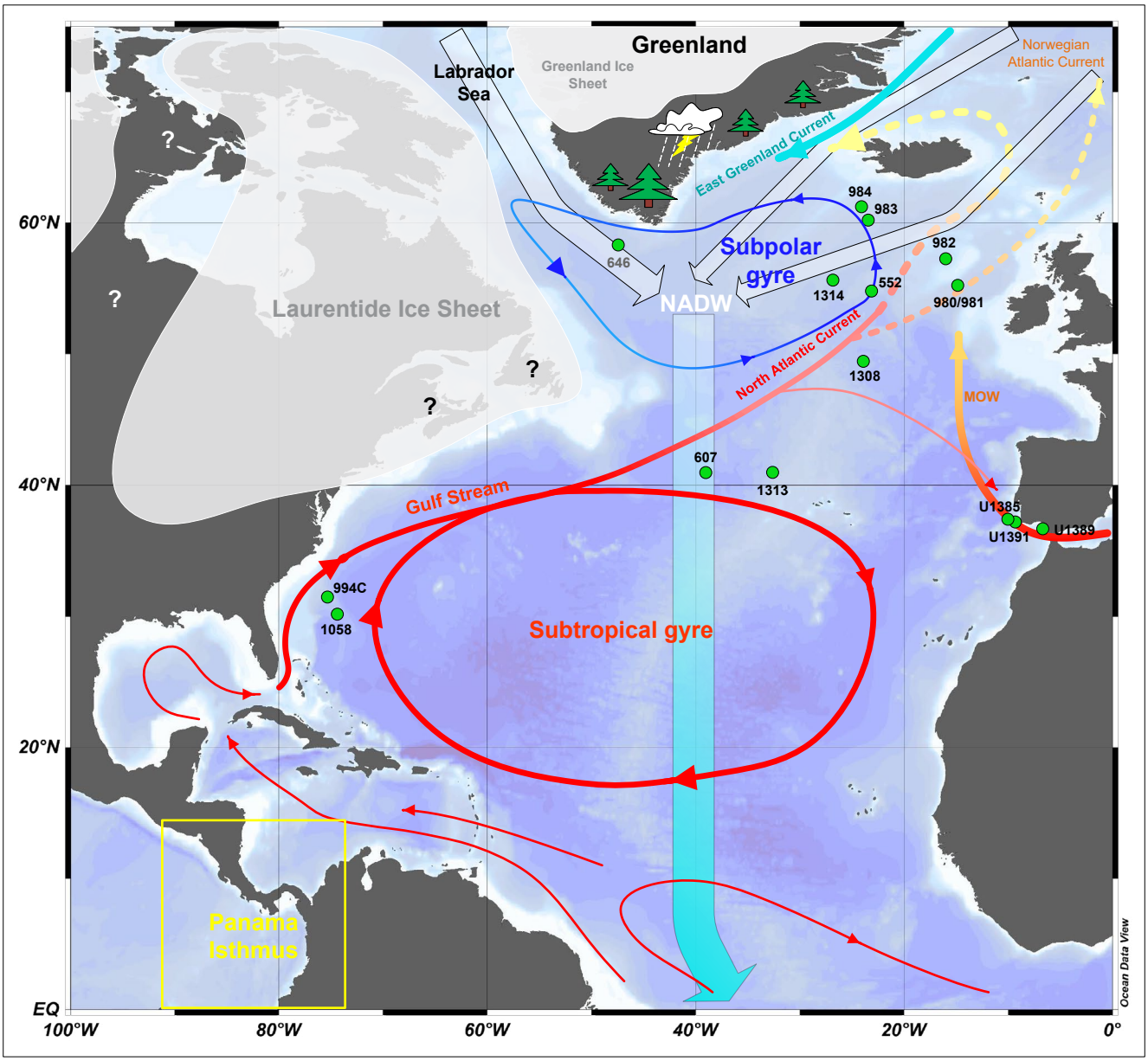

Figure 5: Potential configuration of North Atlantic surface currents during the unprecedented Greenland "greening" at the glacial maximum of MIS 22 due to a major episode in the restriction of the transisthmian seaways and the shutdown of the East Greenland Current at 0.89 Ma. Green circles mark the positions of ODP and IODP sites mentioned in the text and graphs. Hypothesised reconstructions of ice-sheet extent based on Batchelor et al. [141]. Map designed using Ocean Data View software [142].

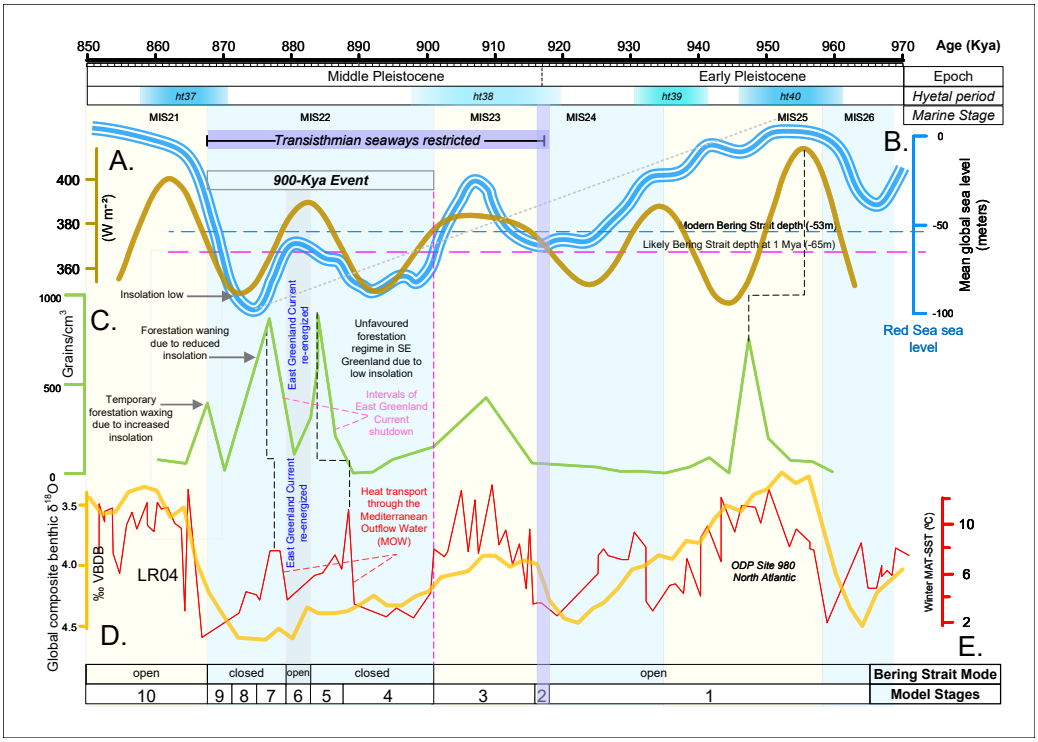

Figure 6: A closer look at the paleoenvironmental parameters that are probably related to the climate perturbation of the 900-Ka event across the MPT. A) Insolation oscillations at 65°N high latitude [143]. B) Mean global sea level fluctuation [144]. C) Pollen content of spermatophytes as an independent proxy of vegetation and forested episodes in South Greenland [119]. D) Stack of 57 globally distributed benthic δ18O records (palaeotemperature proxy) [145]. E) Sea surface temperatures (SSTs) from ODP Site 980 [120]. Hyetal spectrum according to Brikiatis [126].

Discussion

It has long been believed that the final formation of the Isthmus of Panama took place at ~3-3.5 Ma [7, 8, 121]. This view has been taken with such certainty that hundreds, or perhaps thousands, of works have based conclusions on that date [1, 2]. Although the concept of the final formation of the isthmus at ~3–3.5 Ma was initially proposed on the basis of biostratigraphical and geochemical data from the Deep Sea Drilling Project (DSDP) more than 40 years ago [7, 114], the main arguments of the concept are based on geotectonic data that were first presented 25 years ago and have not been reconsidered in light of more recent findings [7, 8, 18 112]. The present review does not reject the possibility of an ephemeral exposure of the Isthmus of Panama at ~3 Ma; however, it suggests that the final formation of the isthmus was a much more recent event caused by rapid tectonic uplifts due to movements of the Cocos Ridge and Nazca Plates in the Early to Middle Pleistocene (i.e., within the last one million years), although the precise times of these events are still under investigation. Indeed, the exposure of the Barú Seaway, in particular, may be a result of tectonic reconstructions that took place since ~3 Ma [37], the complete definition of which is still under discussion [29, 40]. For example, the initiation of seamount and rough crust subduction of the Cocos Plate began before the Cocos Ridge subduction and, especially, before the subduction of the crest of the Cocos Ridge, which resulted in the emergence of the Burica Peninsula during the last one million years [40]. The Panama Triple Junction was located more north-westerly (in the vicinity of the Osa Peninsula) 2–3 Myr ago [40] than it is today (Figure 2), so that the onset of the Cocos Ridge collision (<3 Ma) resulted in a new uplift episode in the Cordillera de Talamanca [39]. During this episode, the Barú Seaway to the east of that mountain range might have developed as a right-lateral basin.

The strati graphical information invoked here regarding the age and distribution of the Quibdó Formation in the Atrato Basin, along with the data from the Urabá Basin, leaves open the possibility that a shallow Atrato seaway persisted until the late Early Pleistocene. In particular, the presence of Quibdó Formation deposits in the Salaquí river area suggests the past existence of a hidden marine connection of the Atrato Seaway to the Pacific via an independent trough (Salaquí Trough) that crossed the northern Baudó mountain range westwards (Figure 2 and Figure 3). This connection was probably severed during the Early Pleistocene orogeny in the area.

In sum, the interpretation of the available data suggests that as many as three shallow transisthmian seaways persisted until as recently as the onset of the Middle Pleistocene (~0.65 Ma). Most importantly, evidence for a fourth transisthmian seaway, the Barú Seaway, which probably featured a deeper sill, was destroyed by the uplift of the ~3000 meters high Barú Volcano. Similarly, the

exposure of an Early Pleistocene shallow transoceanic seaway through the Panama Canal Basin is also questionable because of the complete absence of sediments that testify to its presence. Therefore, although the current stratigraphical evidence supports the exposures of only two of the four hypothesised seaways (i.e. the Nicaraguan and the Atrato), the existence of the other two seaways (i.e. the Barú and the Panama) is suggested by the absence of stratigraphical evidence against their exposure and the relatively young (Pleistocene) age of the topographical barriers developed within them.

The palaeogeographical scenario regarding the very recent formation of the Isthmus of Panama is also in agreement with multiple lines of indirect phylogeographic, biostratigraphic, oceanographic, and paleoclimatic data. For example, the relationship between the elevation of the Isthmus of Panama and oceanographic conditions in the Tropical Eastern Pacific suggests that although today the isthmus is one of the most mountainous regions in Central America (with peaks rising over 3000 m), the modern topography of the region is largely a consequence of rapid uplift during the last few hundred thousand years (since the mid-to-late Pleistocene) [48].

The available phylogeographic data presented here show the existence of a number of transisthmian geminate marine and coastal species (Category A species; see Table 1) with too recent molecular divergence dates (from 1 to 0.65 Ma) that are not consistent with even the youngest estimations for the age of the isthmus (1.8 Ma [9-11]). Instead, the data suggest that the isthmus was not finally and completely formed until 1–0.6 Ma. Most of the relevant species are marine species for which, if a long-distance dispersal and/or a "sweepstake" dispersal is excluded, there is no way of dispersal to either side of the isthmus other than an exposed transisthmian seaway. The above two biogeographical concepts are used frequently to support phylogeographical conclusions, adding "noise" to the biogeographical signal; however, they might be the result of poorly understood palaeogeographic evolution and/or inaccurate dates for clade divergences due to incorrectly calibrated molecular clocks [94]. This is probably also the case in the biogeography of the Isthmus of Panama, where molecular divergence dates earlier than the "benchmark" date of 3 Ma have been easily attributed to "sweepstake" dispersals. A classic example is the case of the marine snails of the genus *Cerithideopsis*, which have been proposed to have dispersed from the Pacific to the Atlantic 750,000 years ago, but also in the opposite direction about 72,000 years ago [122]. Accordingly, the first *Cerithideopsi*s dispersal is congruent with the scenario of the recent isthmus formation proposed here, but the latter dispersal is compatible with a "sweepstake" dispersal. The original authors of the survey concluded that both were cases of "sweepstake" dispersals because they believed that the final formation of the Isthmus of Panama occurred at 3 Ma. However, because that study, as well as many others, used the "benchmark" date of 3 Ma as a calibration point (in the absence of fossils), its chronological results are not suitable for making conclusions related to the final formation of the Isthmus of Panama (or to dispersal scenarios), because they are biased.

In addition to shallow-water species, the presence of a deep-sea bivalve (*Abyssogena* in Table 1) could suggest that at least one exposed seaway maintained a deep sill until ~1.1 Ma. Because of the current biogeographical distribution of these geminate species in the Central Atlantic and the Central-East Pacific (close to and on either side of the Isthmus of Panama), an alternative dispersal through high-latitude sea corridors is not the most parsimonious scenario.

Aside from the Category A geminate species, Supplementary Tables 1 and 2 contain bird and plant species (Category B) with molecular divergence dates that suggest allopatric speciation due to the same vicariant event. Moreover, specific phylogeographic data point to the existence of biogeographical barriers to terrestrial dispersals within the Isthmus of Panama that conclusively correspond to the proposed exposures of the four distinct seaways (see Supplementary Table 3 and Figure 3): the Nicaraguan Seaway, the Barú Seaway, the Canal Seaway, and the Atrato Seaway. In accordance with the phylogeographical and geotectonic data, marine and terrestrial biostratigraphic data suggest that the final formation of the Isthmus of Panama was more recent than previously thought.

When the various phylogeographic, biostratigraphic, oceanographic, and paleoclimatic data are evaluated separately, experts from each discipline may doubt whether the data provide strong enough evidence to support the scenario of a very recent isthmus formation, as alternative explanations are also possible. In this respect, researchers may be in a hurry to reject the proposed scenario and remain true to the current and widespread view of a latest Pliocene (~3 Ma) final exposure of the isthmus. That view was established on geological evidence that can be challenged with more recent lines of evidence, however, and should therefore be carefully reconsidered. Indeed, if the data from the various sources presented in this review are considered independently, they cannot independently support the proposed scenario for the recent final exposure of the isthmus. However, if all the data are considered together as the result of a single event, they show a pattern that supports a novel palaeogeographical scenario, which in turn sheds light on some currently unexplained phenomena that took place during the great paleoclimatic change known as the MPT [16]. I discuss this prospect in the following section within the context of two different palaeoceonographical scenarios, both of which are based on the effects of the recent formation of the Isthmus of Panama on the thermohaline circulation and the production of the NADW. The first scenario favours a northwards heat advection through a strong subtropical gyre and a North Atlantic Current able to penetrate the subpolar gyre, whereas the second scenario favours a northwards heat advection through a strong Mediterranean Outflow Water (MOW). The effect of the latter was probably dominated by the intensity of the cold East Greenland Current, which in turn is driven by the Bering Strait gateway modulated by the open/close modes of the CAS.

Northwards heat advection through the North Atlantic Current

Various oceanographic models predict that termination of inter-oceanic seawater exchange through the Panama seaways should result in perturbation of oceanic circulation and physical properties(e.g. [105]). Such physical and sedimentological changes have been identified ~0.89 Ma and ~0.7 Ma, suggesting major restrictions of the transisthmian seaways around these ages (see Figure 4). Furthermore, contemporaneous changes in heat transport to the North Atlantic via the Gulf Stream (Figure 5) can be shown using variation in the sea surface temperatures (SSTs) as a proxy. Indeed, North Atlantic SSTs during glacial stages were unusually high, in contrast to the contemporaneous low global mean temperatures of deep waters, suggesting a remarkable intensification of the Gulf Stream that is congruent with the restriction of the transisthmian seaways (Supplementary Figure 2). The episodic climatic optimum suggested by the culminations of pollen and spore records from South Greenland during the glacial maximum of marine isotope stage 22 (MIS 22) [119] (Supplementary Figure 2) further supports the hypothesis that there was a major restriction of the transisthmian seaway ~0.89 Ma The culminations required a heat source capable of driving an increase in precipitation and plant growth. Deep-sea cores from around the course of the North Atlantic Current, the ocean surface current that conveys the warm Gulf Stream northwards, display episodic increases of ~4.5°C in SSTs during the MIS 22 interval, whereas cores within the subpolar gyre do not (Supplementary Figure 2).

Indeed, at the time of its formation, the Isthmus of Panama maintained a lowland profile and was therefore sensitive to relative sea level changes. The global mean sea level reached its lowest level of the entire Cenozoic interval at 0.89 Ma [123]. There was also an exceptional climate deterioration around that time, known as the "900-Ka event," which can be added to the evidence supporting a recent final formation of the Isthmus of Panama. The cause of the 900-Ka event is a great mystery [16, 124-125]; however it was recently demonstrated that the event was not orbitally forced but was instead due to a currently undefined feedback perturbation of the Earth's internal climate system [126] (Figure 7). There are examples of major and permanent changes in phenomenally unrelated terrestrial and marine records around that time, such as the permanent reduction in the loess grain-size rate (>63 μm particle content) in the Otindag sandy desert in northeast China (Figure 7C) and the change in the sedimentation rate of the Bering Sea area [128] (MIS24; Figure 7B). These changes are contemporaneous with geochemical changes in the oceans (Figure 7), which could only be explained by a major reorganisation of surface and bottom currents Such a perturbation of the ocean currents could in turn only be achieved through a major palaeogeographical change.

Indeed, the closure of the Bering Strait due to the major sea level fall at 0.89 Ma was previously suggested [128] as a main reason for the 900-Ka event and, more generally, the MPT, the age suggested by paleoenvironmental data as the threshold for the transition of glacial/interglacial periodicity from 41-Kyr cycles to quasi-100-Kyr cycles as well as a significant change in glacial behaviour in general (e.g. [124-125]). However, because the time window for a possible closure of the Bering Strait was short, such a closure cannot explain the long-term procedure of the MPT, which ranged from 1.2 Ma to 0.6 Ma [16]. A longer procedure, such as the restriction of transisthmian seaways due to tectonic uplift driven by Cocos Plate subduction, seems to fit better with the available data.

Recent modelling experiments showed that the open/close modes of a ~2,000-m deep and ~100-km wide transisthmian seaway could have profound effects on the global ocean mean state and deep-water mass properties and circulation [105]. In particular, the models showed North Atlantic Deep Water (NADW) penetration into the Pacific below a depth of 1,469 m, with 12.8% of total net mass transport occurring below that depth [105]. Thus, the deep sill property of a transisthmian seaway has implications for global changes in deep-water circulation and could be a driver of long-term changes in climate [105]. Furthermore, in contrast to present-day and previous CAS simulations, the recent experiments showed that the open/close modes of a transisthmian seaway with the afore said dimensions would be able to essentially influence the transportation of heat and salt southward into the South Atlantic, strongly influencing the palaeoceanography of the Southern Hemisphere.

Accordingly, the exceptional geochemical changes observed in the Southern hemisphere (Figure 7G and 7H) during the MIS24 (~920 Ka) could be attributed to the shoaling of the Barú Seaway. Indeed, the geotectonic data presented here indicate that the only likely transisthmian seaway (among the four proposed here) with such a deep sill property was the Barú Seaway (Figure 3). At the south end of that seaway, fine-grained turbidite deposits of the upper Burica Member contain faunas indicating a gradual shoaling from an initial depth of 2,000 m to a final depth of 1,400 m in Late Pliocene through Early Pleistocene times, and strata assigned to the lowermost Armuelles Formation (late Early Pleistocene time) contain faunas indicative of water depths between 1,200 m and 1,300 m [44]. By contrast, the shallow-water molluscs in stratigraphically higher exposures of the Armuelles Formation are indicative of shelf deposits, indicating that within the deposition interval of the Armuelles Formation, rapid shoaling took place at the end of the Early Pleistocene On the basis of these data, Corrigan et al. [44] concluded that rapid uplift due to Cocos Plate subduction took place after the Early Pleistocene More recently, uplift rates of 1–8 m Ka−1 were estimated for the Burica Peninsula over the Late Pleistocene [129]. With a mean uplift rate of 4 m Ka−1, it would take only 0.6 Ma for a 2400 m deep Barú Seaway to become subaerially exposed, meaning that such an exposure could have occurred during the MPT phenomenon, which occurred from 1.2 Ma to 0.6 Ma [16]. Furthermore, with a combined uplift and volcanic accretion rate of 6 m Ka−1, the Barú volcano (3,474 m) could have emerged during the last 0.6 Myr. Accordingly, the Cocos Plate subduction could correspond to a major step in the shallowing of the formally deep-water Barú Seaway, with important implications for

interoceanic deep-water interchange. This hypothesis is supported by the Atlantic/Pacific divergence of the deep-sea bivalve species Abyssogena from ~0.95 Ma (Table 1). Interestingly, apart from the biostratigraphical data from the Armuelles Formation at the south end (Burica Peninsula) of the assumed Barú Seaway, Cronin & Dowsett [11] noted the presence of the deep-water planktonic foraminifer *Bradleya* among shallow-water taxa collected from the Cangrejos Creek section, Moín Formation, Limon Basin (1.5-0.9 Ma) [45], which may represent facies of an upper-bathyal environment in the area at the north of the Barú Seaway Alternatively, Cronin & Dowsett [11] suggested that the Bradleya may have reached shallow waters because of upwelling currents created by the closure of the CAS [11]. Given the age of the Cangrejos Creek section (1.5-0.9 Ma), this claim can also be used to support the recent formation of the Isthmus of Panama.

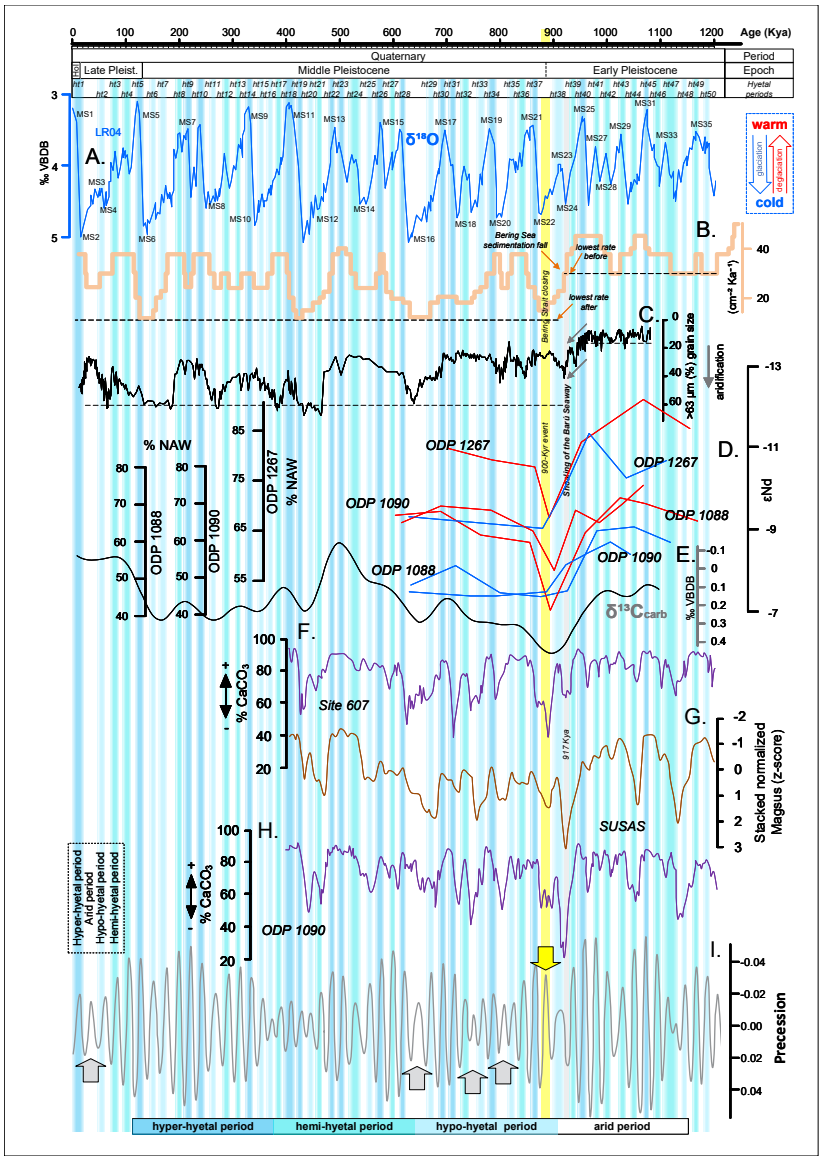

Figure 7: Strict sedimentological and geochemical changes across the MPT. A) Stack of 57 globally distributed benthic $\delta^{18}O$ records (palaeotemperature proxy) [145]. B) Sedimentation rate at the Bering Sea shelf (North Pacific) [128]. C) Loess grain-size rate (>63 µm particle content) in the Otindag sandy desert, north eastern China [127]. D) Comparison of planktic foraminiferal Fe-Mn oxide coating εNd from South Atlantic sites 1267, 1088, and 1090 and percent calculated North Atlantic Water (modified from Supplementary Figure 1 of Farmer et al. [146]). E) Stacked and smoothed carbonate carbon isotope ($\delta^{13}Ccarb$) from benthic foraminifera of the global ocean [147]. F) DSDP Site 607 %CaCO3 [148]. G) SUSAS South Atlantic magnetic susceptibility stack [149]. H) South Atlantic DSDP Site 1090 %CaCO3 [150]. I) Precessional oscillations of the Earth's rotational axis [143]. Hyetal spectrum according to Brikiatis [126]. The grey arrows note that precession minima correspond to hypo-hyetal and/or arid periods only during periods of eccentricity minima [126]. The only exception to that rule occurs at ~880 kyr (marked by a yellow arrow and a yellow vertical bar) and coincides with the 900-Ka event [126].

Figure 6 shows a detailed view of the interval preceding the 900-Ky event. A glacioeustatic sea level drop that started at ~950 Ka (stage 1) culminated at ~917 Ka (stage 2). This interval probably signals the final shoaling of the Barú Seaway and the establishment of a shallow setting in all four remaining transisthmian seaways (Figure 3). The culmination at 917 Ka signals the onset of the failed MIS23 deglacial, which is characterised by increased duration of relatively high insolation and increased SSTs in the North Atlantic (stage 3). During stage 4, reduced insolation contributed to the extremely cold MIS22 glacial, which led to a new low record in eustatic sea level. This low stand probably resulted in subaerial exposure of the Bering Strait and temporary interruption of the East Greenland Current, which was previously forced by water flowing through the Bering Strait [130, 131]. The interruption of the East Greenland Current reduced the supply of fresh and cold Arctic water into East and South Greenland (stage 5), which, combined with an interval of increased insolation and increased heat transport from the North Atlantic Current due to restriction of the transisthmian seaways, resulted in climate optimisation in South Greenland. The restriction of the transisthmian seaways was intensified by the extreme glacioeustatic sea level fall at 0.89 Ma. A glacioeustatic sea level rise (stage 6) then resulted in a temporary opening of the Bering Strait, intensification of the East Greenland Current, cooling of East and South Greenland, and, finally, temporary interruption of the climatic optimum in South Greenland. A subsequent sea level fall (stage 7) brought back the favourable conditions for another climatic optimum in South Greenland, which lasted until the end of the high insolation period.

The above scenario is contradicted by two lines of evidence. The first is that Nd isotope data used as a proxy of the ocean thermohaline circulation show an exceptional weakening at the end of the MIS 23 interglacial, ~900 thousand years ago [111]. This is contrary to the assumption of an enhanced NADW due to a strong North Atlantic Current. The second contradictory line of evidence is that during the MIS22, although the subtropical gyre was intensified [107], its warm waters were not able to penetrate the subpolar gyre and reach the subpolar Deep Sea Drilling Project Site 552 [107]. This can be explained by recent modelling and drifter studies of North Atlantic inter-gyre exchange indicating that communication between the gyres at the surface is limited by the southward Ekman velocities and a strong surface potential vorticity gradient [132-133]. Indeed, the MOW was recently proposed to be an alternative source of heat advection in the North Atlantic [133]. In the following section, I consider this prospect.

Northwards heat advection and Mediterranean Outflow Water (MOW)

On the basis of new evidence attributing a more important role to the MOW in the northwards heat advection in the North Atlantic [133-134], all of the previously mentioned phenomena can be better explained with a slightly different oceanographical scenario Specifically, given the property of the Bering Strait to operate as a valve regulating the salinity of the North Atlantic waters through the transport of relatively fresh North Pacific water into the North Atlantic Ocean (through the East Greenland Current), the open/close modes of the strait are able to mute the meridional overturning circulation, leading either to cooling and ice-sheet advance in the Northern Hemisphere (at full open mode) [135] or to saltier North Atlantic surface waters and enhanced AMOC [136] and Global Ocean Circulation (at closed mode) [137]. The power of this Bering Strait property depends in turn on the open/close modes of the CAS: it is stronger during a closed CAS and weaker during an open CAS [132, 138]. Specifically, an open CAS with the dimensions considered here (~2,000 m deep and ~100 km wide), or even with lesser dimensions, could decrease mass transport into the Arctic Ocean via the Bering Strait, thereby reducing southward mass transport into the North Atlantic from the Arctic by ~36–55% [105]. Moreover, the closure of the CAS and the opening of the Bering Strait were found to induce strong effects on the AMOC that may partly cancel each other out, as they both cause AMOC changes of around 2 Sv (strengthening and weakening, respectively) [138].

From this view, during the complete closing of the CAS at the time of the recent formation of the Isthmus of Panama, the flow of cold and relatively fresh Pacific water into the North Atlantic Ocean through an open Bering Strait and the East Greenland Current should have been remarkably intensified, resulting in a reduction of the NADW and AMOC during the "900-Ka event" (Figure 6 and Figure 7). On the other hand, the closed CAS should have had the same reduction effect on the NADW and AMOC during all subsequent glacial periods. This is exactly what is suggested by the palaeooceanographical results based on Nd isotope data [111].

The continuing sea level fall probably had closed the Bering Strait at 0.9 Ma (Figure 6). Indeed, as seesaw-like climate change between the North Pacific and North Atlantic is a characteristic result of a closed Bering Strait [136, 139], the otherwise unexplained warming [128] of the North Pacific recorded in the Integrated Ocean Drilling Program (IODP) Site U1343 located on the northern Bering Sea slope is probably evidence of that closure (Figure 8) Similarly, the oscillations of the sea level shown in Figure 6 during the "900-Ka event" would temporally open and close the strait, resulting in the phenomena described in the previous section and displayed in Figure 6.

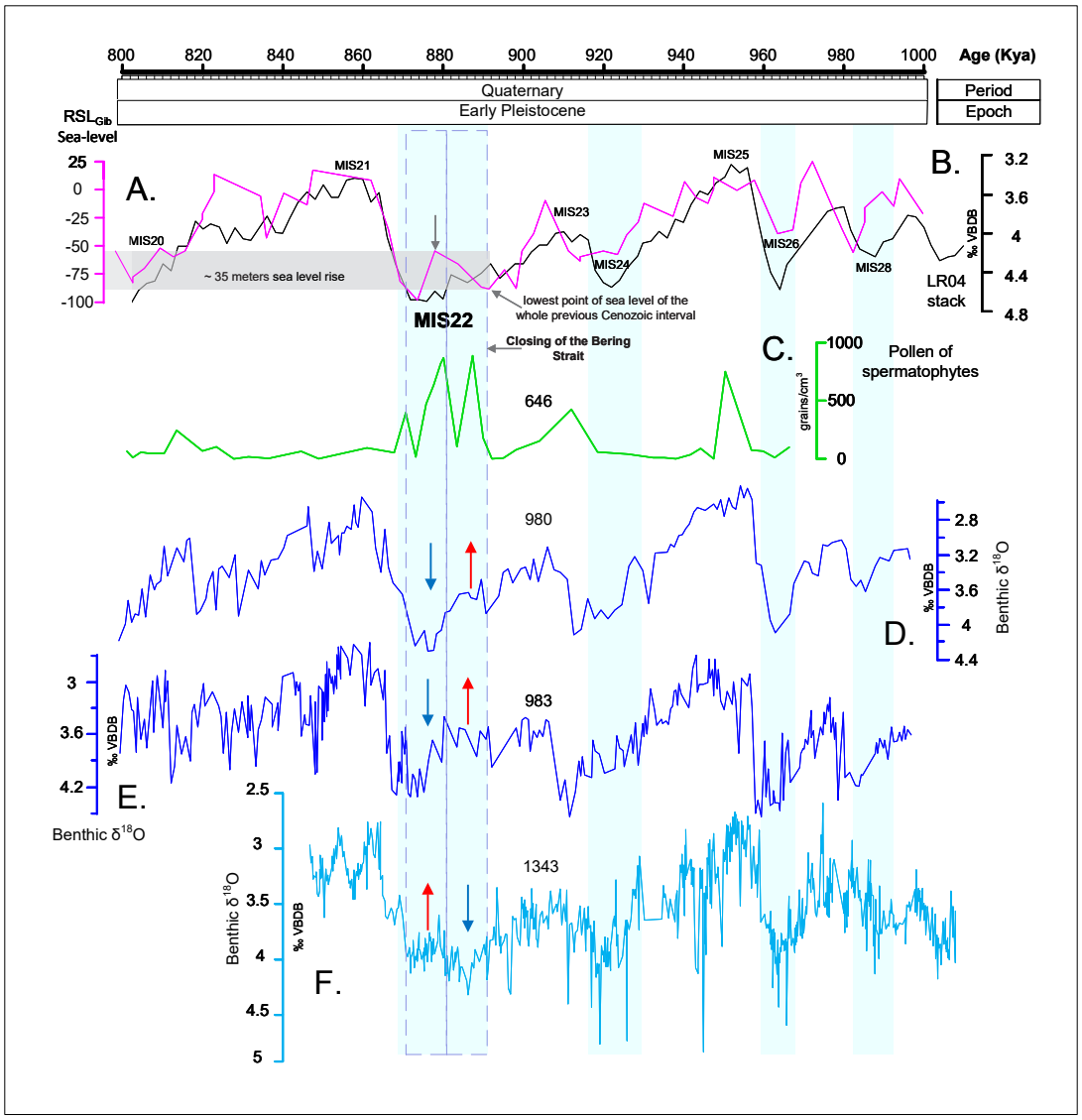

Figure 8: The closing of the Bering Strait during the remarkable MIS 22 glacial, as evidenced by the seesaw temperature pattern (extracted from benthic foraminifera) between the North Atlantic and North Pacific. A) Sea level reconstruction of the Red Sea [144]. B) A stack of 57 globally distributed benthic δ18O records (palaeotemperature proxy) [145]. C) Pollen content of spermatophytes as an independent proxy of vegetation and forested episodes in South Greenland, ODP Site 646 [119]. D) Benthic δ18O from ODP Site 980, North Atlantic (55ºN) [151]. E) Benthic $\delta^{18}O$ from ODP Site 983, North Atlantic (60ºN) [152]. F) Benthic δ18O from IODP Site U1343, North Pacific (57ºN) [128].

As a precondition of this scenario is a weak North Atlantic Current, all of the previously mentioned phenomena of northwards heat advection (including the unusual "greening" of South Greenland during the MIS 22 glacial maximum) (Figure 6 and Figure 8C) can be attributed to the effect of an intensified MOW (Supplementary Figure 3), as recently suggested [133].

Conclusions

Using the most updated data available, I reconsidered geotectonic evidence that was first presented 25 years ago and has been invoked to support a ~3 Ma age for the final closing of the CAS and the final formation of the Isthmus of Panama. More recent data suggest that this age is no longer supported by the available evidence. Specifically, recent geotectonic evidence in conjunction with multiple indirect phylogeographic, biostratigraphic, oceanographic, and paleoclimatic indications suggests that as many as four transisthmian seaways persisted until as recently as the onset of the Middle Pleistocene (~0.65 Ma). Nevertheless, direct stratigraphical evidence is available for the exposures of only two of the hypothesised seaways (the Nicaraguan and Atrato Seaways). Subduction of the Cocos Ridge beneath the Barú Seaway (the only seaway that likely featured a deep sill) might have caused rapid tectonic shoaling and reorganisation of oceanic currents ~1.2–0.6 Ma, coinciding with the mid-Pleistocene climate transition (MPT).

This suggests a tight relationship between these events, although the exact mechanism explaining the transition of glacial/interglacial periodicity from 41-Kyr cycles to quasi-100-Kyr cycles is not yet known. During the MPT, the most essential contribution of the Isthmus of Panama to the global palaeoclimate and the AMOC was control of the Bering Strait gateway as a conveyor of relatively fresh North Pacific waters to the North Atlantic. The palaeogeographical and palaeoceonographical scenario proposed here can explain unusual and contrasting climate phenomena, including the "900-Ka (cold) event" and the "greening" of South Greenland during the MIS 22 glacial maximum.

Data availability statement

All data generated or analysed during this study are included in this published article (and its supplementary information files).

Acknowledgements

This research was not funded by public, commercial, or not-for-profit grants.

References

1. Bacon, C. D., Silvestro, D., Jaramillo, C., Smith, B. T., Chakrabarty, P., & Antonelli, A. (2015). Biological evidence supports an early and complex emergence of the Isthmus of Panama. Proceedings of the National Academy of Sciences, 112(19), 6110-6115.
2. Lessios, H. A. (2008). The great American schism: divergence of marine organisms after the rise of the Central American Isthmus. Annual Review of Ecology, Evolution, and Systematics, 39, 63-91.
3. Molnar, P. (2008). Closing of the Central American Seaway and the Ice Age: A critical review. Paleoceanography, 23(2).
4. Brikiatis, L. (2017). A re-evaluation of the basal age in the DSDP hole at Site 534, Central Atlantic. GeoResJ, 14, 59-66.
5. Pindell, J. L., & Kennan, L. (2009). Tectonic evolution of the Gulf of Mexico, Caribbean and northern South America in the mantle reference frame: an update. Geological Society, London, Special Publications, 328(1), 1-55.
6. Montes, C., Cardona, A., Jaramillo, C., Pardo, A., Silva, J. C., Valencia, V., ... & Niño, H. (2015). Middle Miocene closure of the Central American seaway. Science, 348(6231), 226-229.
7. O'Dea, A., Lessios, H. A., Coates, A. G., Eytan, R. I., Restrepo-Moreno, S. A., Cione, A. L., ... & Jackson, J. B. (2016). Formation of the Isthmus of Panama. Science advances, 2(8), e1600883.
8. O'Dea, A., & Jackson, J. (2009). Environmental change drove macroevolution in cupuladriid bryozoans. Proceedings of the Royal Society B: Biological Sciences, 276(1673), 3629-3634.
9. Keller, G., Zenker, C. E., & Stone, S. M. (1989). Late Neogene history of the Pacific-Caribbean gateway. Journal of South American Earth Sciences, 2(1), 73-108.
10. Schwarzhans, W., & Aguilera, O. (2013). Otoliths of the Myctophidae from the Neogene of tropical America. Palaeo Ichthyologica, 13, 83-150.
11. Coates, A. G. (1996). The geological evolution of the Central American Isthmus. Evolution and environment in tropical America.
12. Schmidt, D. N., Williams, M., Haywood, A. M., & Gregory, F. J. (2007). The closure history of the Central American seaway: evidence from isotopes and fossils to models and molecules. Deep Time Perspectives on Climate Change Marrying the Signal from Computer Models and Biological Proxies: London, Geological Society of London, 427-442.
13. Karas, C., Nürnberg, D., Bahr, A., Groeneveld, J., Herrle, J. O., Tiedemann, R., & Demenocal, P. B. (2017). Pliocene oceanic seaways and global climate. Scientific Reports, 7(1), 1-8.
14. Leigh, E. G., O'Dea, A., & Vermeij, G. J. (2014). Historical biogeography of the I sthmus of P anama. Biological Reviews, 89(1), 148-172.
15. Bagley, J. C., & Johnson, J. B. (2014). Testing for shared biogeographic history in the lower C entral A merican freshwater fish assemblage using comparative phylogeography: concerted, independent, or multiple evolutionary responses?. Ecology and Evolution, 4(9), 1686-1705.
16. Clark, P. U., Archer, D., Pollard, D., Blum, J. D., Rial, J. A., Brovkin, V., ... & Roy, M. (2006). The middle Pleistocene transition: characteristics, mechanisms, and implications for long-term changes in atmospheric pCO2. Quaternary Science Reviews, 25(23-24), 3150-3184.
17. Collins, L. S., Coates, A. G., Berggren, W. A., Aubry, M. P., & Zhang, J. (1996). The late Miocene Panama isthmian strait. Geology, 24(8), 687-690.
18. Funk, J., Mann, P., McIntosh, K., & Stephens, J. (2009). Cenozoic tectonics of the Nicaraguan depression, Nicaragua, and Median Trough, El Salvador, based on seismic-reflection profiling and remote-sensing data. Geological Society of America Bulletin, 121(11-12), 1491-1521.
19. Andjić, G., Baumgartner-Mora, C., Baumgartner, P. O., & Petrizzo, M. R. (2018). Tectono-stratigraphic response of the Sandino Forearc Basin (N-Costa Rica and W-Nicaragua) to episodes of rough crust and oblique subduction. The Depositional Record, 4(1), 90-132.
20. Alonso-Henar, J., Schreurs, G., Martinez-Díaz, J. J., Álvarez-Gómez, J. A., & Villamor, P. (2015). Neotectonic development of the El Salvador Fault Zone and implications for deformation in the Central America Volcanic Arc: Insights from 4-D analog modeling experiments. Tectonics, 34(1), 133-151.
21. Lucas, S. G., Garcia, R. A. M. I. R. O., Espinoza, E. D. G. A. R., Alvarado, G. E., Hurtado de Mendoza, L., & VEGA, E. (2008). The fossil mammals of Nicaragua. New Mex. Mus. Nat. Hist. Sci. Bull, 44, 417-430.
22. Stephens, J. H. (2014). Tectonic and depositional history of an active forearc basin, Sandino basin, offshore Nicaragua (Doctoral dissertation).
23. Stoppa, L., Kutterolf, S., Rausch, J., Grobety, B., Pettke, T., Wang, K. L., & Hemming, S. (2018). The Malpaisillo Formation: A sequence of explosive eruptions in the mid to late Pleistocene (Nicaragua, Central America). Journal of volcanology and geothermal research, 359, 47-67.

24. Swain, F. M. (1966). Bottom sediments of lake Nicaragua and lake Managua, Western Nicaragua. Journal of Sedimentary Research, 36(2), 522-540.
25. Eisendle-Flöckner, U., Bezerra, T. N., Decraemer, W., Hodda, M., Holovachov, O., Leduc, D., ... & Vanreusel, A. (2019). Nemys: World Database of Nematodes.
26. Eisendle-Flöckner, U., Bezerra, T. N., Decraemer, W., Hodda, M., Holovachov, O., Leduc, D., ... & Vanreusel, A. (2019). Nemys: World Database of Nematodes.
27. Eisendle-Flöckner, U., Bezerra, T. N., Decraemer, W., Hodda, M., Holovachov, O., Leduc, D., ... & Vanreusel, A. (2019). Nemys: World Database of Nematodes.
28. Barboza, G., Fernandez, J. A., Barrientos, J., & Bottazi, G. (1997). Costa Rica: Petroleum geology of the Caribbean margin. The Leading Edge, 16(12), 1787-1798.
29. Coates, A. G., Collins, L. S., Aubry, M. P., & Berggren, W. A. (2004). The geology of the Darien, Panama, and the late Miocene-Pliocene collision of the Panama arc with northwestern South America. GSA Bulletin, 116(11-12), 1327-1344.
30. Mende, A. (2001). Sedimente und Architektur des Forearc-und Backarc-Becken von Südost-Costa Rica und Nordwest-Panamá. Inst. f. Geologie u. Paläontologie.
31. Brandes, C., Astorga, A., Littke, R., & Winsemann, J. (2008). Basin modelling of the Limón Back-arc Basin (Costa Rica): burial history and temperature evolution of an island arc-related basin-system. Basin Research, 20(1), 119-142.
32. Coates, A. G., Jackson, J. B., Collins, L. S., Cronin, T. M., Dowsett, H. J., Bybell, L. M., ... & Obando, J. A. (1992). Closure of the Isthmus of Panama: the near-shore marine record of Costa Rica and western Panama. Geological Society of America Bulletin, 104(7), 814-828.
33. Escalante, G. (1991). The geology of southern Central America and western Colombia.
34. Brikiatis, L. (2021). Evidence for a Recent Formation of the Isthmus of Panama 0.6 Mya.
35. Brandes, C., Astorga, A., & Winsemann, J. (2009). The Moín High, East Costa Rica: Seamount, laccolith or contractional structure?. Journal of South American Earth Sciences, 28(1), 1-13.
36. Savin, S. M., & Douglas, R. G. (1985). Sea level, climate, and the Central American land bridge. The great American biotic interchange, 303-324.
37. Kolarsky, R. A., Mann, P., & Montero, W. (1995). Island arc response to shallow subduction of the Cocos Ridge, Costa Rica. Special Papers-Geological Society of America, 235-235.
38. Collins, L. S., Coates, A. G., Jackson, J. B., Obando, J. A., & Mann, P. (1995). Timing and rates of emergence of the Limon and Bocas del Toro basins: Caribbean effects of Cocos Ridge subduction?. SPECIAL PAPERS-GEOLOGICAL SOCIETY OF AMERICA, 263-263.
39. Morell, K. D., Kirby, E., Fisher, D. M., & Van Soest, M. (2012). Geomorphic and exhumational response of the Central American Volcanic Arc to Cocos Ridge subduction. Journal of Geophysical Research: Solid Earth, 117(B4).
40. Morell, K. D. (2015). Late M iocene to recent plate tectonic history of the southern C entral A merica convergent margin. Geochemistry, Geophysics, Geosystems, 16(10), 3362-3382.
41. Abratis, M., & Wörner, G. (2001). Ridge collision, slab-window formation, and the flux of Pacific asthenosphere into the Caribbean realm. Geology, 29(2), 127-130.
42. Gardner, T. W., Verdonck, D., Pinter, N. M., Slingerland, R., Furlong, K. P., Bullard, T. F., & Wells, S. G. (1992). Quaternary uplift astride the aseismic Cocos ridge, Pacific coast, Costa Rica. Geological Society of America Bulletin, 104(2), 219-232.
43. Morell, K. D., Fisher, D. M., Gardner, T. W., La Femina, P., Davidson, D., & Teletzke, A. (2011). Quaternary outer forearc deformation and uplift inboard of the Panama Triple Junction, Burica Peninsula. Journal of Geophysical Research: Solid Earth, 116(B5).
44. Corrigan, J., Mann, P., & Ingle Jr, J. C. (1990). Forearc response to subduction of the Cocos ridge, Panama-Costa Rica. Geological Society of America Bulletin, 102(5), 628-652.
45. McNeill, D. F., Coates, A. G., Budd, A. F., & Borne, P. F. (2000). Integrated paleontologic and paleomagnetic stratigraphy of the upper Neogene deposits around Limon, Costa Rica: a coastal emergence record of the Central American Isthmus. Geological Society of America Bulletin, 112(7), 963-981.
46. McNeill, D. F., Klaus, J. S., O'Connell, L. G., Coates, A. G., & Morgan, W. A. (2013). Depositional sequences and stratigraphy of the Colón carbonate platform: Bocas Del Toro Archipelago, Panama. Journal of Sedimentary Research, 83(2), 183-195.
47. Coates, A. G., McNeill, D. F., Aubry, M. P., Berggren, W. A., & Collins, L. S. (2005). An introduction to the geology of the Bocas del Toro Archipelago, Panama. Caribbean Journal of Science.
48. O'Dea, A., Hoyos, N., Rodríguez, F., Degracia, B., & De Gracia, C. (2012). History of upwelling in the Tropical Eastern Pacific and the paleogeography of the Isthmus of Panama. Palaeogeography, Palaeoclimatology, Palaeoecology, 348, 59-66.
49. Lowrie, A., Stewart, J., Stewart, R. H., Van Andel, T. J., & McRaney, L. (1982). Location of the eastern boundary of the Cocos plate during the Miocene. Marine Geology, 45(3-4), 261-279.
50. Marshall, J. S. (2007). The geomorphology and physiographic provinces of Central America. Central America: geology, resources and hazards, 1, 75-121.
51. Buchs, D. M., Irving, D., Coombs, H., Miranda, R., Wang, J., Coronado, M., ... & Redwood, S. D. (2019). Volcanic contribution to emergence of Central Panama in the Early Miocene. Scientific reports, 9(1), 1-16.
52. Montes, C., & Hoyos, N. (2020). Isthmian bedrock geology: tilted, bent, and broken. In J. Gómez, & D. Mateus–Zabala (Eds.), The Geology of Colombia, Volume 3 Paleogene –Neogene (Publicaciones Geológicas Especiales 37, pp. 451–467.). Servicio Geológico Colombiano, Bogotá.
53. Woodring, W. P. (1957). Geology and paleontology of Canal

Zone and adjoining parts of Panama. United States Geological Survey Professional Paper 306.
54. Stewart, R. H., & Stewart, J. L. (1980). Geologic map of the Panama Canal and vicinity, Republic of Panama (No. 1232).
55. Kirby, M. X., Jones, D. S., & MacFadden, B. J. (2008). Lower Miocene stratigraphy along the Panama Canal and its bearing on the Central American Peninsula. PLoS One, 3(7), e2791.
56. Jones, S. M. (1950). Geology of Gatun Lake and vicinity, Panama. Geological Society of America Bulletin, 61(9), 893-922.
57. Pratt, T. L., Holmes, M., Schweig, E. S., Gomberg, J., & Cowan, H. A. (2003). High resolution seismic imaging of faults beneath Limón Bay, northern Panama Canal, Republic of Panama. Tectonophysics, 368(1-4), 211-227.
58. URS Holdings (2007). Environmental Impact Study: Panama Canal Expansion Project - Third Set of Locks. URS Holdings, Inc.: Panama City, Panama.
59. Redwood, S. D. (2020). Late Pleistocene to Holocene sea level rise in the Gulf of Panama, Panama, and its influence on early human migration through the Isthmus. Caribb J Earth Sci, 51, 15-31.
60. Rockwell, T. K., Bennett, R. A., Gath, E., & Franceschi, P. (2010a). Unhinging an indenter: A new tectonic model for the internal deformation of Panama. Tectonics, 29, TC4027.
61. Rockwell, T., Gath, E., González, T., Madden, C., Verdugo, D., Lippincott, C., ... & Franceschi, P. (2010). Neotectonics and Paleoseismology of the Limón and Pedro Miguel Faults in Panamá: Earthquake Hazard to the Panamá CanalNeotectonics and Paleoseismology of the Limón and Pedro Miguel Faults in Panamá. Bulletin of the Seismological Society of America, 100(6), 3097-3129.
62. Farris, D. W., Cardona, A., Montes, C., Foster, D., & Jaramillo, C. (2017). Magmatic evolution of Panama Canal volcanic rocks: A record of arc processes and tectonic change. PloS one, 12(5), e0176010.
63. Woodring, W. P. (1966). The Panama land bridge as a sea barrier. Proceedings of the American Philosophical Society, 110(6), 425-433.
64. Barat, F., de Lépinay, B. M., Sosson, M., Müller, C., Baumgartner, P. O., & Baumgartner-Mora, C. (2014). Transition from the Farallon Plate subduction to the collision between South and Central America: Geological evolution of the Panama Isthmus. Tectonophysics, 622, 145-167.
65. Duque-Caro, H. (1990). Neogene stratigraphy, paleoceanography and paleobiogeography in northwest South America and the evolution of the Panama Seaway. Palaeogeography, Palaeoclimatology, Palaeoecology, 77(3-4), 203-234.
66. Duque-Caro, H. (1990). The Choco Block in the northwestern corner of South America: Structural, tectonostratigraphic, and paleogeographic implications. Journal of South American Earth Sciences, 3(1), 71-84.
67. Cediel, F., Restrepo, I., Marín-Cerón, M. I., Duque-Caro, H., Cuartas, C., Mora, C., ... & Muñoz, G. (2010). Geology and Hydrocarbon Potential, Atrato and San Juan Basins, Chocó (Panamá) Arc, Colombia, Tumaco Basin (Pacific Realm). Colombia, Agencia Nacional de Hidrocarburos (ANH)-EAFIT, Medellín.
68. Rodríguez, M. S. (2007). Geological framework of the Pacific Coast sedimentary Basins, Western Colombia. Geología Colombiana, 32, 47–62.
69. Mojica, J., Briceño, L. A., & Vargas, A. (2011). Los Ríos Atrato y San Juan de la región pacífica de Colombia: Han corrido siempre en las direcciones actuales? Conference paper, Congreso Colombiano de Geología, Medellin, Colombia.
70. Cediel, F., Restrepo, I. (2011) Geology and Hydrocarbon Potential, Atrato, San Juan and Urabá Basins. In F. Cediel (Ed.), Petroleum Geology of Colombia series, Vol. 3. University EAFIT, Medellin, Colombia.
71. ANH-Servigecol Ltda (2008). Geología de superficie y geoquímica de rocas y crudos de la subcuenca del San Juan (Chocó). Technical Report, Agencia National de Hidrocarburos. https://www.anh.gov.co/
72. ANH-G2 Seismic (2010). Informe final programa sísmico Choco - Buenaventura 2d 2006, subcuenca del Río San Juan, Colombia. Technical Report, Agencia National de Hidrocarburos. https://www.anh.gov.co/
73. Loeblich, A. R. Jr., & Tappan, H. (1988). Foraminiferal genera and their classification. Boston, MA: Springer.
74. Paleobiology Database. Search for Orbulina universa. Access on August 21, 2022.
75. Paleobiology Database. Search for Ammonia. Access on August 21, 2022.
76. Redwood, S. D. (2019). The geology of the Panama-Chocó arc. Geology and Tectonics of Northwestern South America: The Pacific-Caribbean-Andean Junction, 901-932.
77. León, S., Cardona, A., Parra, M., Sobel, E. R., Jaramillo, J. S., Glodny, J., ... & Pardo-Trujillo, A. (2018). Transition from collisional to subduction-related regimes: An example from Neogene Panama-Nazca-South America interactions. Tectonics, 37(1), 119-139.
78. Egbue, O., & Kellogg, J. (2010). Pleistocene to present North Andean "escape". Tectonophysics, 489(1-4), 248-257.
79. Garzón Varón, F. (2012). Modelamiento estructural de la zona límite entre la microplaca de Panamá y el bloque norandino a partir de la interpretación de imágenes de radar, cartografía geológica, anomalías de campos potenciales y líneas sísmicas. Departamento de Geociencias.
80. Flinch, J. F. (2003). Structural evolution of the Sinu-Lower Magdalena area (northern Colombia).
81. Martínez, J. O., & Ramos, E. L. (2011). High-resolution seismic stratigraphy of the late Neogene of the central sector of the Colombian Pacific continental shelf: A seismic expression of an active continental margin. Journal of South American Earth Sciences, 31(1), 28-44.
82. Brikiatis, L. (2016). Late mesozoic North Atlantic land bridges. Earth-Science Reviews, 159, 47-57.
83. Marek, C. (2015). The emergence of the Isthmus of Panama: a biological perspective.
84. Alfaro, J. W. L., Boubli, J. P., Paim, F. P., Ribas, C. C., da

Silva, M. N. F., Messias, M. R., ... & Farias, I. P. (2015). Biogeography of squirrel monkeys (genus Saimiri): South-central Amazon origin and rapid pan-Amazonian diversification of a lowland primate. Molecular Phylogenetics and Evolution, 82, 436-454.
85. Morris-Pocock, J. A., Steeves, T. E., Estela, F. A., Anderson, D. J., & Friesen, V. L. (2010). Comparative phylogeography of brown (Sula leucogaster) and red-footed boobies (S. sula): the influence of physical barriers and habitat preference on gene flow in pelagic seabirds. Molecular Phylogenetics and Evolution, 54(3), 883-896.
86. Steeves, T. E., Anderson, D. J., & Friesen, V. L. (2005). The Isthmus of Panama: a major physical barrier to gene flow in a highly mobile pantropical seabird. Journal of Evolutionary Biology, 18(4), 1000-1008.
87. Van der Stocken, T., Wee, A. K., De Ryck, D. J., Vanschoenwinkel, B., Friess, D. A., Dahdouh-Guebas, F., ... & Webb, E. L. (2019). A general framework for propagule dispersal in mangroves. Biological Reviews, 94(4), 1547-1575.
88. Knowlton, N., & Weigt, L. A. (1998). New dates and new rates for divergence across the Isthmus of Panama. Proceedings of the Royal Society of London. Series B: Biological Sciences, 265(1412), 2257-2263.
89. Ochoa-Zavala, M., Jaramillo-Correa, J. P., Piñero, D., Nettel-Hernanz, A., & Núñez-Farfán, J. (2019). Contrasting colonization patterns of black mangrove (Avicennia germinans (L.) L.) gene pools along the Mexican coasts. Journal of Biogeography, 46(5), 884-898.
90. Galván-Quesada, S., Doadrio, I., Alda, F., Perdices, A., Reina, R. G., García Varela, M., ... & Domínguez-Domínguez, O. (2016). Molecular phylogeny and biogeography of the amphidromous fish genus Dormitator Gill 1861 (Teleostei: Eleotridae). PLoS One, 11(4), e0153538.
91. Martin, A. P., & Bermingham, E. (2000). Regional endemism and cryptic species revealed by molecular and morphological analysis of a widespread species of Neotropical catfish. Proceedings of the Royal Society of London. Series B: Biological Sciences, 267(1448), 1135-1141.
92. Loaiza, J. R., Scott, M. E., Bermingham, E., Sanjur, O. I., Wilkerson, R., Rovira, J., ... & Conn, J. E. (2010). Late Pleistocene environmental changes lead to unstable demography and population divergence of Anopheles albimanus in the northern Neotropics. Molecular Phylogenetics and Evolution, 57(3), 1341-1346.
93. Smith, K. E., VanEkeris, L. A., Okech, B. A., Harvey, W. R., & Linser, P. J. (2008). Larval anopheline mosquito recta exhibit a dramatic change in localization patterns of ion transport proteins in response to shifting salinity: a comparison between anopheline and culicine larvae. Journal of Experimental Biology, 211(19), 3067-3076.
94. Brikiatis, L. (2020). An early Pangaean vicariance model for synapsid evolution. Scientific Reports, 10, 13091.
95. Woodburne, M. O. (2010). The Great American Biotic Interchange: dispersals, tectonics, climate, sea level and holding pens. Journal of mammalian evolution, 17, 245-264.
96. Beu, A. G. (2010). Neogene tonnoidean gastropods of tropical and South America: contributions to the Dominican Republic and Panama Paleontology Projects and uplift of the Central American Isthmus.
97. MacFadden, B. J. (2013). Dispersal of Pleistocene Equus (Family Equidae) into South America and calibration of GABI 3 based on evidence from Tarija, Bolivia. PloS one, 8(3), e59277.
98. Jackson, J. B., Budd, A. F., & Coates, A. G. (Eds.). (1996). Evolution and environment in tropical America. University of Chicago Press.
99. Allmon, W. D. (2001). Nutrients, temperature, disturbance, and evolution: a model for the late Cenozoic marine record of the western Atlantic. Palaeogeography, Palaeoclimatology, Palaeoecology, 166(1-2), 9-26.
100. Budd, A. F. (2000). Diversity and extinction in the Cenozoic history of Caribbean reefs. Coral Reefs, 19, 25-35.
101. Landau, B., Vermeij, G., & da Silva, C. M. (2008). Southern Caribbean Neogene palaeobiogeography revisited. New data from the Pliocene of Cubagua, Venezuela. Palaeogeography, Palaeoclimatology, Palaeoecology, 257(4), 445-461.
102. Landau, B., Marques Da Silva, C., & Vermeij, G. (2009). Pacific elements in the Caribbean Neogene gastropod fauna: the source-sink model, larval development, disappearance, and faunal units. Bulletin de la Société géologique de France, 180(4), 343-352.
103. León-Rodríguez, L., & Collins, L. (2005). Large paleobathymetric changes indicate rapid pleistocene tectonic uplift of the pacific margin of western Panama-eastern Costa Rica. In Geological Society of America Annual Meeting, Abstracts with Programs (Vol. 37, p. 160).
104. Beu, A. G. (2001). Gradual Miocene to Pleistocene uplift of the Central American Isthmus: evidence from tropical American tonnoidean gastropods. Journal of Paleontology, 75(3), 706-720.
105. Sentman, L. T., Dunne, J. P., Stouffer, R. J., Krasting, J. P., Toggweiler, J. R., & Broccoli, A. J. (2018). The mechanistic role of the central American seaway in a GFDL earth system model. Part 1: Impacts on global ocean mean state and circulation. Paleoceanography and Paleoclimatology, 33(7), 840-859.
106. Bhaumik, A. K., Gupta, A. K., & Ray, S. (2014). Surface and deep-water variability at the Blake Ridge, NW Atlantic during the Plio-Pleistocene is linked to the closing of the Central American Seaway. Palaeogeography, Palaeoclimatology, Palaeoecology, 399, 345-351.
107. Kaiser, E. A., Caldwell, A., & Billups, K. (2019). North Atlantic upper-ocean hydrography during the mid-Pleistocene transition evidenced by Globorotalia truncatulinoides coiling ratios. Paleoceanography and Paleoclimatology, 34(4), 658-671.
108. Poore, H. R., Samworth, R., White, N. J., Jones, S. M., & McCave, I. N. (2006). Neogene overflow of northern compo-

nent water at the Greenland-Scotland Ridge. Geochemistry, Geophysics, Geosystems, 7(6).
109. Hernández-Molina, F. J., Stow, D. A., Alvarez-Zarikian, C. A., Acton, G., Bahr, A., Balestra, B., ... & Xuan, C. (2014). Onset of Mediterranean outflow into the North Atlantic. Science, 344(6189), 1244-1250.
110. Lofi, J., Voelker, A. H. L., Ducassou, E., Hernández-Molina, F. J., Sierro, F. J., Bahr, A., ... & Williams, T. (2016). Quaternary chronostratigraphic framework and sedimentary processes for the Gulf of Cadiz and Portuguese Contourite Depositional Systems derived from Natural Gamma Ray records. Marine Geology, 377, 40-57.
111. Pena, L. D., & Goldstein, S. L. (2014). Thermohaline circulation crisis and impacts during the mid-Pleistocene transition. Science, 345(6194), 318-322.
112. Sepulchre, P., Arsouze, T., Donnadieu, Y., Dutay, J. C., Jaramillo, C., Le Bras, J., ... & Waite, A. J. (2014). Consequences of shoaling of the Central American Seaway determined from modeling Nd isotopes. Paleoceanography, 29(3), 176-189.
113. Berggren, W. A. (1982). Role of ocean gateways in climatic change. Climate in Earth History, 20, 118-125.
114. Keigwin, L. (1982). Isotopic paleoceanography of the Caribbean and East Pacific: role of Panama uplift in late Neogene time. Science, 217(4557), 350-353.
115. Murdock, T. Q., Weaver, A. J., & Fanning, A. F. (1997). Paleoclimatic response of the closing of the Isthmus of Panama in a coupled ocean-atmosphere model. Geophysical Research Letters, 24(3), 253-256.
116. Lunt, D. J., Valdes, P. J., Haywood, A., & Rutt, I. C. (2008). Closure of the Panama Seaway during the Pliocene: implications for climate and Northern Hemisphere glaciation. Climate Dynamics, 30, 1-18.
117. Schneider, B., & Schmittner, A. (2006). Simulating the impact of the Panamanian seaway closure on ocean circulation, marine productivity and nutrient cycling. Earth and Planetary Science Letters, 246(3-4), 367-380.
118. Klocker, A., Prange, M., & Schulz, M. (2005). Testing the influence of the Central American Seaway on orbitally forced Northern Hemisphere glaciation. Geophysical Research Letters, 32(3).
119. de Vernal, A., & Hillaire-Marcel, C. (2008). Natural variability of Greenland climate, vegetation, and ice volume during the past million years. Science, 320(5883), 1622-1625.
120. Marino, M., Maiorano, P., & Flower, B. P. (2011). Calcareous nannofossil changes during the Mid-Pleistocene Revolution: Paleoecologic and paleoceanographic evidence from North Atlantic Site 980/981. Palaeogeography, Palaeoclimatology, Palaeoecology, 306(1-2), 58-69.
121. Keigwin, L. D. (1978). Pliocene closing of the Isthmus of Panama, based on biostratigraphic evidence from nearby Pacific Ocean and Caribbean Sea cores. Geology, 6, 630–634.
122. Miura, O., Torchin, M. E., Bermingham, E., Jacobs, D. K., & Hechinger, R. F. (2011). Flying shells: historical dispersal of marine snails across Central America. Proceedings of the Royal Society B, 279, 1061–1067.
123. Miller, K. G., Browning, J. V., Schmelz, W. J., Kopp, R. E., Mountain, G. S., & Wright, J. D. (2020). Cenozoic sea-level and cryospheric evolution from deep-sea geochemical and continental records. Science Advances, 6, eaaz1346
124. Maslin, M. A., & Brierley, C. M. (2015). The role of orbital forcing in the early middle Pleistocene transition. Quaternary International, 389, 47–55.
125. Ford, H.L., & Chalk, T.B. (2020). The Mid-Pleistocene enigma. Oceanography 33, 101–103.
126. Brikiatis, L. (2021). Astronomical control of the hydroclimate during the past 1.2 million years. Geology, Earth & Marine Sciences, 3, 1–11.
127. Zeng, L., Yi., S., Zhang, W., Feng, H., Lv, A., Zhao, W. () Lu, H. (2020). Provenance of loess deposits and stepwise expansion of the desert environment in NE China since ~1.2 Ma: evidence from Nd-Sr isotopic composition and grain-size record. Global and Planetary Change, 185, 103087.
128. Kender, S., Ravelo, A.C., Worne, S., Swann, G. E. A., Leng, M. J., Asahi, H. () Hall, I. R. (2018). Closure of the Bering Strait caused Mid-Pleistocene Transition cooling. Nature Communications, 9, 5386.
129. Leon-Rodriguez, L. (2007). Benthic foraminiferal record of the Pleistocene uplift of the sedimentary deposits of the Burica Peninsula (Costa Rica-Panama) as a result of Cocos Ridge subduction beneath the Central American Arc. M.S. thesis, Florida International University, Miami, Florida.
130. De Schepper, S., Schreck, M., Beck, K., Matthiessen, J., Fahl, K., & Mangerud, G. (2015). Early Pliocene onset of modern Nordic Seas circulation related to ocean gateway changes. Nature Communications, 6, 8659.
131. Horikawa, K., Martin, E., Basak, C., Onodera, J., Seki, O., Sakamoto, T. () Kawamura, K. (2015). Pliocene cooling enhanced by flow of low-salinity Bering Sea water to the Arctic Ocean. Nature Communications, 6, 7587.
132. Burkholder, K. C., & Lozier, M. S. (2014), Tracing the pathways of the upper limb of the North Atlantic Meridional Overturning Circulation. Geophysical Research Letters, 41, 4254–4260.
133. Catunda, M. C. A., Bahr, A., Kaboth-Bahr, S., Zhang, X., Foukal, N. P., & Friedrich, O. (2021). Subsurface heat channel drove sea surface warming in the high-latitude North Atlantic during the Mid-Pleistocene Transition. Geophysical Research Letters, 48, e2020GL091899.
134. Kaboth-Bahr, S., Bahr, A., Stepanek, C., Catunda, M. C. A., Karas, C., Ziegler, M. () Grunert, P. (2021). Mediterranean heat injection to the North Atlantic delayed the intensification of Northern Hemisphere glaciations. Communications Earth & Environment, 2, 158.
135. Hu, A., Meehl, G. A., Otto-Bliestner, B., Waelbroeck, C., Han, W., Loutre, M.-F., () Rosenbloom, N. (2010). Influence of Bering Strait flow and North Atlantic circulation on glacial sea-level changes. Nature Geoscience, 3, 118–121.
136. Hu, A., Meehl, G. A., Han, W., Otto-Bliestner, B., Abe-Ouchi,

A., & Rosenbloom, N. (2015). Effects of the Bering Strait closure on AMOC and global climate under different background climates. Progress in Oceanography, 132, 174–196.
137. Hu, A., Meehl, G. A., Rosenbloom, N., Molina, M. J., & Strand, W. G. (2021). The influence of variability in meridional overturning on global ocean circulation. Journal of Climate, 18, 7697–7716.
138. Brierley, C. & Fedorov, A. V. (2016). Comparing the impacts of Miocene–Pliocene changes in inter-ocean gateways on climate: Central American Seaway, Bering Strait, and Indonesia. Earth and Planetary Sciences Letters, 444, 116–130.
139. Hu, A., Meehl, G. A., Han, W., Abe-Ouchi, A., Morrill, C., Okazaki, Y., & Chikamoto, M. O. (2012). The Pacific-Atlantic seesaw and the Bering Strait. Geophysical Research Letters, 39, L03702.
140. Montes, C., Cardona, A., McFadden, R., Morón, S. E., Silva, C. A., Restrepo-Moreno, S. () Flores, J. A. (2012). Evidence for middle Eocene and younger land emergence in central Panama: implications for isthmus closure. GSA Bulletin, 124, 780–799.
141. Batchelor, C. L., Margold, M., Krapp, M., Murton, D. K., Dalton, A. S., Gibbard, P. L. () Manica, A. (2019). The configuration of Northern Hemisphere ice sheets through the Quaternary. Nat Commun, 10, 3713.
142. Schlitzer, R. (2018). Ocean Data View.
143. Laskar, J., Robutel, P., Joutel, F., Gastineau, M., Correia, A. C. M., & Levrard, B. (2004). A long-term numerical solution for the insolation quantities of the Earth. Astronomy and Astrophysics, 428, 261e285.
144. Rohling, E. J., Foster, G. L., Grant, K. M., Marino, G., Roberts, A. P., Tamisiea, M. E., & Williams, F. (2014). Sea-level and deep-sea-temperature variability over the past 5.3 million years. Nature, 508, 477–482.
145. Lisiecki, L. E., & Raymo, M. E. (2005). A Pliocene-Pleistocene stack of 57 globally distributed benthic d18O records. Paleoceanography, 20, PA1003.
146. Farmer, J.R., Hönisch, B., Haynes, L. L., Kroon, D., Jung, S., Ford, H. L. () Kim. J. (2019). Deep Atlantic Ocean carbon storage and the rise of 100,000-year glacial cycles. Nature Geoscience, 12, 355–360.
147. Hoogakker, B. A. A., Rohling, E. J., Palmer, M. R., Tyrrell, T., & Rothwell, R. G. (2006). Underlying causes for long-term global ocean delta C-13 fluctuations over the last 1.20 Myr. Earth and Planetary Science Letters, 248, 15–29.
148. Sosdian, S. M., Rosenthal, Y., & Toggweiler, J. R. (2018). Deep Atlantic carbonate ion and CaCO3 compensation during the Ice Ages. Paeloceanography and Paleoclimatology, 33, 546–562.
149. Schmieder, F., von Dobeneck, T., & Bliel, U. (2000). The Mid-Pleistocene climate transition as documented in the deep South Atlantic Ocean: initiation, interim state and terminal event. Earth and Planetary Science Letters, 179, 539–549.
150. Hodell, D. A., Venz, K. A., Charles, C. D., & Ninnemann, U. S. (2003). Pleistocene vertical carbon isotope and carbonate gradients in the South Atlantic sector of the Southern Ocean. Geochemistry, Geophysics, Geosystems, 4, 1–19.
151. Flower, B. P., Oppo, D. W., McManus, J. F., Venz, K. A., Hodell, D. A., & Cullen, J. L. (2000). North Atlantic Intermediate to Deep Water circulation and chemical stratification during the past 1 Myr. Paleoceanography, 15, 388–403.
152. Kleiven, H. F., Jansen, E., Curry, W. B., Hodell, D. A., & Venz, K. (2003). Atlantic Ocean thermohaline circulation changes on orbital to suborbital timescales during the mid-Pleistocene. Paleoceanography, 18, 1008.
153. Egana, J. P., Bloom, D. D., Kuo, C.-H., Hammer, M. P., Tongnunui, P., Iglésias, S. P. () Simons, A. M. (2018). Phylogenetic analysis of trophic niche evolution reveals a latitudinal herbivory gradient in Clupeoidei (herrings, anchovies, and allies). Molecular Phylogenetics and Evolution, 124, 151–161.
154. Silva, G., Cunha, R.L., Ramos, A., & Castilho, R. (2017). Wandering behaviour prevents inter and intra oceanic speciation in a coastal pelagic fish. Scientific Reports, 7, 2893.
155. Katz, A. D. (2018). The influence of vicariance and dispersal on the diversification and evolution of springtails (collembola). PhD Dissertation, University of Illinois at Urbana-Champaign.
156. LaBella, A. L., Van Dover, C. L., Jollivet, D., & Cunningham, C. W. (2017). Gene flow between Atlantic and Pacific Ocean basins in three lineages of deep-sea clams (Bivalvia: Vesicomyidae: Pliocardiinae) and subsequent limited gene flow within the Atlantic. Deep-Sea Research II, 137, 307–317.
157. Archer, F. I., Morin, P. A., Hancock-Hanser, B. L., Robertson, K.M., Leslie, M. S., Bérubé, M. () Taylor, B. L. (2013). Mitogenomic phylogenetics of fin whales (Balaenoptera physalus spp.): genetic evidence for revision of subspecies. PLoS ONE, 8, e63396.
158. Hernández-Almeida, I., Sierro, F. J., Cacho, I., & Flores, J. A. (2012). Impact of suborbital climate changes in the North Atlantic on ice sheet dynamics at the Mid-Pleistocene Transition. Paleoceanography, 27(3).
159. McClymont, E. L., Rosell-Melé, A., Haug, G. H., & Lloyd, J. M. (2008). Expansion of subarctic water masses in the North Atlantic and Pacific oceans and implications for mid-Pleistocene ice sheet growth. Paleoceanography, 23(4).
160. Naafs, B. D. A., Hefter, J., Ferretti, P., Stein, R., & Haug, G. H. (2011). Sea surface temperatures did not control the first occurrence of Hudson Strait Heinrich Events during MIS 16. Paleoceanography, 26(4).
161. Rodrigues, T., Alonso-García, M., Hodell, D. A., Rufino, M., Naughton, F., Grimalt, J. O., ... & Abrantes, F. (2017). A 1-Ma record of sea surface temperature and extreme cooling events in the North Atlantic: A perspective from the Iberian Margin. Quaternary Science Reviews, 172, 118-130.
162. Ruddiman, W. F., Raymo, M., Martinson, D. G., Clement, B. M., & Backman, J. (1989). Pleistocene evolution: Northern hemisphere ice sheets and North Atlantic Ocean. Paleoceanography, 4(4), 353-412.
163. Lawrence, K. T., Herbert, T. D., Brown, C. M., Raymo, M.

E., & Haywood, A. M. (2009). High-amplitude variations in North Atlantic sea surface temperature during the early Pliocene warm period. Paleoceanography, 24(2).
164. Johnson, K. P., & Weckstein, J. D. (2011). The Central American land bridge as an engine of diversification in New World doves. Journal of Biogeography, 38(6), 1069-1076.
165. Smith, B. T., & Klicka, J. (2010). The profound influence of the Late Pliocene Panamanian uplift on the exchange, diversification, and distribution of New World birds. Ecography, 33(2), 333-342.
166. Ireland, H. E., Kite, G. C., Veitch, N. C., Chase, M. W., Schrire, B., Lavin, M., ... & Pennington, R. T. (2010). Biogeographical, ecological and morphological structure in a phylogenetic analysis of Ateleia (Swartzieae, Fabaceae) derived from combined molecular, morphological and chemical data. Botanical Journal of the Linnean Society, 162(1), 39-53.
167. Wagner, N., Silvestro, D., Brie, D., Ibisch, P. L., Zizka, G., Weising, K., & Schulte, K. (2013). Spatio-temporal evolution of Fosterella (Bromeliaceae) in the Central Andean biodiversity hotspot. Journal of Biogeography, 40(5), 869-880.
168. Schaefer, H., Hechenleitner, P., Santos-Guerra, A., de Sequeira, M. M., Pennington, R. T., Kenicer, G., & Carine, M. A. (2012). Systematics, biogeography, and character evolution of the legume tribe Fabeae with special focus on the middle-Atlantic island lineages. BMC Evolutionary Biology, 12, 1-19.
169. Smith, B. T., McCormack, J. E., Cuervo, A. M., Hickerson, M. J., Aleixo, A., Cadena, C. D., ... & Brumfield, R. T. (2014). The drivers of tropical speciation. Nature, 515(7527), 406-409.
170. Ward, P. S., & Branstetter, M. G. (2017). The acacia ants revisited: convergent evolution and biogeographic context in an iconic ant/plant mutualism. Proceedings of the Royal Society B: Biological Sciences, 284(1850), 20162569.
171. Wang, B., Ding, Z., Liu, W., Pan, J., Li, C., Ge, S., & Zhang, D. (2009). Polyploid evolution in Oryza officinalis complex of the genus Oryza. BMC Evolutionary Biology, 9, 1-13.
172. Vargas, O. M., Goldston, B., Grossenbacher, D. L., & Kay, K. M. (2020). Patterns of speciation are similar across mountainous and lowland regions for a Neotropical plant radiation (Costaceae: Costus). Evolution, 74(12), 2644-2661.
173. Aguilar, C., Miller, M. J., Loaiza, J. R., González, R., Krahe, R., & De León, L. F. (2019). Tempo and mode of allopatric divergence in the weakly electric fish Sternopygus dariensis in the Isthmus of Panama. Scientific reports, 9(1), 1-11.
174. Jones, C. P., & Johnson, J. B. (2009). Phylogeography of the livebearer Xenophallus umbratilis (Teleostei: Poeciliidae): glacial cycles and sea level change predict diversification of a freshwater tropical fish. Molecular Ecology, 18(8), 1640-1653.
175. Bagley, J. C., Alda, F., Breitman, M. F., Bermingham, E., van den Berghe, E. P., & Johnson, J. B. (2015). Assessing species boundaries using multilocus species delimitation in a morphologically conserved group of neotropical freshwater fishes, the Poecilia sphenops species complex (Poeciliidae). PLoS One, 10(4), e0121139.
176. Bagley, J. C., Hickerson, M. J., & Johnson, J. B. (2018). Testing hypotheses of diversification in Panamanian frogs and freshwater fishes using hierarchical approximate Bayesian computation with model averaging. Diversity, 10(4), 120.
177. Santos, J. C., Coloma, L. A., Summers, K., Caldwell, J. P., Ree, R., & Cannatella, D. C. (2009). Amazonian amphibian diversity is primarily derived from late Miocene Andean lineages. PLoS biology, 7(3), e1000056.
178. Mendoza, A. M., Bolívar-García, W., Vázquez-Domínguez, E., Ibáñez, R., & Olea, G. P. (2019). The role of Central American barriers in shaping the evolutionary history of the northernmost glassfrog, Hyalinobatrachium fleischmanni (Anura: Centrolenidae). PeerJ, 7, e6115.
179. Crawford, A. J. (2003). Huge populations and old species of Costa Rican and Panamanian dirt frogs inferred from mitochondrial and nuclear gene sequences. Molecular Ecology, 12(10), 2525-2540.
180. Fritz, U., Stuckas, H., Vargas-Ramírez, M., Hundsdörfer, A. K., Maran, J., & Päckert, M. (2012). Molecular phylogeny of Central and South American slider turtles: implications for biogeography and systematics (Testudines: Emydidae: Trachemys). Journal of Zoological Systematics and Evolutionary Research, 50(2), 125-136.
181. Parham, J. F., Papenfuss, T. J., Van Dijk, P. P., Wilson, B. S., Marte, C., Schettino, L. R., & Simison, W. B. (2013). Genetic introgression and hybridization in Antillean freshwater turtles (Trachemys) revealed by coalescent analyses of mitochondrial and cloned nuclear markers. Molecular Phylogenetics and Evolution, 67(1), 176-187.
182. Castoe, T. A., Daza, J. M., Smith, E. N., Sasa, M. M., Kuch, U., Campbell, J. A., ... & Parkinson, C. L. (2009). Comparative phylogeography of pitvipers suggests a consensus of ancient Middle American highland biogeography. Journal of Biogeography, 36(1), 88-103.
183. MAUCK III, W. M., & Burns, K. J. (2009). Phylogeny, biogeography, and recurrent evolution of divergent bill types in the nectar-stealing flowerpiercers (Thraupini: Diglossa and Diglossopis). Biological Journal of the Linnean Society, 98(1), 14-28.
184. Rocha-Méndez, A., Sánchez-González, L. A., González, C., & Navarro-Sigüenza, A. G. (2019). The geography of evolutionary divergence in the highly endemic avifauna from the Sierra Madre del Sur, Mexico. BMC Evolutionary Biology, 19, 1-21.
185. Morales-Jimenez, A. L., Cortés-Ortiz, L., & Di Fiore, A. (2015). Phylogenetic relationships of Mesoamerican spider monkeys (Ateles geoffroyi): Molecular evidence suggests the need for a revised taxonomy. Molecular phylogenetics and evolution, 82, 484-494.
186. Silvestro, D., Tejedor, M. F., Serrano-Serrano, M. L., Loiseau, O., Rossier, V., Rolland, J., ... & Salamin, N. (2019). Early

arrival and climatically-linked geographic expansion of New World monkeys from tiny African ancestors. Systematic Biology, 68(1), 78-92.
187. Perelman, P., Johnson, W. E., Roos, C., Seuánez, H. N., Horvath, J. E., Moreira, M. A., ... & Pecon-Slattery, J. (2011). A molecular phylogeny of living primates. PLoS genetics, 7(3), e1001342.
188. Nigenda-Morales, S. F., Gompper, M. E., Valenzuela-Galván, D., Lay, A. R., Kapheim, K. M., Hass, C., ... & Koepfli, K. P. (2019). Phylogeographic and diversification patterns of the white-nosed coati (Nasua narica): Evidence for south-to-north colonization of North America. Molecular phylogenetics and evolution, 131, 149-163.

Supplementary Information

Supplementary Table 1. Molecular divergence dates of of possible geminate species or populations with clear current transisthmian distribution.

	Type of Life Form	North/Central America	South America	Divergence Time (Mya)	Calibration	Reference
1	Birds/Montane birds	Leptotila verreauxi fulviventris	L. v. decipiens/ chalcauchenia/ decolor	0.865	Date of island formation	[164]
2	Birds/Montane birds	Piranga leucoptera populations	Piranga leucoptera populations	0.74	Standard "bird mutation rate"	[165]
3	Birds	Elaenia flavogaster populations	Elaenia flavogaster populations	0.66	Standard "bird mutation rate"	[165]
4	Birds	Lepidothrix coronata populations	Lepidothrix coronata populations	0.557	Standard "bird mutation rate"	[165]
5	Birds	Mionectes oleagineus populations	Mionectes oleagineus populations	0.886	Standard "bird mutation rate"	[165]
6	Birds	Myioborus miniatus populations	Myioborus miniatus populations	0.86	Standard "bird mutation rate"	[165]
7	Birds	Xiphorhynchus erythropygius populations	Xiphorhynchus erythropygius populations	0.798	Standard "bird mutation rate"	[165]
8	Birds	Psarocolius montezuma	Psarocolius bifasciatus	0.634	Standard "bird mutation rate"	[1, 165]
9	Birds	Pyrrhura eisenmanni	Pyrrhura picta/ emma	0.64	Standard "bird mutation rate"	[165]
10	Plants	Ateleia standleyana	Ateleia guaraya	0.52-0.88	Fossil-based divergence date	[166]
11	Plants	Fosterella micrantha	Fosterella villosula	0.6	Fossil-based divergence date	[167]
12	Plants	Vicia gigantea	Vicia nigricans	0.78	Fossil-based divergence dates	[168]

Supplementary Table 2. Molecular divergence dates of possible geminate species or populations with current overlapped trans-isthmian distribution

	Type of Life Form	Species/Variety	Distribution	Diverg. Time (Mya)	Calibration	Ref.
1	Birds	"Capito maculicoronatus vs C. squamatus "	Central America and South America	0.77	Standard "bird mutation rate"	[165]
2	Birds	Querula purpurata	Central America/ Chocó and S. America	0.82	Standard "bird mutation rate"	[169]
3	Plants	Vachellia hindsii vs V. globulifera/collinsii	Central America and South America	~0.9	Fossils	[170]
4	Plants	Oryza latifolia vs O. alta/ grandiglumis	Central America and South America	~0.6	Fossil-based divergence date	[171]
5	Plants	Herbs Costus plicatus vs C. nitidus	Central America	0.95	Fossils	[172]
6	Plants	Herbs Costus osae vs C. comosus var. comosus	Central America and South America	0.95	Fossils	[172]
7	Plants	Herbs Costus wilsonii vs C. laevis	Central America and South America	0.92	Fossils	[172]

Supplementary Table 3. Molecular divergence dates of possible geminate species or populations currently distributed on either sides of specific potential Panama Isthmus seaways.

	Type of Life Form	Species/Variety	Potential seaway	Diverg. Time (Mya)	Calibration	Ref.
1	Insects/ mosquito	Anopheles albimanus CEPCO-PCOLE populations	Atrato-Darien Seaway	0.827	Standard mutation rate	[92]
2	Insects/ mosquito	Anopheles albimanus NCRWP-CEPCO populations	Barú Seaway	0.85	Standard mutation rate	[92]
3	Fresh water fishes	Pimelodella chagresi populations 19 vs 16,17	Barú Seaway	~0.9	Isolation date of the Maracaibo Lake	[91]
4	Fresh water fishes	Pimelodella chagresi populations 12-15 vs 5, 1-2	Canal Seaway	~0.9	Isolation date of the Maracaibo Lake	[91]
5	Fresh water fishes	Pimelodella chagresi populations 4 vs3, Atrato	Atrato-Darien Seaway	~0.9	Isolation date of the Maracaibo Lake	[91]
6	Fresh water fishes	Pimelodella chagresi populations 1, 2 vs 8,11-5	Atrato-Darien Seaway	0.65	Isolation date of the Maracaibo Lake	[91]
7	Fresh water fishes	Sternopygus dariensis populations	Atrato-Darien Seaway	1.1	Fossils	[173]
8	Fresh water fishes	Xenophallus umbratilis populations 1-10 vs 11-12, 21-23	Nicaraguan Seaway	0.769	Rate of related genus	[174]

9	Fresh water fishes	Poecilia gillii populations	Barú Seaway	1.14	Fossils and geological	[175]
10	Amphibians/ Frogs	Agalychnis callidryas populations	Canal Seaway	0.62	Standard "frog mutation rate"	[176]
11	Amphibians/Frogs	Dendrobates auratus populations	Canal Seaway	0.578	Multi-calibration amphibian chronogram	[177]
12	Amphibians/Frogs	Hyalinobatrachium fleischmanni, Nicaragua vs Costa Rica populations	Nicaraguan Seaway	0.81	On previously published divergence times	[178]
13	Amphibians/Frogs	Hyalinobatrachium fleischmanni, Bocas del Toro vs rest of Panama populations	Barú Seaway	1.175	On previously published divergence times	[178]
14	Amphibians/Frogs	Engystomops (Physalaemus) pustulosus	Barú Seaway	~0.83	Standard "frog mutation rate"	[176]
15	Amphibians/Frogs	Eleutherodactylus stejnegerianus	Barú Seaway	0.727	Recalibration of rates estimated from toads	[179]
16	Amphibians/Frogs	Dendropsophus ebraccatus populations	Barú Seaway	~0.87 Mya	Standard "frog mutation rate"	[176]
17	Amphibians/ FW turtles	Trachemys emolli vs T. grayi	Nicaraguan Seaway	0.92-1.11	Fossils	[180-181]
18	Reptiles/ Snakes	Atropoides mexicanum	Nicaraguan Seaway	~ 1 Mya	Fossils and geological	[182]
19	Montane birds	Diglossa plumbea vs D. baritula	Nicaraguan Seaway	0.8	Standard mutation rate	[183]
20	Montane birds	Geotrygon goldmani vs G. chiriquensis	Canal Seaway	0.953	Date of island formation	[164]
21	Montane birds	Toucanets (genus Aulacorhynchus) populations	Nicaraguan Seaway	0.924	Standard "bird mutation rate"	[184]
22	Montane birds	Bush-tanagers (genus Chlorospingus) populations	Nicaraguan Seaway	0.924	Standard "bird mutation rate"	[184]
23	Montane birds	Hummingbirds (Eupherusa eximia eximia vs E. e. nelsoni)	Nicaraguan Seaway	0.924	Standard "bird mutation rate"	[184]
24	Montane birds	Myadestes melanops and M. coloratus	Canal Seaway	0.85	Standard "bird mutation rate"	[165]
25	Birds	Chlorophanes spiza	Atrato-Darien Seaway	0.62	Standard "bird mutation rate"	[169]
26	Birds	Pteroglossus frantzii vs P. sanguineus/erythropygius	Atrato-Darien Seaway	0.763	Standard "bird mutation rate"	[165]
27	Mammals/ Primates	Ateles geoffroyi azuerensis vs A. g. ornatus	Barú Seaway	0.75	A. geoffroyi - A. fusciceps at 2.20 ± 0.62 mya	[185]
28	Mammals/ Primates	Saguinus geoffroyi vs S. oedipus	Atrato-Darien Seaway	1-1.04	1. fossils; 2. fossils	[186-187]

29	Mammals/ Carnivora	White-nosed coati (Nasua narica)	Nicaraguan Seaway	0.6	On fossils-derived reference date	[188]

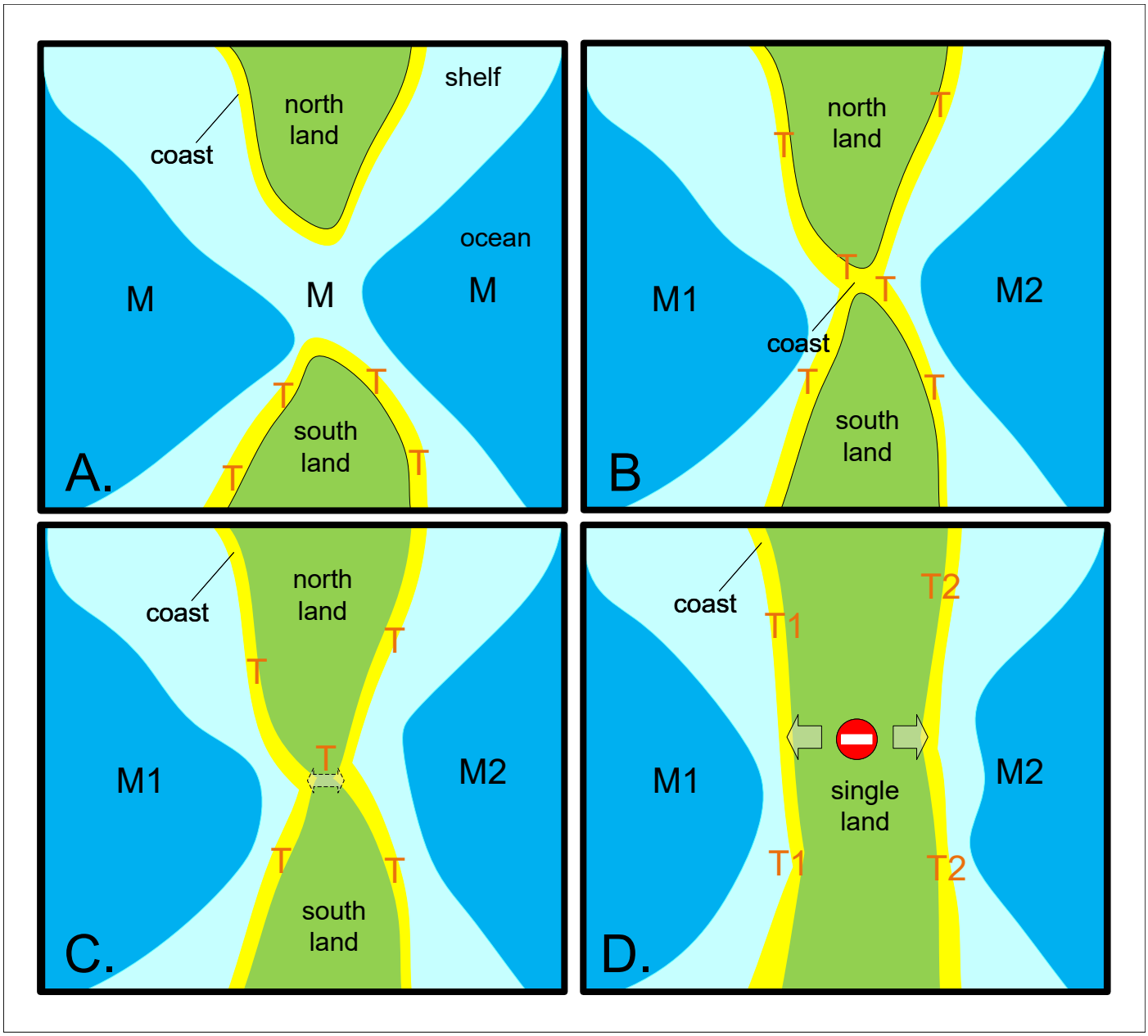

Supplementary Figure 1: Parallel vicariant effects on marine and terrestrial coastal dwellers during isthmus formation. M = single ancestral marine population; T = single ancestral terrestrial coastal population; M1, M2 = divergent marine populations leading to new species; T1, T2 = divergent terrestrial coastal populations leading to new species. Arrows denote interbreeding. A, B, C, and D are succeeding stages of palaeogeographical evolution.

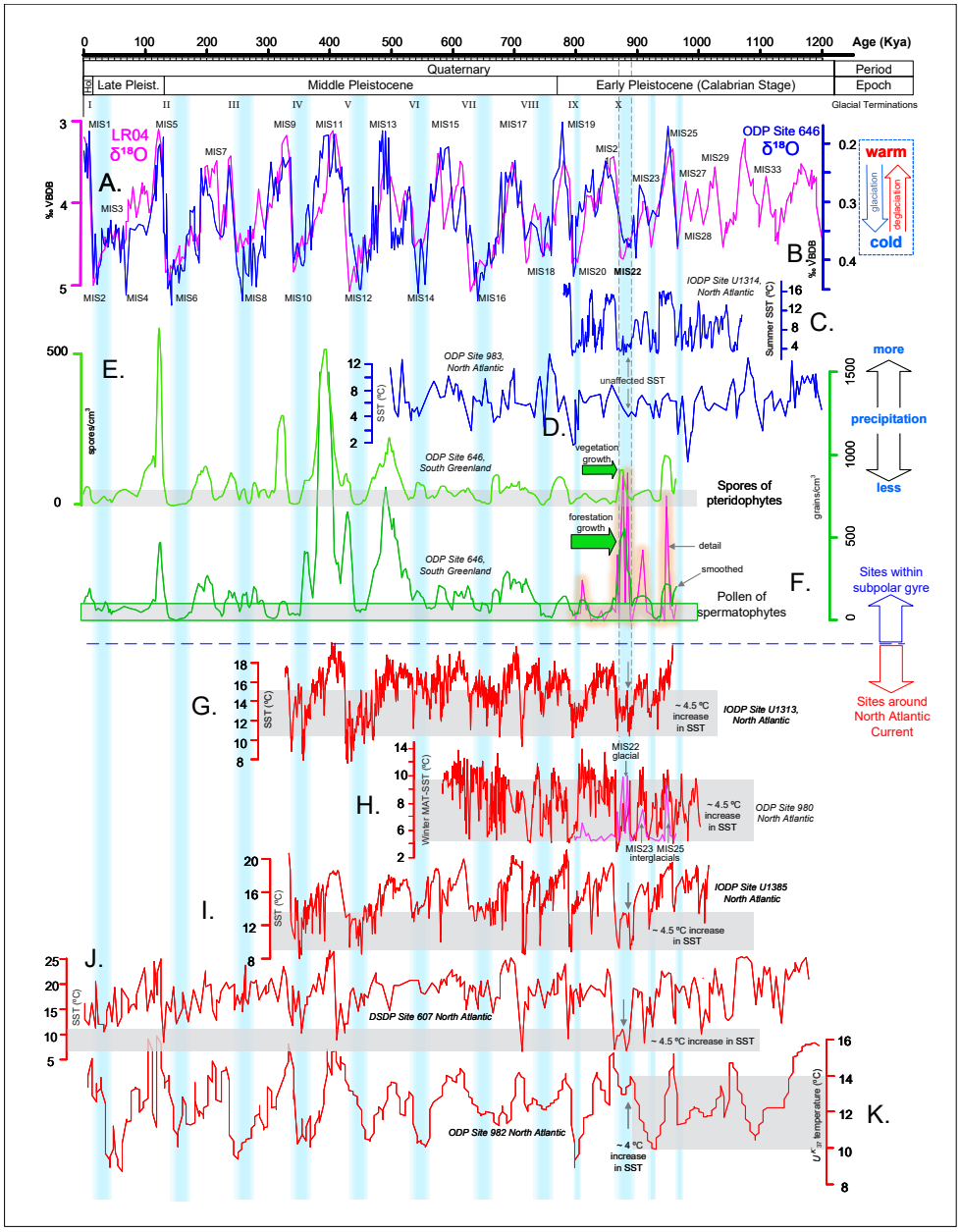

Supplementary Figure 2: Comparison of geochemical and stratigraphical data highlighting the episode of increased forestation in South Greenland during the glacial maximum of MIS22. The chronological accuracy of the greening records (E & F) is supported by the correlation of the 18O measurements of the cores (B) and the reference $\delta^{18}O$ curve LR04 (A). This otherwise exceptionally cold and dry period is known as the "900-Kyr event". Graphs: A) Stack of 57 globally distributed benthic $\delta^{18}O$ records (palaeotemperature proxy) [145]. B) ^{18}O isotopic measurements in foraminifer shells (Neogloboquadrina pachyderma) of the upper 76 m at ODP Site 646 [119]. C) Fauna-based summer sea surface temperatures (SSTs) from IODP Site U1314, North Atlantic [158]. D) $U^{K}37$-derived SSTs from Site 983, North Atlantic [159]. E) Spore content of pteridophytes as an independent proxy of vegetation growth from ODP Site 646 [119]; the grey horizontal band denotes the values of the current interglacial period for comparison. F) Pollen content of spermatophytes as an independent proxy of vegetation and forested episodes from ODP Site 646 [119]. G) High-resolution alkenone-based SSTs from IODP Site U1313, North Atlantic [160]. H) Winter MAT-SST from ODP Site 980, North Atlantic [120]. I) SSTs from IODP Site U1385, SW Iberian Margin [161]. J) SST record based on census counts of foraminifera from DSDP Site 607, North Atlantic [162]. K) $U^{K}37$-derived SSTs from Site 982, North Atlantic [163]. Grey horizontal stripes denote the initial increase in SSTs at the onset of the event. Light blue vertical strips and MIS numbers denote glacial periods after 0.89 Mya with their terminations on the top. All records are plotted on their original timescales. For site locations see Figure 5.

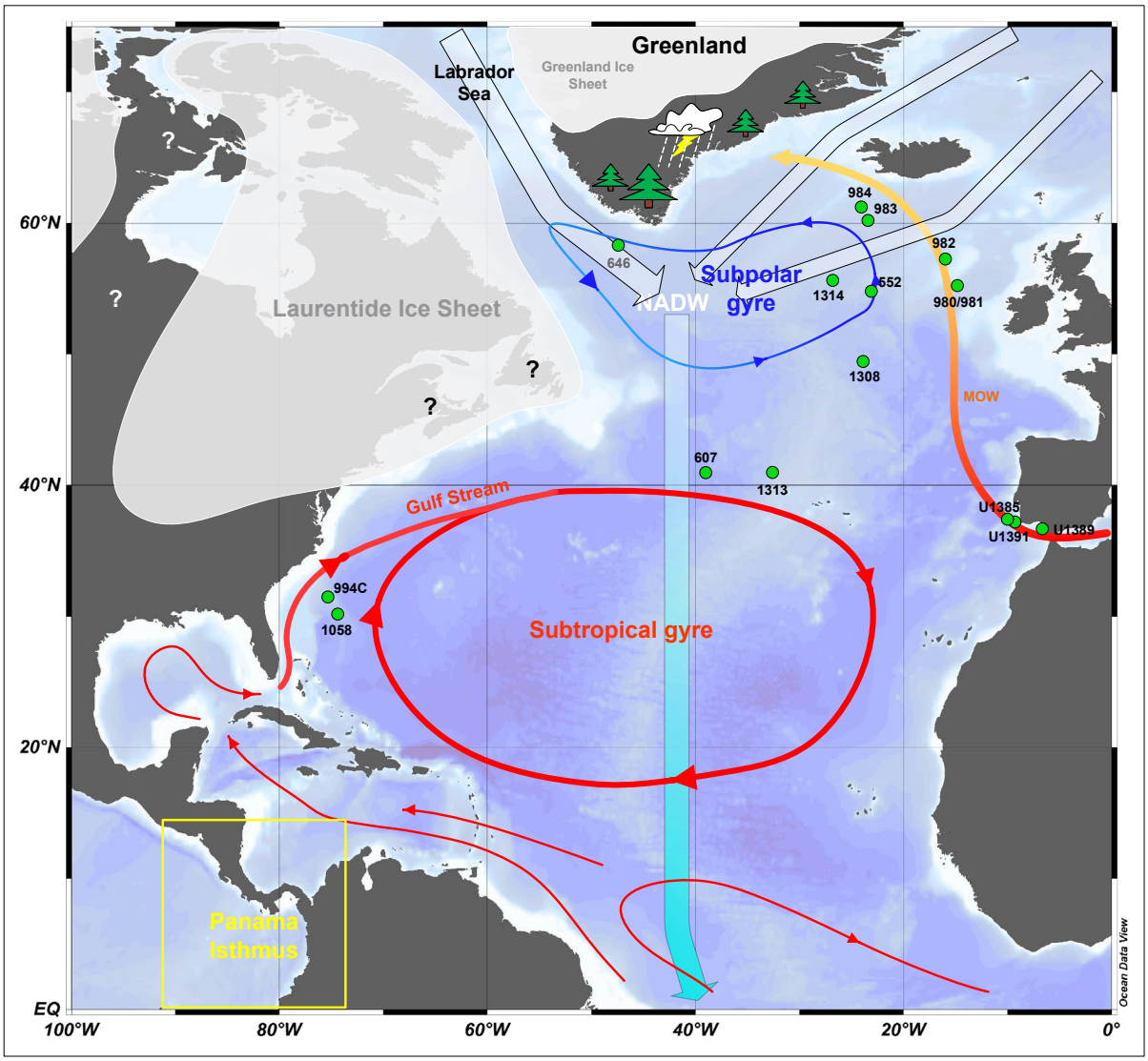

Supplementary Figure 3: Potential configuration of North Atlantic surface currents during the unprecedented Greenland "greening" at the glacial maximum of MIS 22 due to a major episode in the restriction of the transisthmian seaways, the temporal closing of the Bering Strait and the shutdown of the East Greenland Current at 0.89 Ma. Northwards heat advection through the Mediterranean Outflow Water (MOW).

Supplementary References

158. Hernández-Almeida, I., Sierro, F. J., Cacho, I., & Flores, J. A. (2012). Impact of suborbital climate changes in the North Atlantic on ice sheet dynamics at the Mid-Pleistocene Transition. Paleoceanography 27, PA3214.

159. McClymont, E. L., Rosell-Mele´, A., Haug, G. H., & Lloyd, J. M. (2008). Expansion of subarctic water masses in the North Atlantic and Pacific oceans and implications for mid-Pleistocene ice sheet growth. Paleoceanography, 23, PA4214.

160. Naafs, B. D. A., Hefter, J., Ferretti, P., Stein, R., & Haug, G. H. (2011). Sea surface temperatures did not control the first occurrence of Hudson Strait Heinrich Events during MIS 16. Paleoceanography, 26, PA4201.

161. Rodrigues, T., Alonso-García, M., Hodell, D. A., Rufino, M., Naughton, F., Grimalt, J. O. () Abrantes, F. (2017). A 1-Ma record of sea surface temperature and extreme cooling events in the North Atlantic: a perspective from the Iberian Margin. Quaternary Science Reviews, 172, 118e130.

162. Ruddiman, W., Raymo, M., Martinson, D., Clement, B., & Backman, J. (1989). Pleistocene evolution: Northern Hemisphere ice sheets and North Atlantic Ocean. Paleoceanography, 4, 353-412.

163. Lawrence, K. T., Herbert, T. D., Brown, C. M., Raymo, M. E., & Haywood, A. M. (2009). High-amplitude variations in North Atlantic sea surface temperature during the early Pliocene warm period. Paleoceanography, 24, PA2218.

164. Johnson, K. P., & Weckstein, J. D. (2011). The Central American land bridge as an engine of diversification in New World

doves. Journal of Biogeography, 38, 1069-1076.
165. Smith, B.T., & Klicka, J. (2010). The profound influence of the Late Pliocene Panamanian uplift on the exchange, diversification, and distribution of New World birds. Ecography, 33, 333-342.
166. Ireland, H. E., Kite, G. C., Veitch, N. C., Chase, M. W., Schrire, B., Lavin, M. () Pennington, R. T. (2010). Biogeographical, ecological and morphological structure in a phylogenetic analysis of Ateleia (Swartzieae, Fabaceae) derived from combined molecular, morphological and chemical data. Botanical Journal of the Linnean Society, 162, 39-53.
167. Wagner, N., Silvestro, D., Brie, D., Ibisch, P. L., Zizka, G., Weising, K., & Schulte, K. (2012). Spatio-temporal evolution of Fosterella (Bromeliaceae) in the Central Andean biodiversity hotspot. Journal of Biogeography, 40, 869-880.
168. Schaefer, H., Hechenleitner, P., Santos-Guerra, A., de Sequeira, M. M., Pennington, R. T., Kenicer, G., Carine, M. A. (2012). Systematics, biogeography, and character evolution of the legume tribe Fabeae with special focus on the middle-Atlantic island lineages. BMC Evolutionary Biology, 12, 250.
169. Smith, B. T., McCormack, J. E., Cuervo, A. M., Hickerson, M. J., Aleixo, A., & Cadena, C. D. (2014). The drivers of tropical speciation. Nature, 515, 406-409.
170. Ward, P.S., & Branstetter, M.G. (2017). The acacia ants revisited: convergent evolution and biogeographic context in an iconic ant/plant mutualism. Proceedings of the Royal Society B, 284, 20162569.
171. Wang, B., Ding, Z., Liu, W., Pan, J., Li, C., Ge, S., Zhang, D. (2009). Polyploid evolution in Oryza officinalis complex of the genus Oryza. BMC Evolutionary Biology, 9, 250.
172. Vargas, O. M., Goldston, B., Grossenbacher, D. L., & Kay, K. M. (2020). Patterns of speciation are similar across mountainous and lowland regions for a Neotropical plant radiation (Costaceae: Costus). Evolution, 74, 2644-2661.
173. Aguilar, C., Miller, M. J., Loaiza, J. R., González, R., Krahe, R., & De León L. F. (2019). Tempo and mode of allopatric divergence in the weakly electric fish Sternopygus dariensis in the Isthmus of Panama. Scientific Reports, 9, 18828.
174. Jones, C. P. (2007). Phylogeography of the Livebearer Xenophallus umbratilis (Teleostei: Poeciliidae): glacial cycles and sea level change predict diversification of a freshwater tropical fish. All Theses and Dissertations. 1565.
175. Bagley, J. C., Alda, F., Breitman, M. F., Bermingham, E., van den Berghe, E. P., & Johnson, J. B. (2015). Assessing species boundaries using multilocus species delimitation in a morphologically conserved group of neotropical freshwater fishes, the Poecilia sphenops species complex (Poeciliidae). PLoS ONE, 10, e0121139.
176. Bagley, J. C. Hickerson, M. J., & Johnson, J. B. (2018). Testing hypotheses of diversification in Panamanian frogs and freshwater fishes using hierarchical approximate bayesian computation with model averaging. Diversity, 10, 120.
177. Santos, J. C., Coloma, L. A., Summers, K., Caldwell, J. P., Ree, R., Cannatella, D. C. (2009). Amazonian amphibian diversity is primarily derived from Late Miocene Andean lineages. PLoS Biology, 7, e1000056.
178. Mendoza, A. M., Bolívar-García, W., Vázquez-Domínguez, E., Ibáñez, R., Olea, G. P. (2019). The role of Central American barriers in shaping the evolutionary history of the northernmost glassfrog, Hyalinobatrachium fleischmanni (Anura: Centrolenidae). PeerJ, 7, e6115.
179. Crawford, A. J. (2003). Huge populations and old species of Costa Rican and Panamanian dirt frogs inferred from mitochondrial and nuclear gene sequences. Molecular Ecology, 12, 2525-2540.
180. Fritz, U., Stuckas, H., Vargas-Ramírez, M., Hundsdörfer, A. K., Maran, J., & Päckert, M. (2012). Molecular phylogeny of Central and South American slider turtles: implications for biogeography and systematics (Testudines: Emydidae: Trachemys). Journal of Zoological Systematics and Evolutionary Research, 50, 125-136.
181. Parham, J. F., Papenfuss, T. J., van Dijk, P. P., Wilson, B. S., Marte, C., Schettino, L. R., & Simison, W. B. (2013). Genetic introgression and hybridization in Antillean freshwater turtles (Trachemys) revealed by coalescent analyses of mitochondrial and cloned nuclear markers. Molecular Phylogenetics and Evolution, 67, 176-187.
182. Castoe, T. A., Daza, J. M., Smith, E. N., Sasa, M. M., Kuch, U., Campbell, J. () Parkinson, C. L. (2009). Comparative phylogeography of pitvipers suggests a consensus of ancient Middle American highland biogeography. Journal of Biogeography, 36, 88-103.
183. Mauck, W. M., & Burns, K. J. (2009). Phylogeny, biogeography, and recurrent evolution of divergent bill types in the nectar-stealing flowerpiercers (Thraupini: Diglossa and Diglossopis). Biological Journal of the Linnean Society, 98, 14-28.
184. Rocha-Méndez, A., Sánchez-González, L.A., González, C., & Navarro-Sigüenza, A. G. (2019). The geography of evolutionary divergence in the highly endemic avifauna from the Sierra Madre del Sur, Mexico. BMC Evolutionary Biology, 19, 237.
185. Morales-Jimenez, A. L., Cortés-Ortiz, L., & Di Fiore, A. (2015). Phylogenetic relationships of Mesoamerican spider monkeys (Ateles geoffroyi): Molecular evidence suggests the need for a revised taxonomy. Molecular Phylogenetics and Evolution, 82, 484-494.
186. Silvestro, D., Tejedor, M. F., Serrano-Serrano, M. L., Loiseau, O., Rossier, V., Rolland, J. () Salamin, N. (2019). Early arrival and climatically-linked geographic expansion of new world monkeys from tiny African ancestors. Systematic Biology, 68, 78-92.
187. Perelman, P., Johnson, W. E., Roos, C., Seuanez, H. N., Horvath, J. E., Moreira, M. A. M. () Pecon-Slattery, J. (2011). A molecular phylogeny of living primates. PLoS Genetics, 7, e1001342.
188. Nigenda-Moralesa, S. F., Gompper, M. E., Valenzuela-Galván, D., Lay, A. R., Kapheim, K. M., Hass, C. () Koepfli, K.-P. (2019). Phylogeographic and diversification patterns of the white-nosed coati (Nasua narica): evidence for south-to-north colonization of North America. Molecular Phylogenetics and Evolution, 131, 149-163.

Supplementary Appendix

Phylogeographic maps of the taxa listed in Supplementary Table 3.

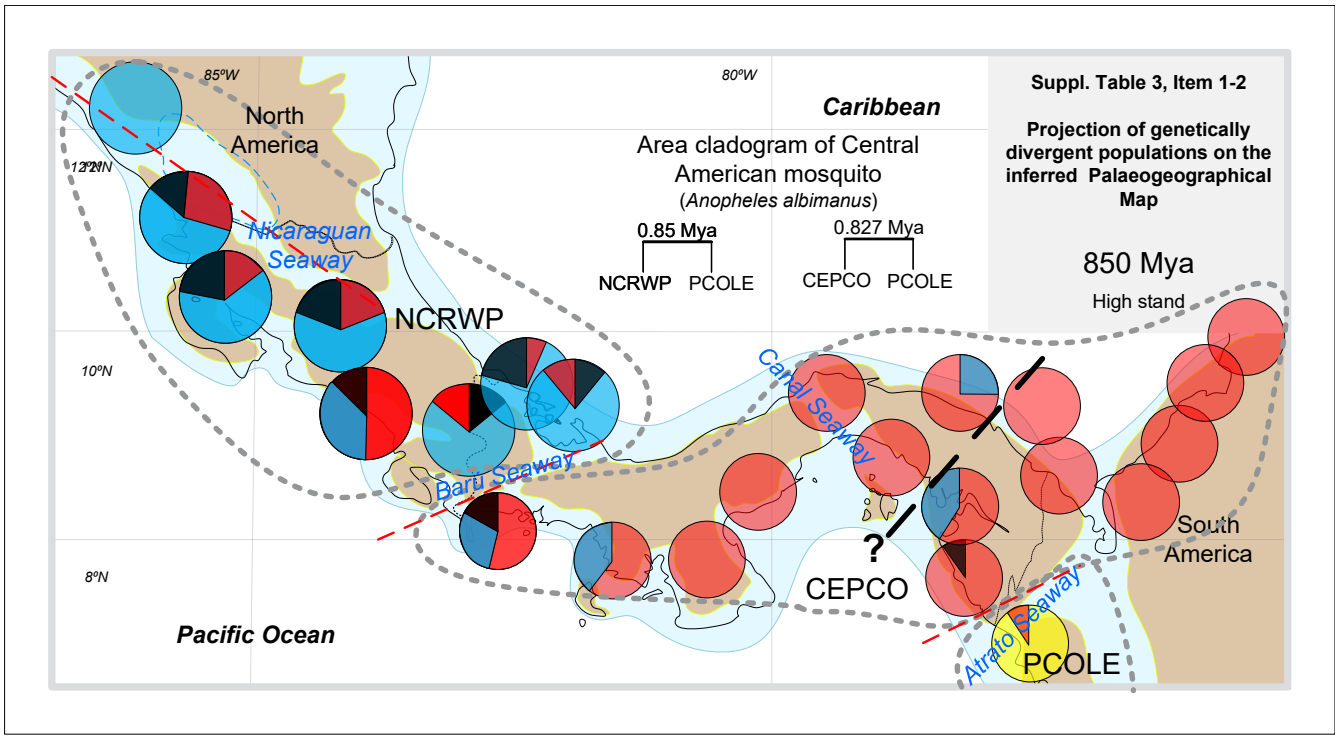

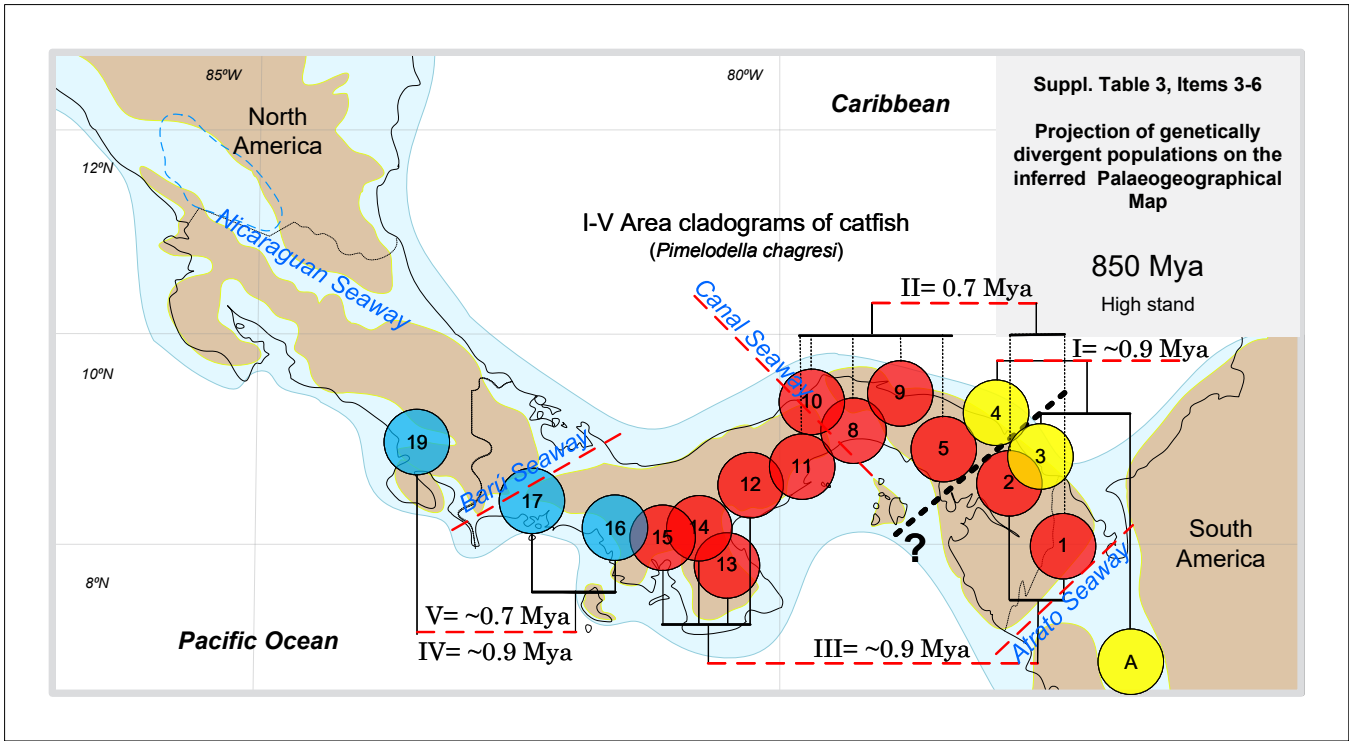

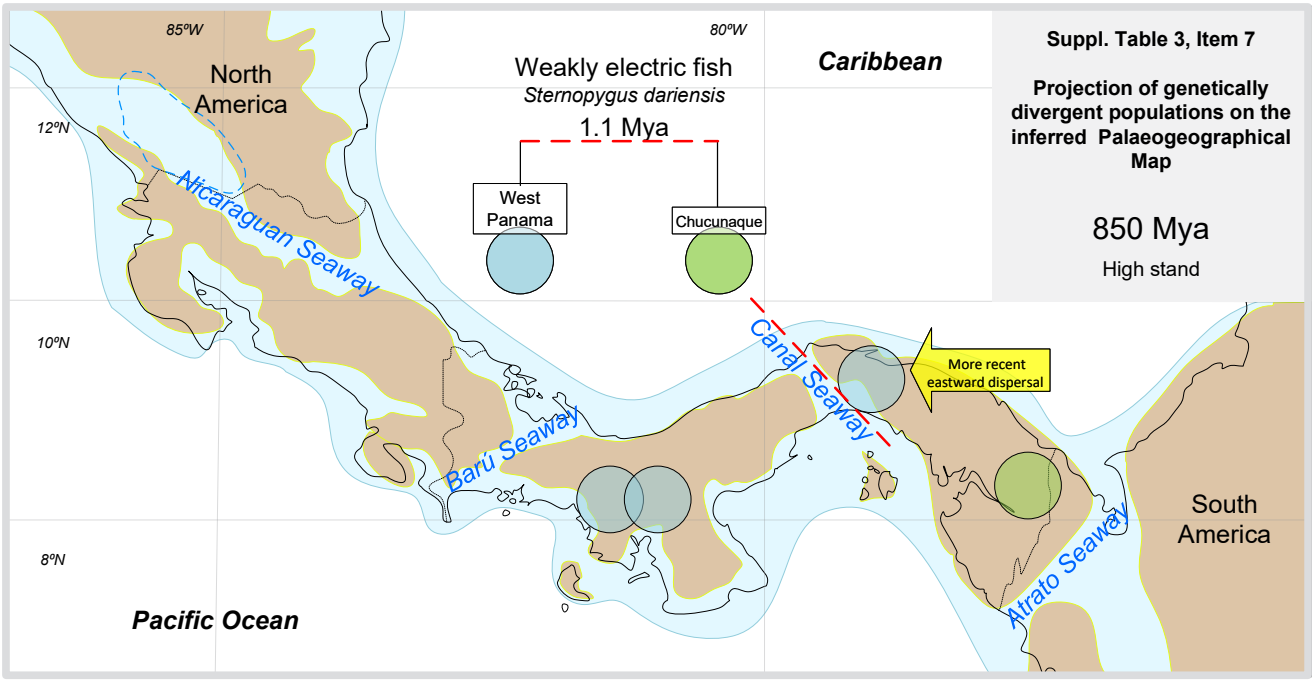
85ºW
80ºW
North America
Weakly electric fish
Sternopygus dariensis
1.1 Mya
Caribbean
Suppl. Table 3, Item 7
Projection of genetically divergent populations on the inferred Palaeogeographical Map
850 Mya
High stand
12ºN
Nicaraguan Seaway
West Panama
Chucunaque
10ºN
Canal Seaway
More recent eastward dispersal
Baru Seaway
South America
8ºN
Atrato Seaway
Pacific Ocean

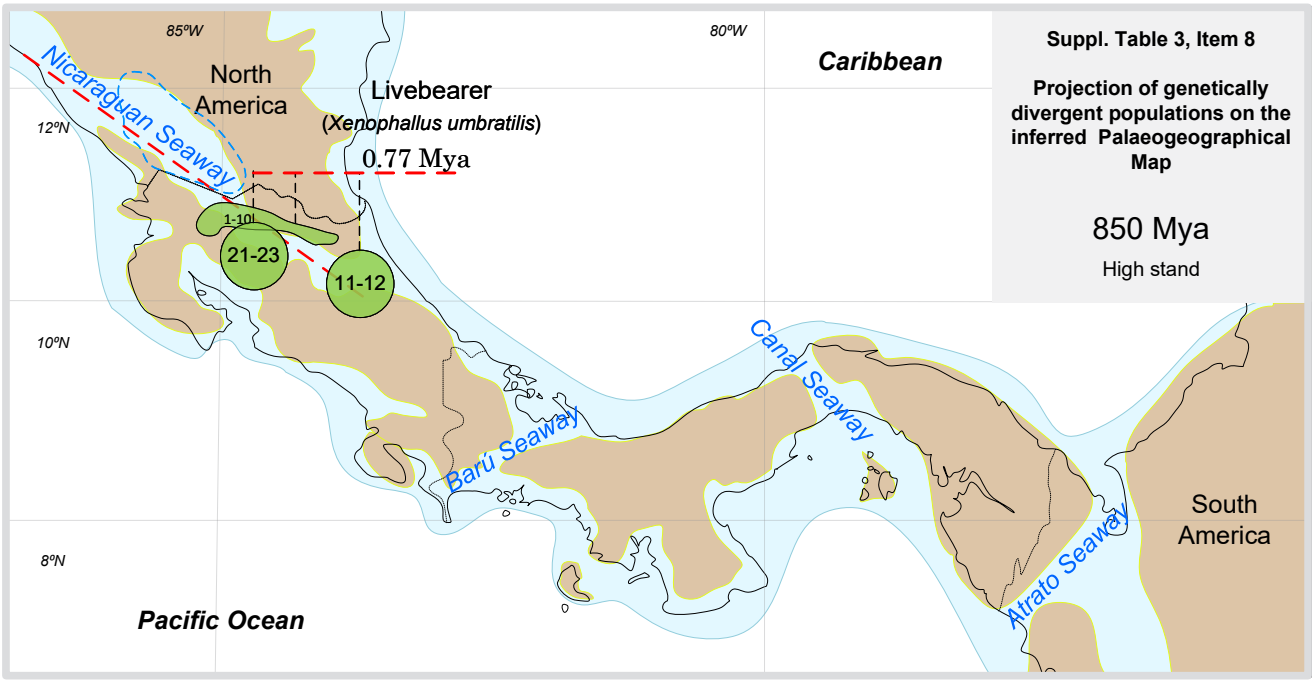
85ºW
80ºW
Nicaraguan Seaway
North America
Livebearer
(Xenophallus umbratilis)
0.77 Mya
Caribbean
Suppl. Table 3, Item 8
Projection of genetically divergent populations on the inferred Palaeogeographical Map
850 Mya
High stand
12ºN
1-10
21-23
11-12
10ºN
Canal Seaway
Baru Seaway
South America
8ºN
Atrato Seaway
Pacific Ocean

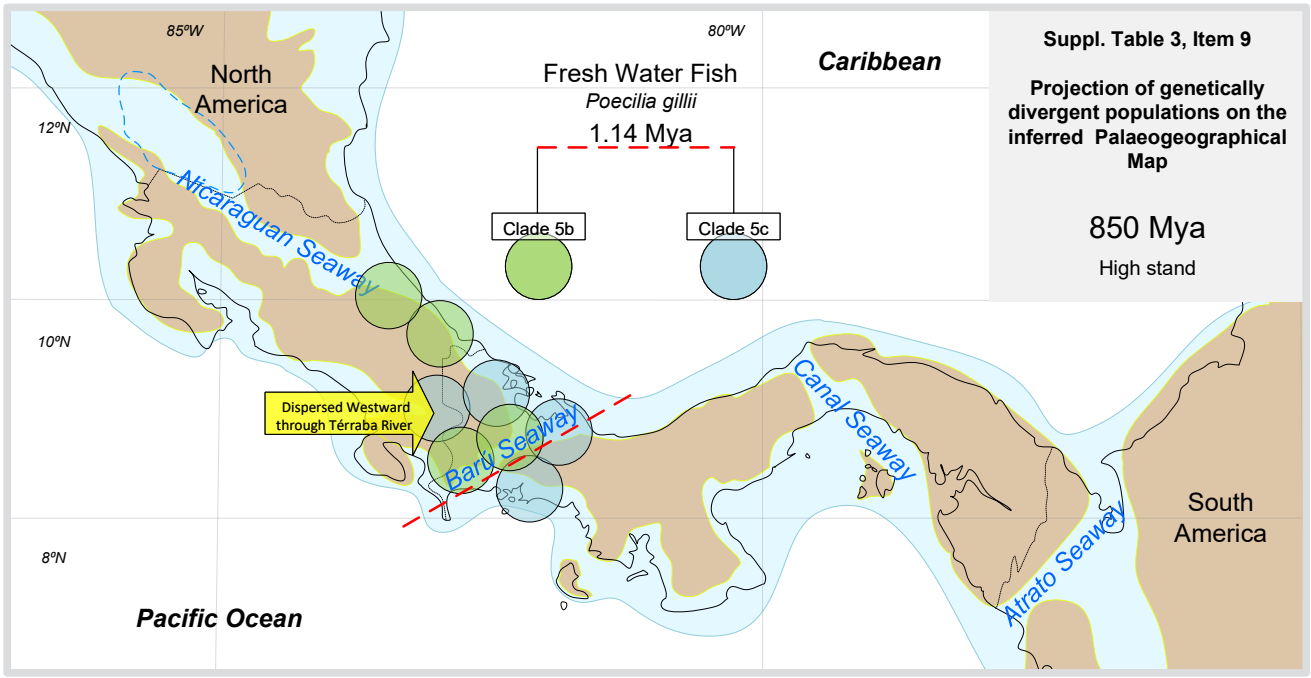
85ºW
80ºW
North America
Caribbean
Fresh Water Fish
Poecilia gillii
1.14 Mya
Clade 5b
Clade 5c
Suppl. Table 3, Item 9
Projection of genetically divergent populations on the inferred Palaeogeographical Map
850 Mya
High stand
12ºN
10ºN
8ºN
Nicaraguan Seaway
Dispersed Westward through Térraba River
Barú Seaway
Canal Seaway
Atrato Seaway
South America
Pacific Ocean

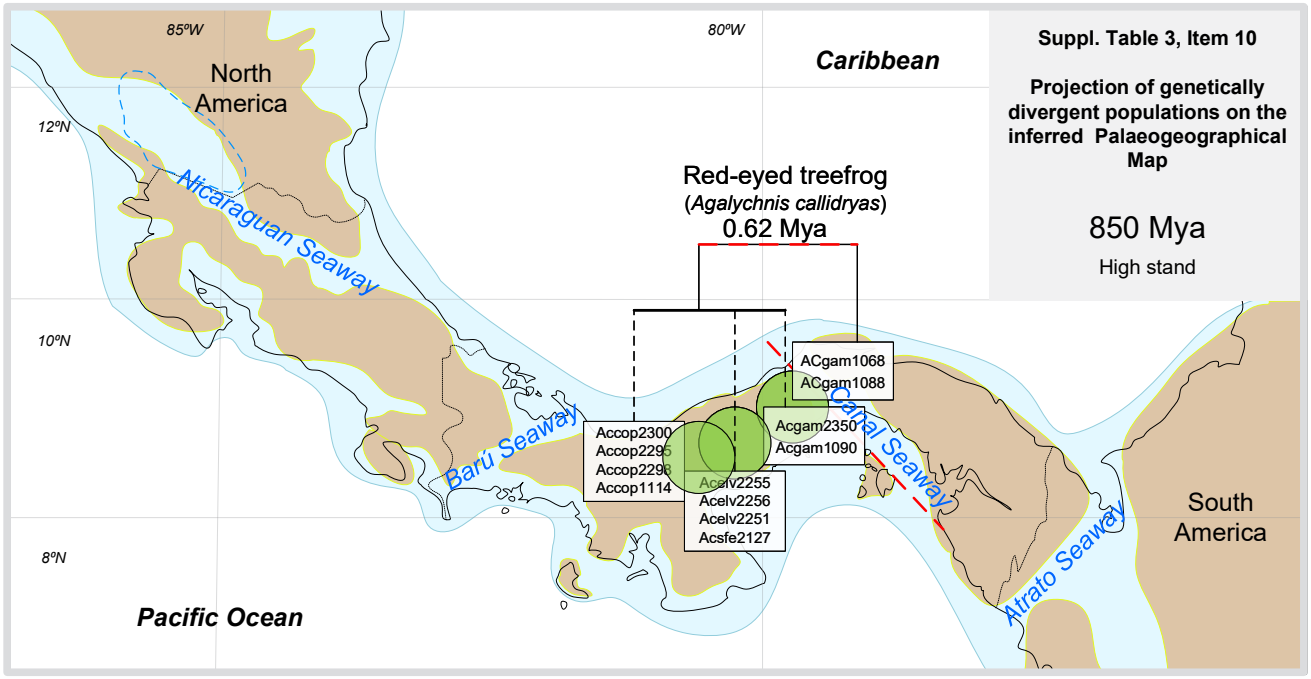
85ºW
80ºW
North America
Caribbean
Suppl. Table 3, Item 10
Projection of genetically divergent populations on the inferred Palaeogeographical Map
850 Mya
High stand
Red-eyed treefrog
(Agalychnis callidryas)
0.62 Mya
12ºN
10ºN
8ºN
Nicaraguan Seaway
ACgam1068
ACgam1088
Acgam2350
Acgam1090
Accop2300
Accop2295
Accop2298
Accop1114
Acelv2255
Acelv2256
Acelv2251
Acsfe2127
Barú Seaway
Canal Seaway
Atrato Seaway
South America
Pacific Ocean

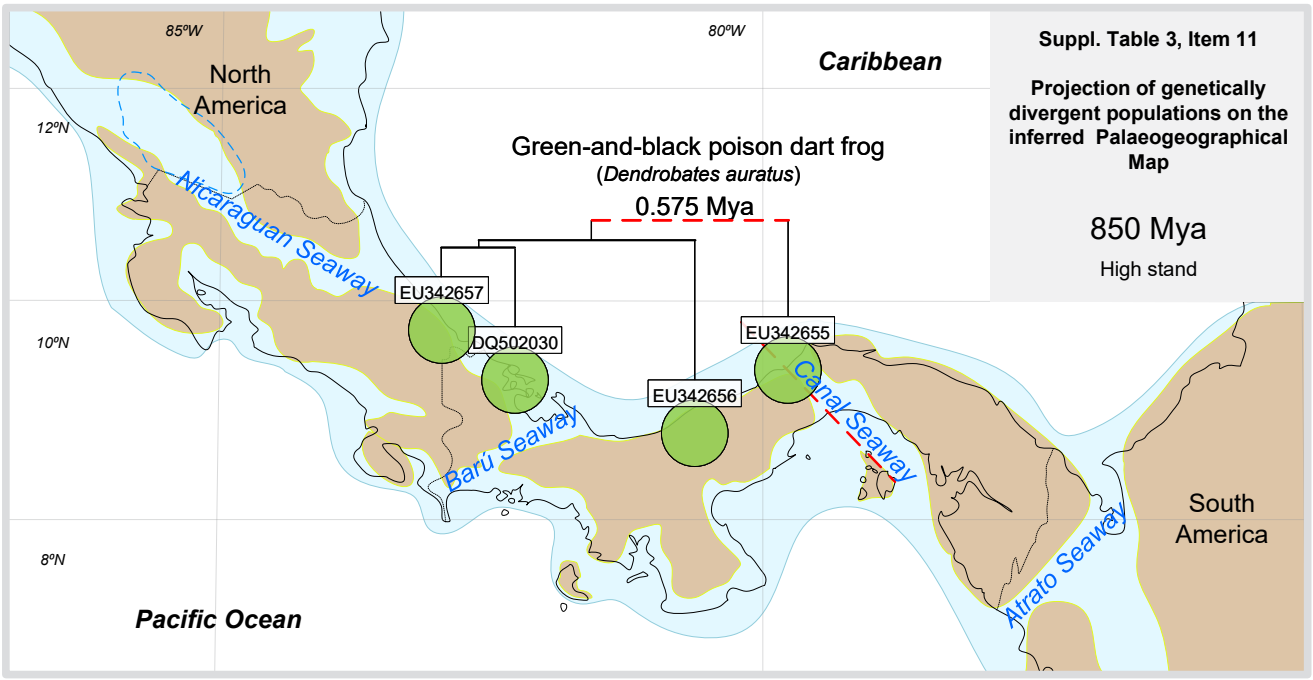
85ºW
80ºW
Caribbean
North America
12ºN
Green-and-black poison dart frog
(Dendrobates auratus)
0.575 Mya
Suppl. Table 3, Item 11
Projection of genetically divergent populations on the inferred Palaeogeographical Map
850 Mya
High stand
Alicaraguan Seaway
EU342657
DQ502030
EU342655
EU342656
10ºN
Canal Seaway
Baru Seaway
South America
8ºN
Atrato Seaway
Pacific Ocean

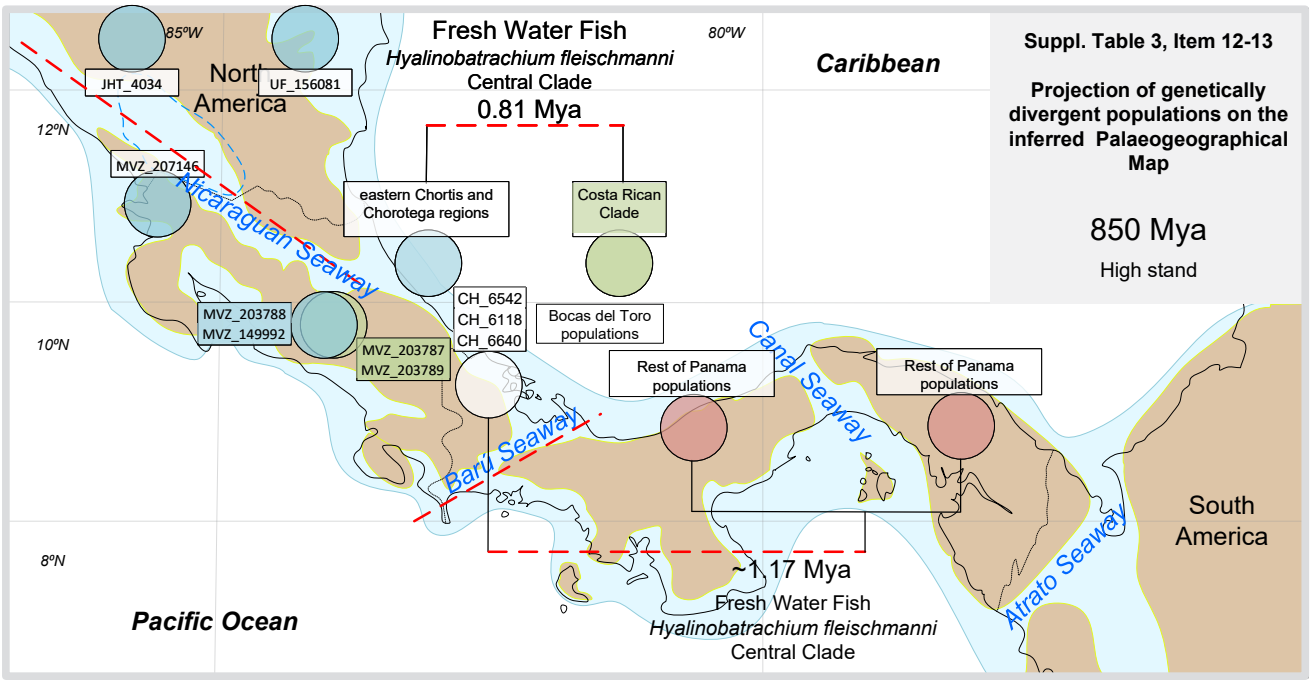
85ºW
Fresh Water Fish
Hyalinobatrachium fleischmanni
Central Clade
0.81 Mya
80ºW
Caribbean
Suppl. Table 3, Item 12-13
Projection of genetically divergent populations on the inferred Palaeogeographical Map
850 Mya
High stand
JHT_4034
North America
UF_156081
12ºN
MVZ_207146
Alicaraguan Seaway
eastern Chortis and Chorotega regions
Costa Rican Clade
CH_6542
CH_6118
CH_6640
Bocas del Toro populations
MVZ_203788
MVZ_149992
MVZ_203787
MVZ_203789
10ºN
Canal Seaway
Rest of Panama populations
Rest of Panama populations
Baru Seaway
South America
8ºN
~1.17 Mya
Fresh Water Fish
Hyalinobatrachium fleischmanni
Central Clade
Atrato Seaway
Pacific Ocean

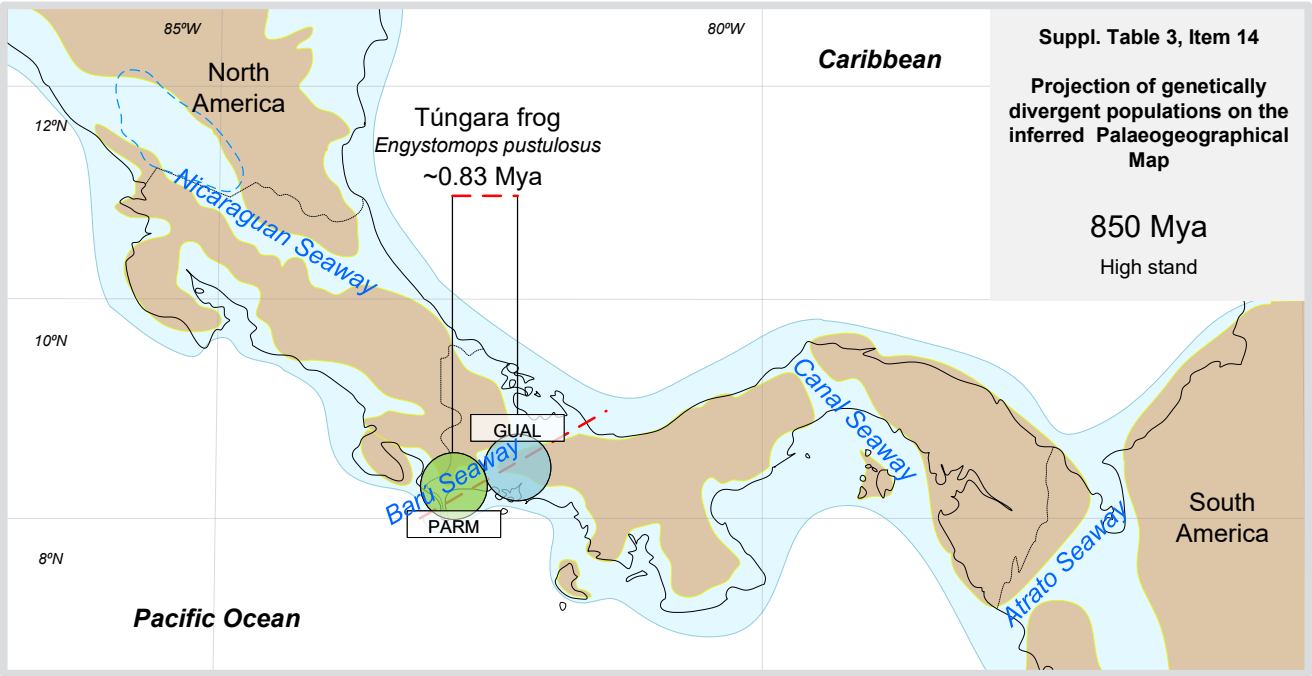
85ºW
80ºW
Caribbean
North America
12ºN
Túngara frog
Engystomops pustulosus
~0.83 Mya
Nicaraguan Seaway
Suppl. Table 3, Item 14
Projection of genetically divergent populations on the inferred Palaeogeographical Map
850 Mya
High stand
10ºN
GUAL
Canal Seaway
Barú Seaway
PARM
South America
8ºN
Atrato Seaway
Pacific Ocean

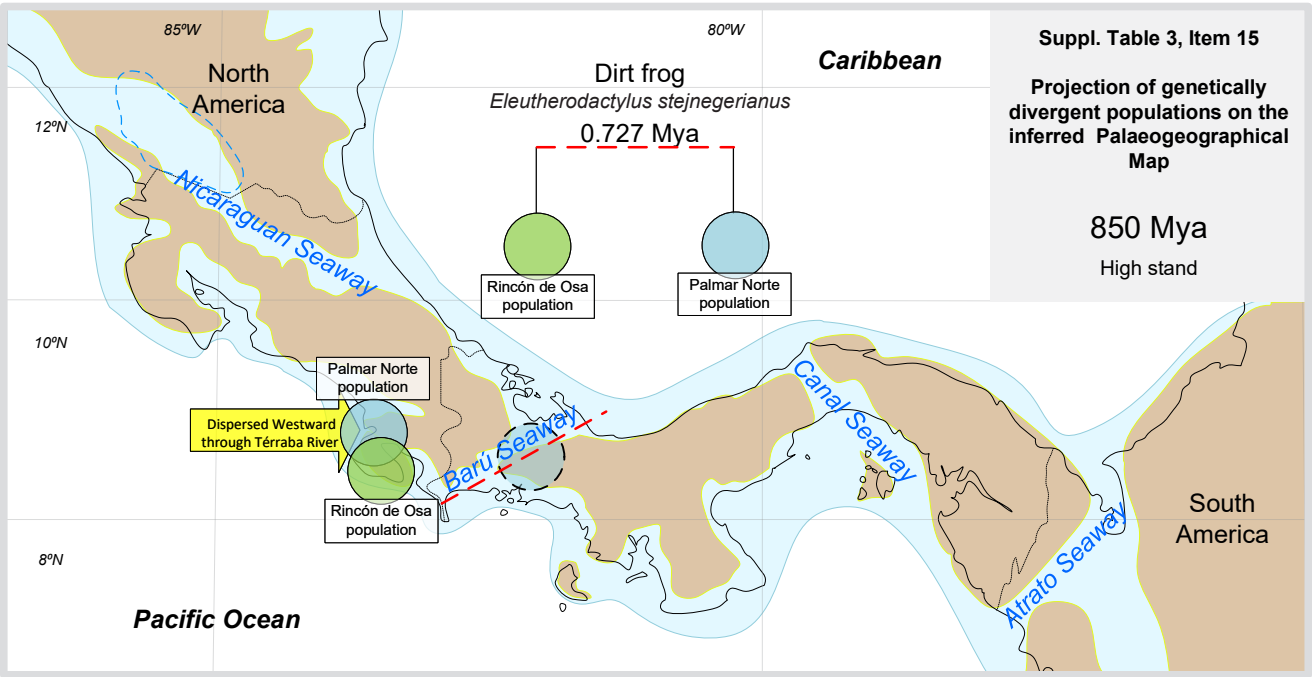
85ºW
80ºW
Caribbean
North America
Dirt frog
Eleutherodactylus stejnegerianus
0.727 Mya
12ºN
Nicaraguan Seaway
Suppl. Table 3, Item 15
Projection of genetically divergent populations on the inferred Palaeogeographical Map
850 Mya
High stand
Rincón de Osa population
Palmar Norte population
10ºN
Palmar Norte population
Dispersed Westward through Térraba River
Canal Seaway
Barú Seaway
Rincón de Osa population
South America
8ºN
Atrato Seaway
Pacific Ocean

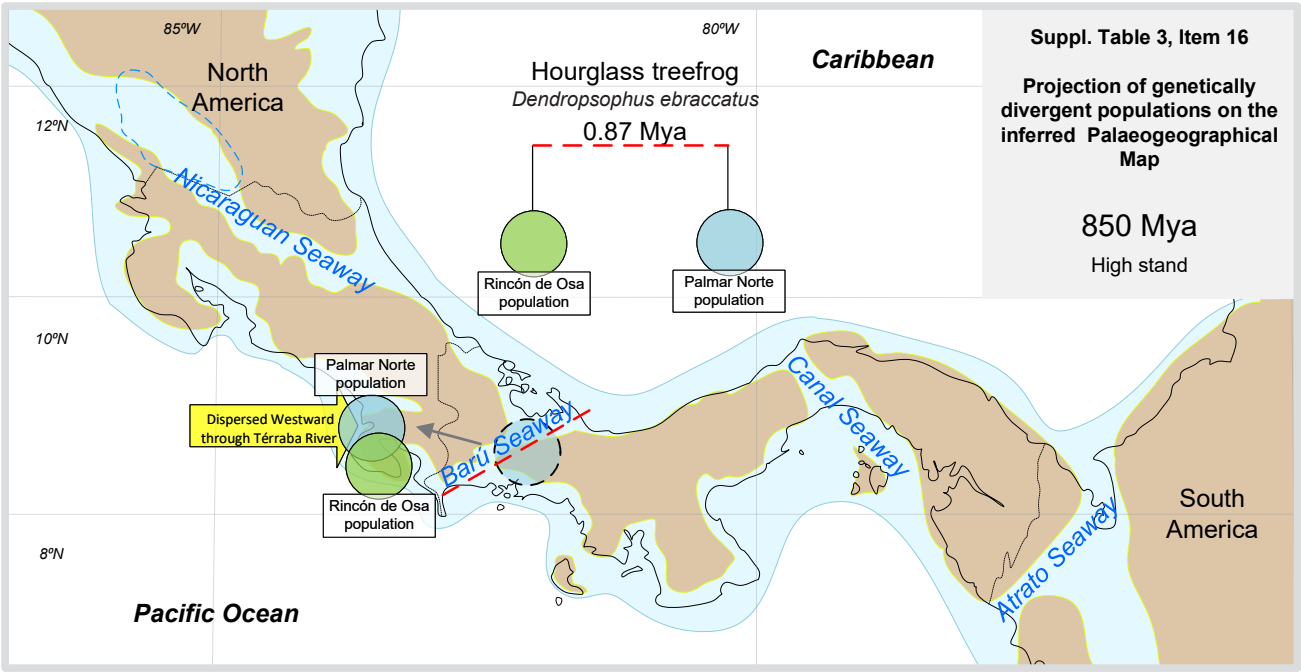
85ºW
80ºW
North America
Caribbean
Hourglass treefrog
Dendropsophus ebraccatus
0.87 Mya
Suppl. Table 3, Item 16
Projection of genetically divergent populations on the inferred Palaeogeographical Map
850 Mya
High stand
12ºN
10ºN
8ºN
Nicaraguan Seaway
Rincón de Osa population
Palmar Norte population
Palmar Norte population
Dispersed Westward through Térraba River
Rincón de Osa population
Barú Seaway
Canal Seaway
Atrato Seaway
South America
Pacific Ocean

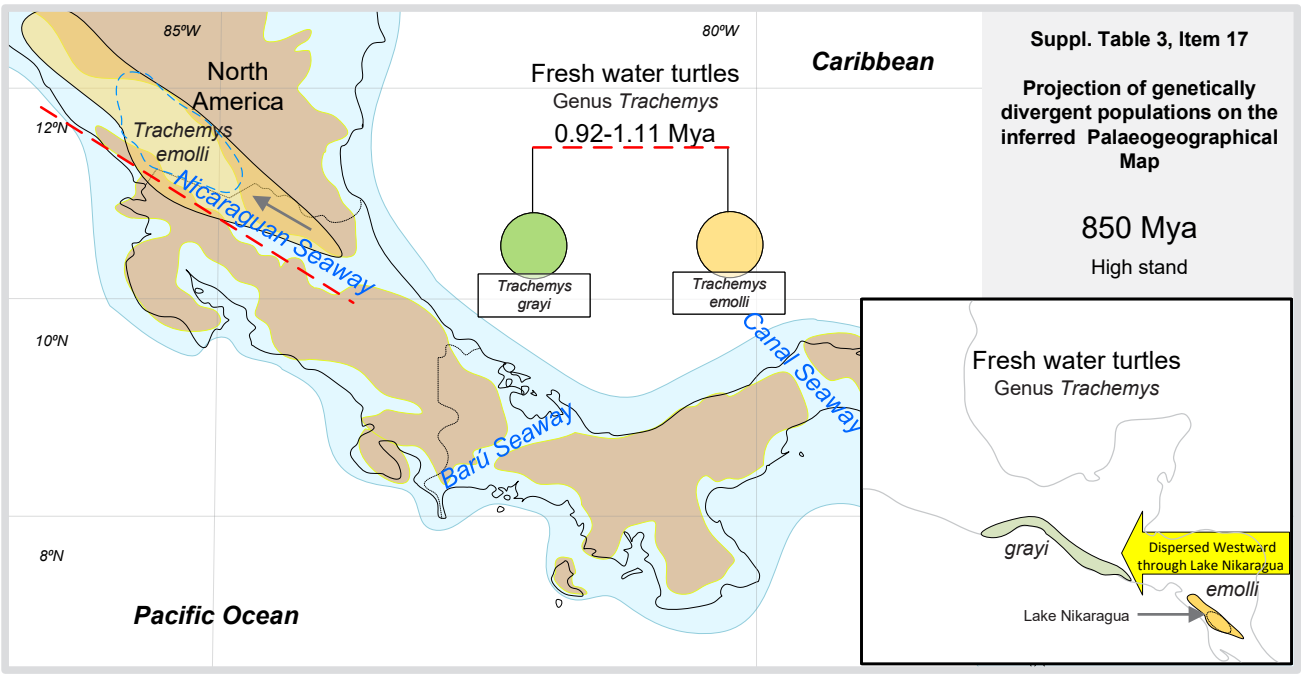
85ºW
80ºW
North America
Caribbean
Fresh water turtles
Genus Trachemys
0.92-1.11 Mya
Suppl. Table 3, Item 17
Projection of genetically divergent populations on the inferred Palaeogeographical Map
850 Mya
High stand
12ºN
10ºN
8ºN
Trachemys emolli
Nicaraguan Seaway
Trachemys grayi
Trachemys emolli
Canal Seaway
Barú Seaway
Pacific Ocean
Fresh water turtles
Genus Trachemys
grayi
Dispersed Westward through Lake Nikaragua
emolli
Lake Nikaragua

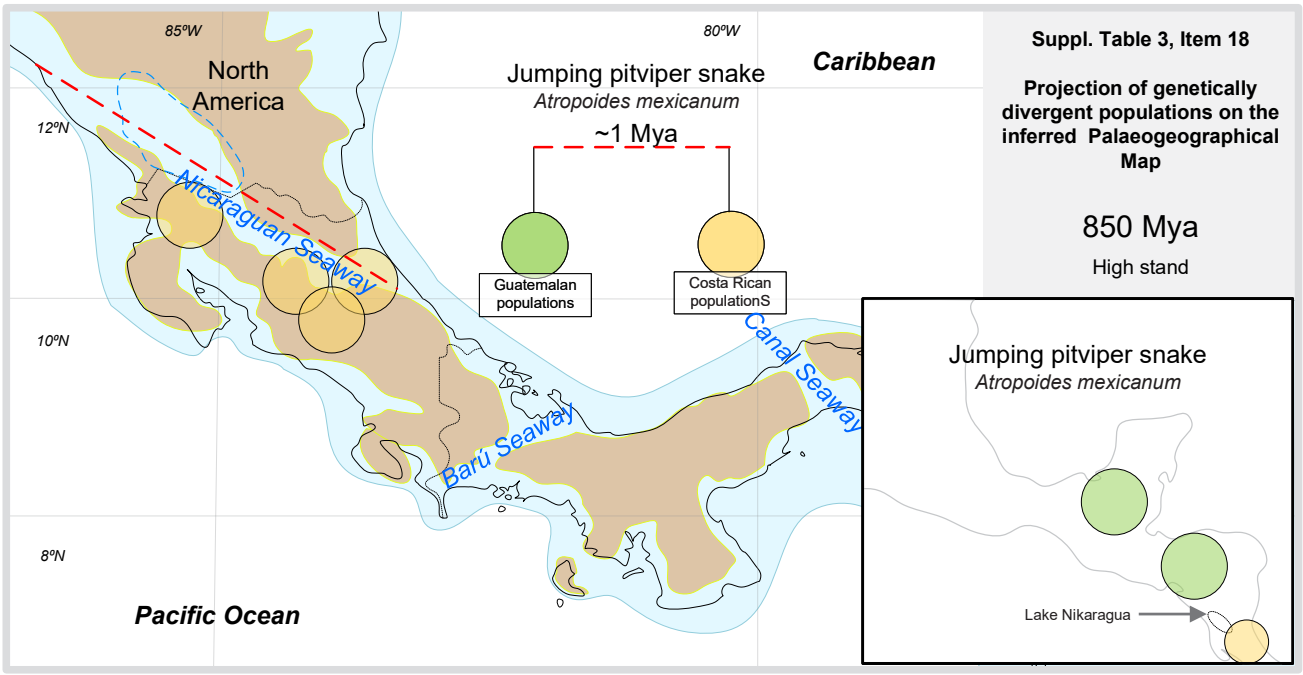
85ºW
80ºW
North America
Caribbean
Jumping pitviper snake
Atropoides mexicanum
~1 Mya
Suppl. Table 3, Item 18
Projection of genetically divergent populations on the inferred Palaeogeographical Map
850 Mya
High stand
12ºN
10ºN
8ºN
Nicaraguan Seaway
Guatemalan populations
Costa Rican populationS
Canal Seaway
Barú Seaway
Pacific Ocean
Jumping pitviper snake
Atropoides mexicanum
Lake Nikaragua

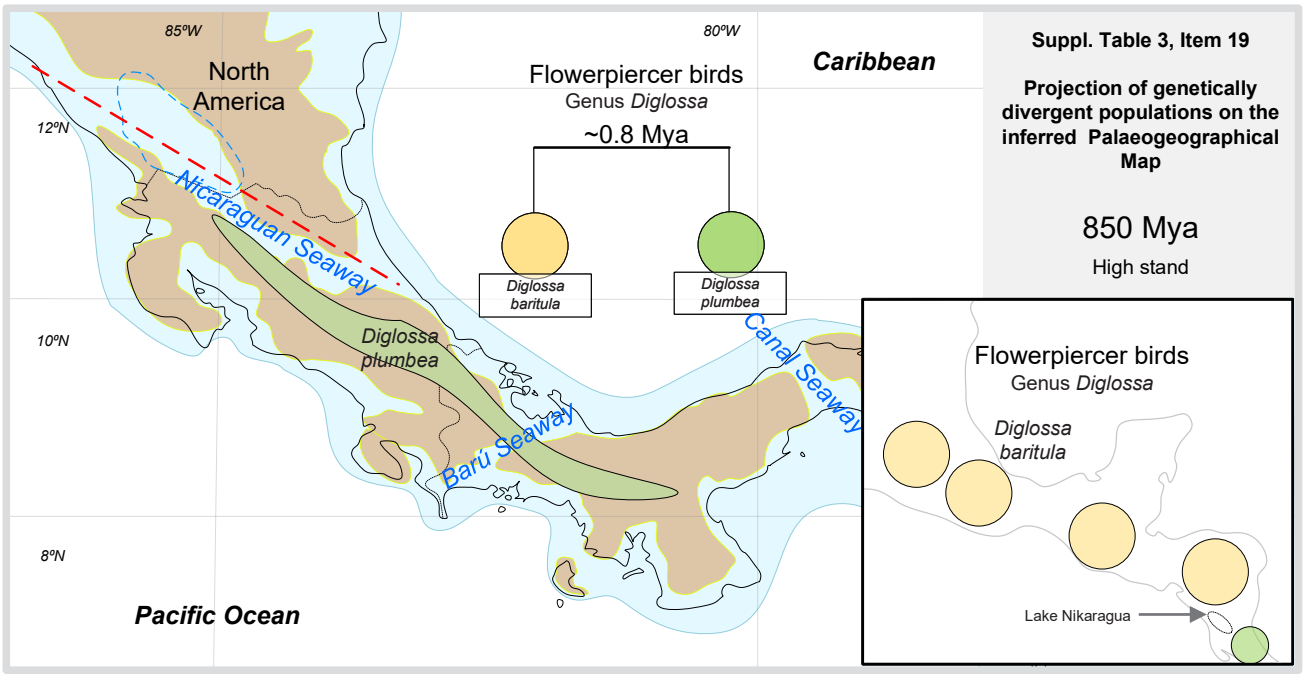
85ºW
80ºW
North America
Caribbean
Flowerpiercer birds
Genus Diglossa
~0.8 Mya
Suppl. Table 3, Item 19
Projection of genetically divergent populations on the inferred Palaeogeographical Map
850 Mya
High stand
12ºN
10ºN
8ºN
Nicaraguan Seaway
Diglossa baritula
Diglossa plumbea
Diglossa plumbea
Canal Seaway
Barú Seaway
Pacific Ocean
Flowerpiercer birds
Genus Diglossa
Diglossa baritula
Lake Nikaragua

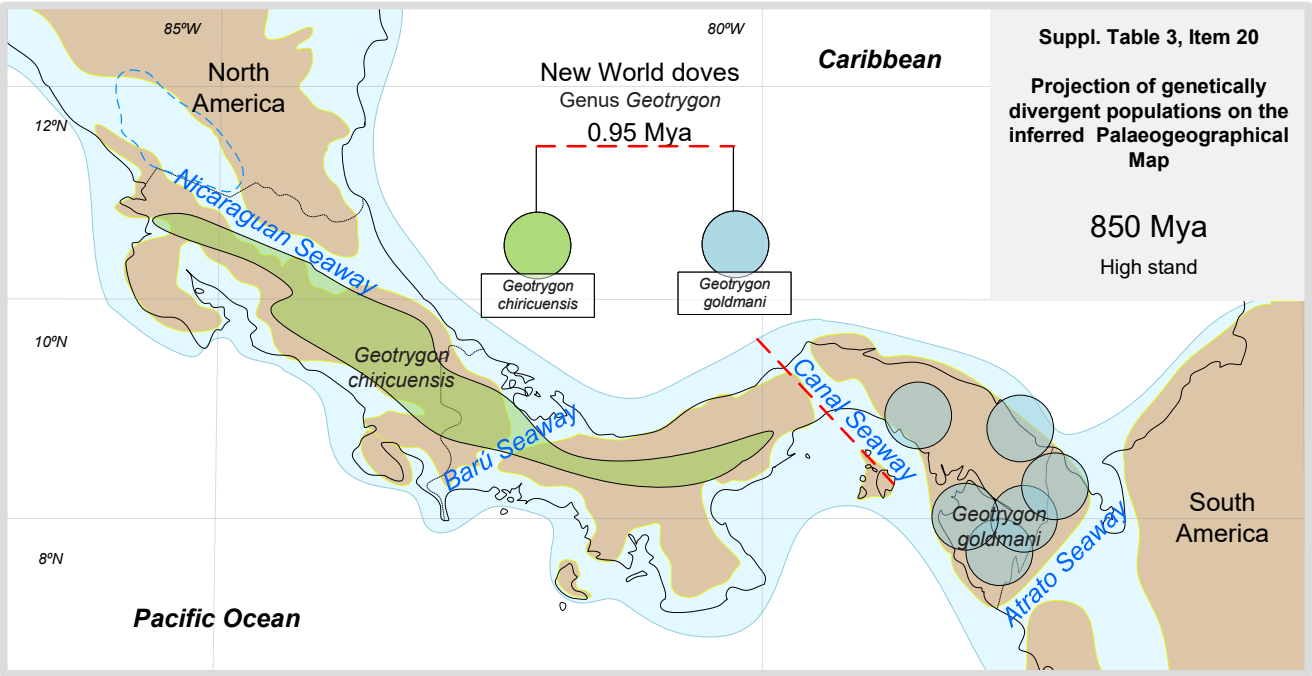
85ºW
80ºW
North America
New World doves
Genus Geotrygon
0.95 Mya
Caribbean
Suppl. Table 3, Item 20
Projection of genetically divergent populations on the inferred Palaeogeographical Map
850 Mya
High stand
12ºN
Nicaraguan Seaway
Geotrygon chiricuensis
Geotrygon goldmani
10ºN
Geotrygon chiricuensis
Barú Seaway
Canal Seaway
Geotrygon goldmani
Atrato Seaway
South America
8ºN
Pacific Ocean

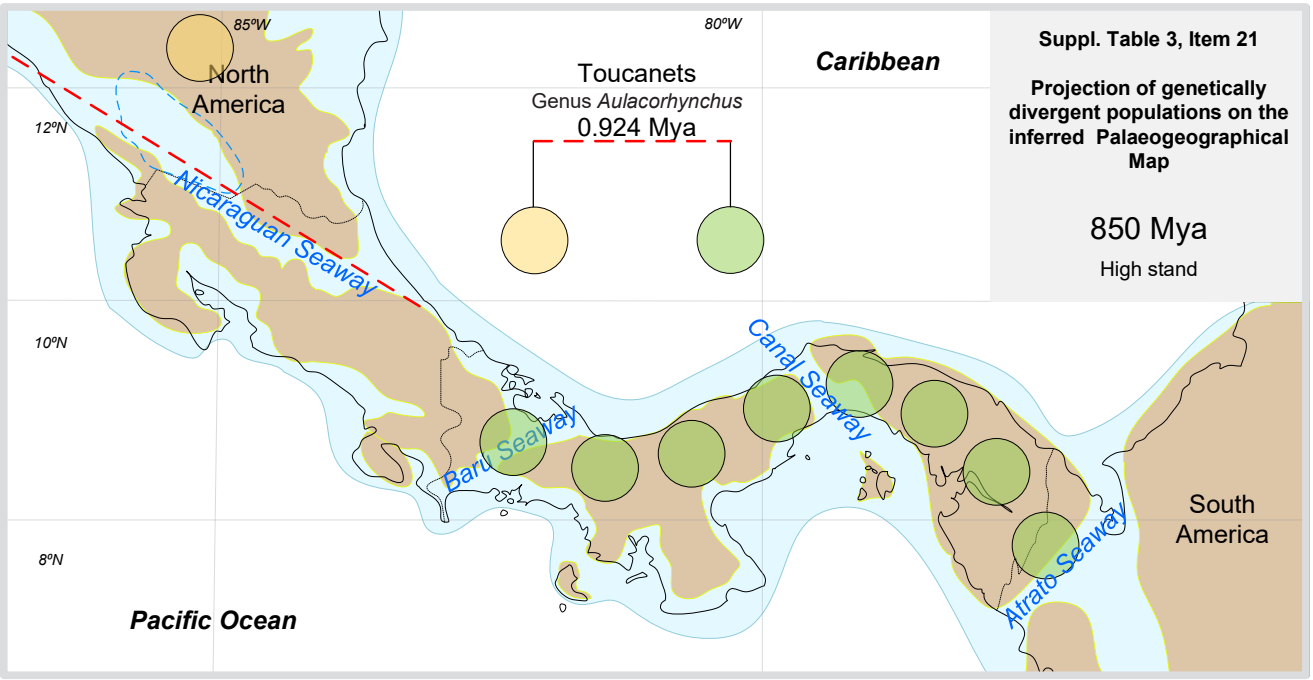
85ºW
80ºW
North America
Toucanets
Genus Aulacorhynchus
0.924 Mya
Caribbean
Suppl. Table 3, Item 21
Projection of genetically divergent populations on the inferred Palaeogeographical Map
850 Mya
High stand
12ºN
Nicaraguan Seaway
10ºN
Canal Seaway
Barú Seaway
South America
Atrato Seaway
8ºN
Pacific Ocean

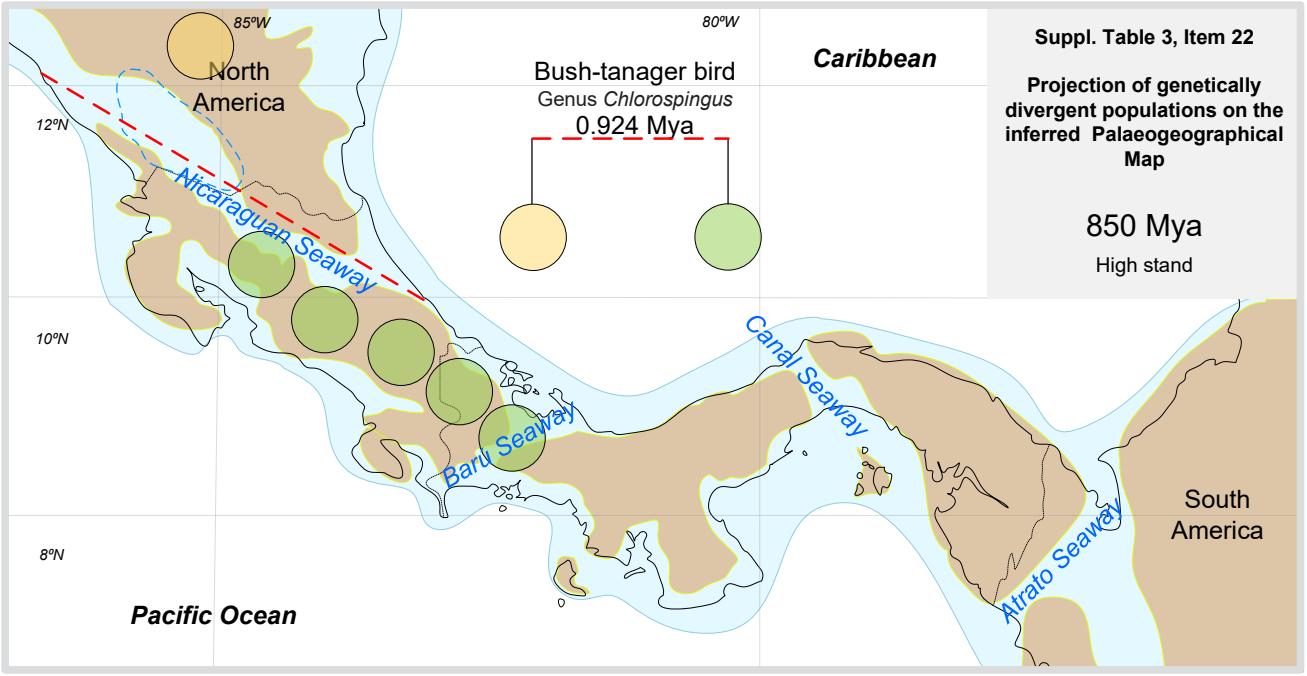
85ºW
80ºW
North America
Caribbean
Bush-tanager bird
Genus Chlorospingus
0.924 Mya
Suppl. Table 3, Item 22
Projection of genetically divergent populations on the inferred Palaeogeographical Map
850 Mya
High stand
12ºN
10ºN
8ºN
Nicaraguan Seaway
Canal Seaway
Barú Seaway
Atrato Seaway
South America
Pacific Ocean

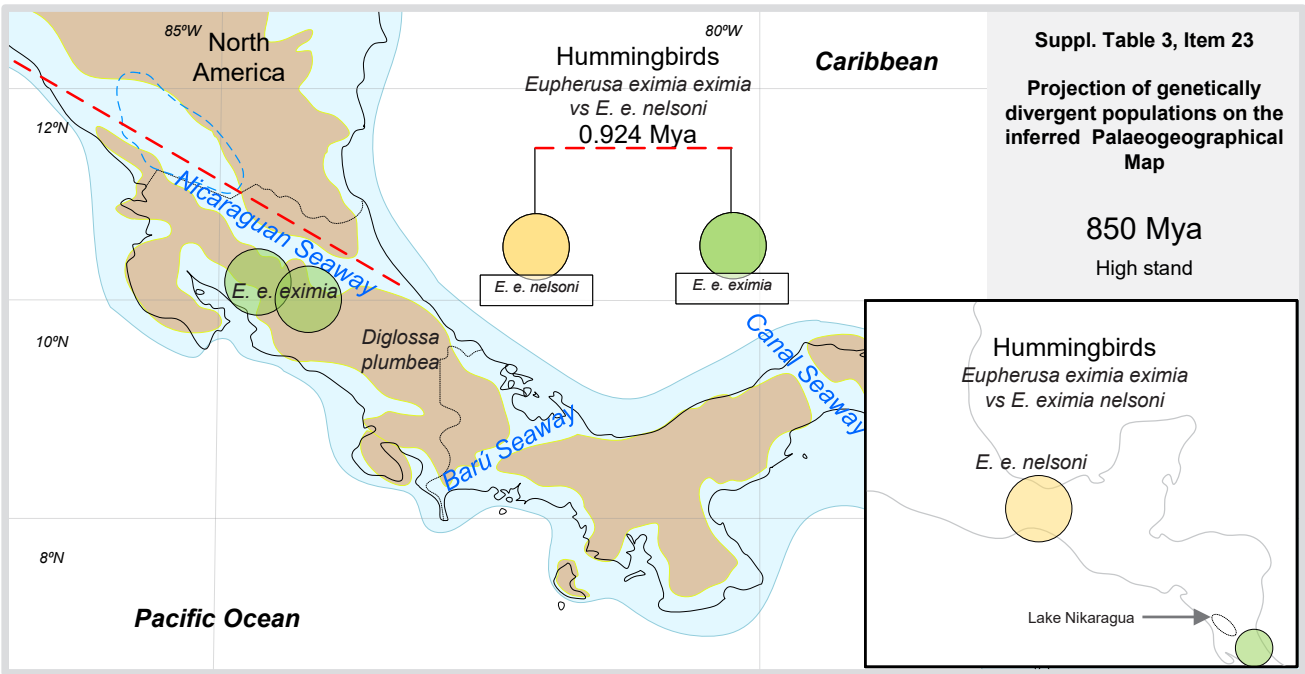
85ºW
80ºW
North America
Caribbean
Hummingbirds
Eupherusa eximia eximia
vs E. e. nelsoni
0.924 Mya
Suppl. Table 3, Item 23
Projection of genetically divergent populations on the inferred Palaeogeographical Map
850 Mya
High stand
E. e. nelsoni
E. e. eximia
12ºN
10ºN
8ºN
Nicaraguan Seaway
E. e. eximia
Diglossa plumbea
Canal Seaway
Barú Seaway
Pacific Ocean
Hummingbirds
Eupherusa eximia eximia
vs E. eximia nelsoni
E. e. nelsoni
Lake Nikaragua

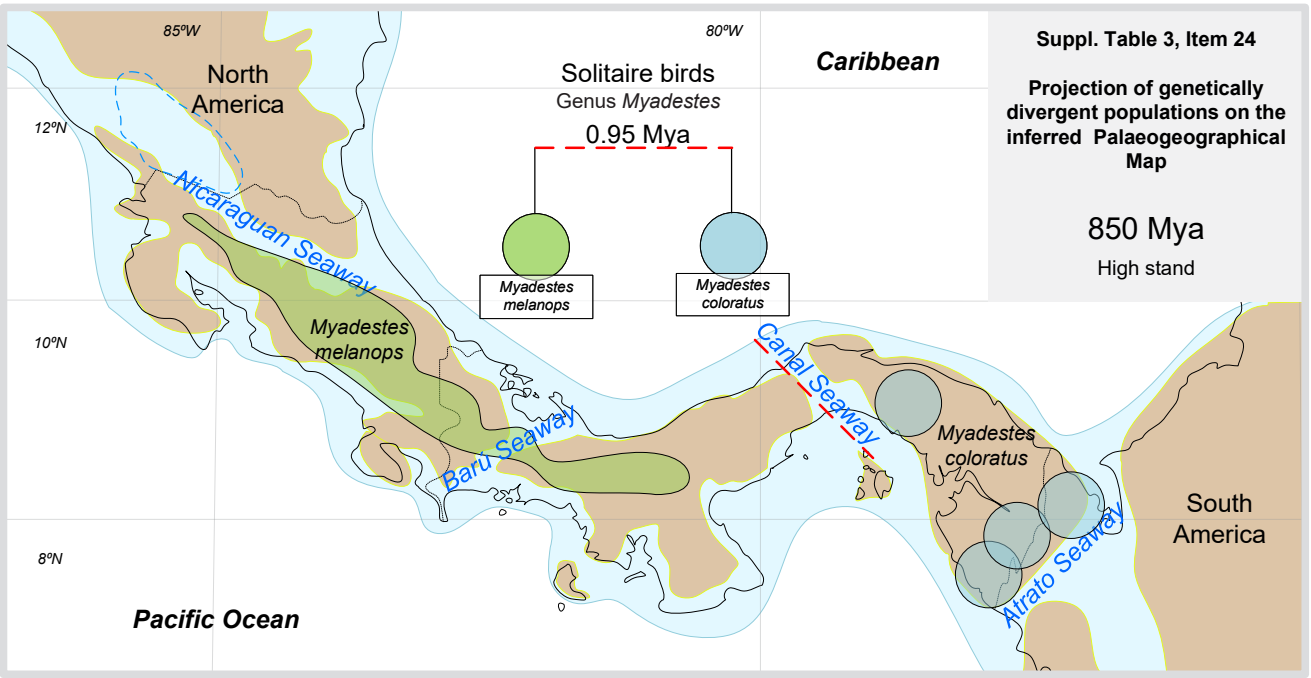
85ºW
80ºW
North America
Caribbean
Solitaire birds
Genus Myadestes
0.95 Mya
Suppl. Table 3, Item 24
Projection of genetically divergent populations on the inferred Palaeogeographical Map
850 Mya
High stand
12ºN
10ºN
8ºN
Nicaraguan Seaway
Myadestes melanops
Myadestes melanops
Myadestes coloratus
Canal Seaway
Baru Seaway
Myadestes coloratus
Atrato Seaway
South America
Pacific Ocean

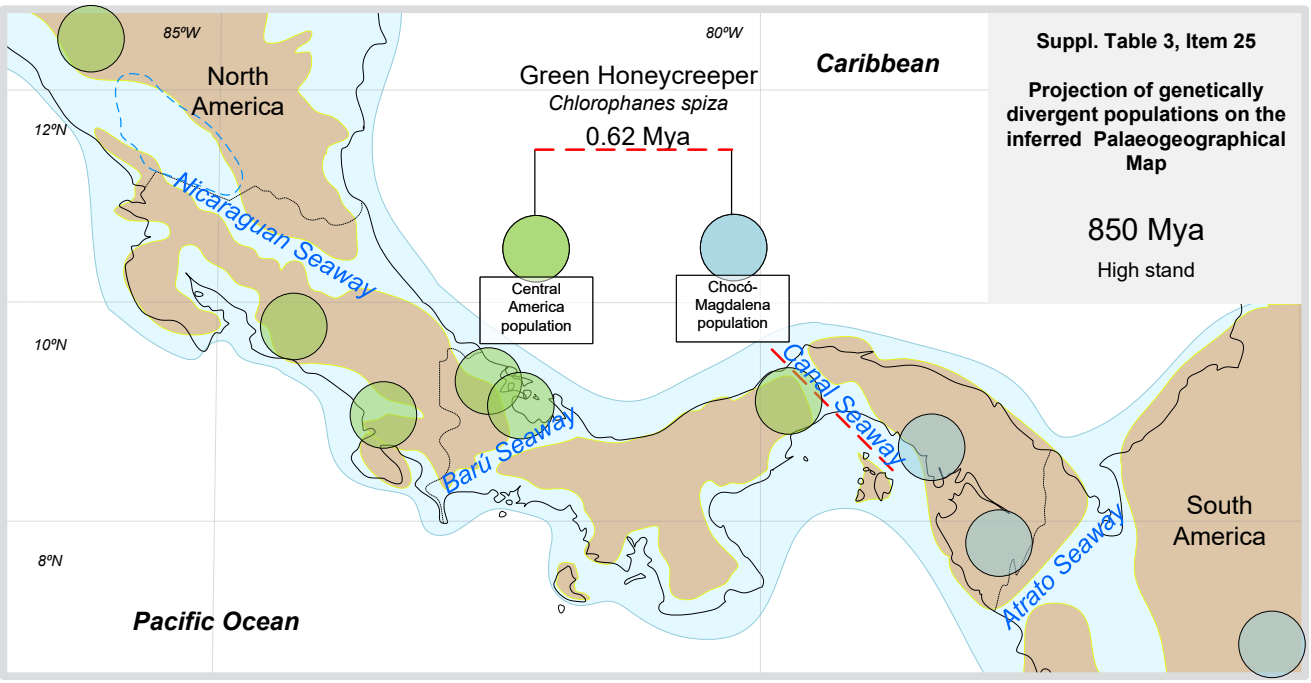
85ºW
80ºW
North America
Caribbean
Green Honeycreeper
Chlorophanes spiza
0.62 Mya
Suppl. Table 3, Item 25
Projection of genetically divergent populations on the inferred Palaeogeographical Map
850 Mya
High stand
12ºN
10ºN
8ºN
Nicaraguan Seaway
Central America population
Chocó-Magdalena population
Canal Seaway
Baru Seaway
Atrato Seaway
South America
Pacific Ocean

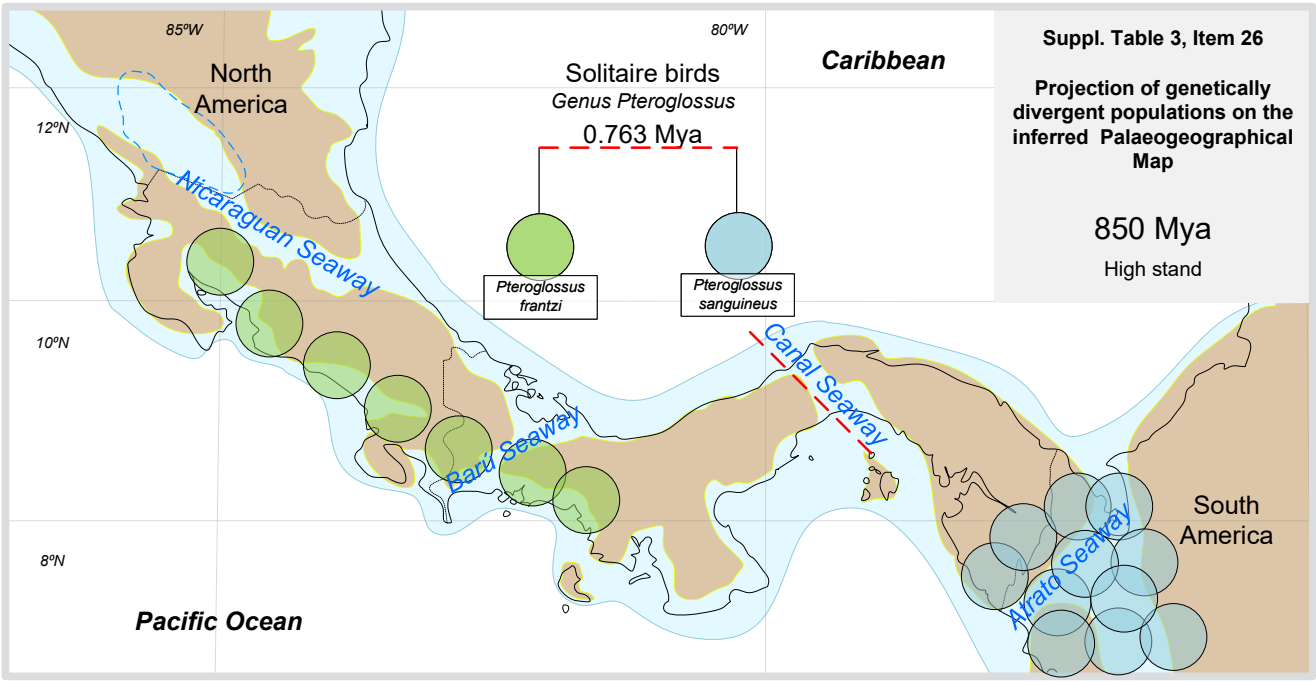
85ºW
80ºW
North America
Caribbean
Solitaire birds
Genus Pteroglossus
0.763 Mya
Suppl. Table 3, Item 26
Projection of genetically divergent populations on the inferred Palaeogeographical Map
850 Mya
High stand
12ºN
10ºN
8ºN
Nicaraguan Seaway
Pteroglossus frantzi
Pteroglossus sanguineus
Canal Seaway
Barú Seaway
Atrato Seaway
South America
Pacific Ocean

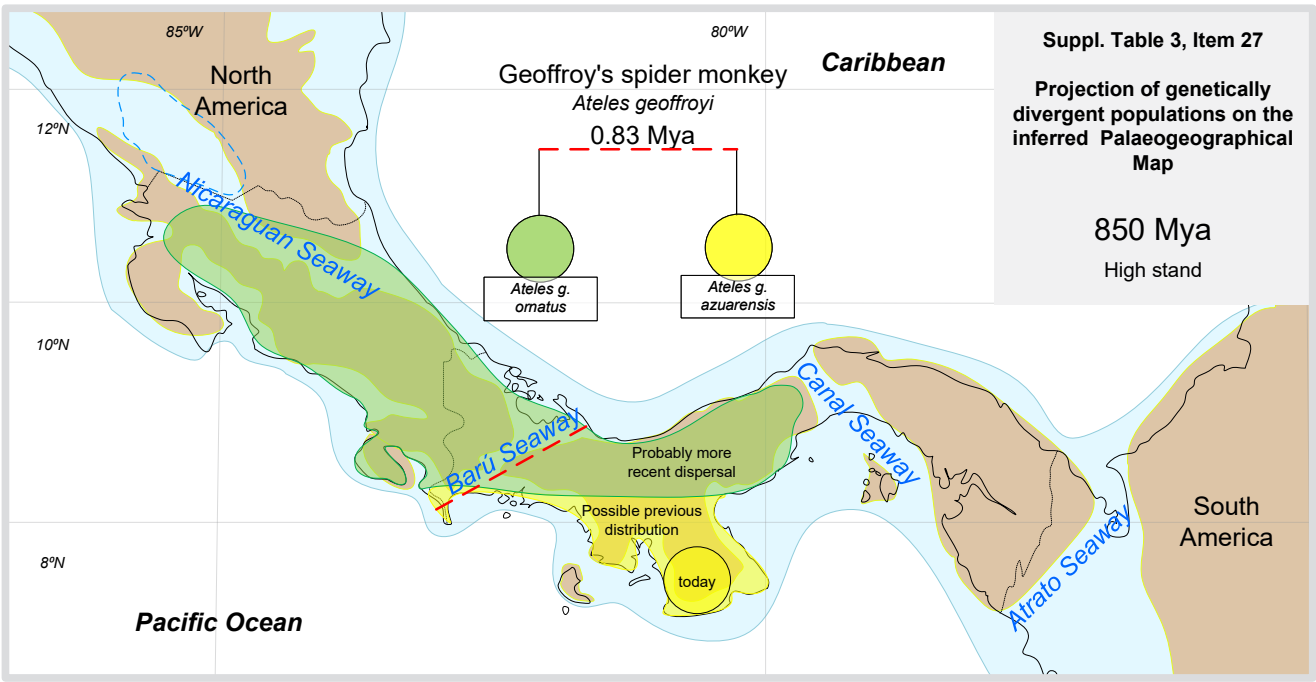
85ºW
80ºW
North America
Caribbean
Geoffroy's spider monkey
Ateles geoffroyi
0.83 Mya
Suppl. Table 3, Item 27
Projection of genetically divergent populations on the inferred Palaeogeographical Map
850 Mya
High stand
12ºN
10ºN
8ºN
Nicaraguan Seaway
Ateles g. omatus
Ateles g. azuarensis
Canal Seaway
Barú Seaway
Probably more recent dispersal
Possible previous distribution
today
Atrato Seaway
South America
Pacific Ocean

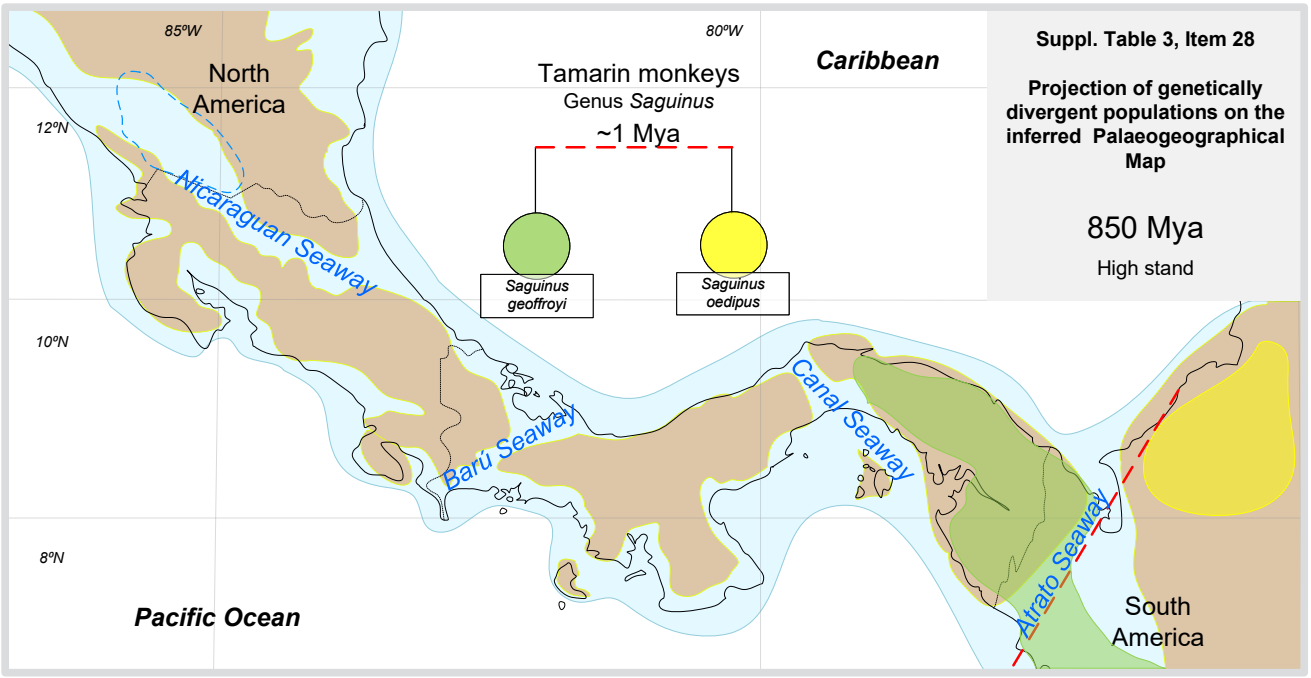

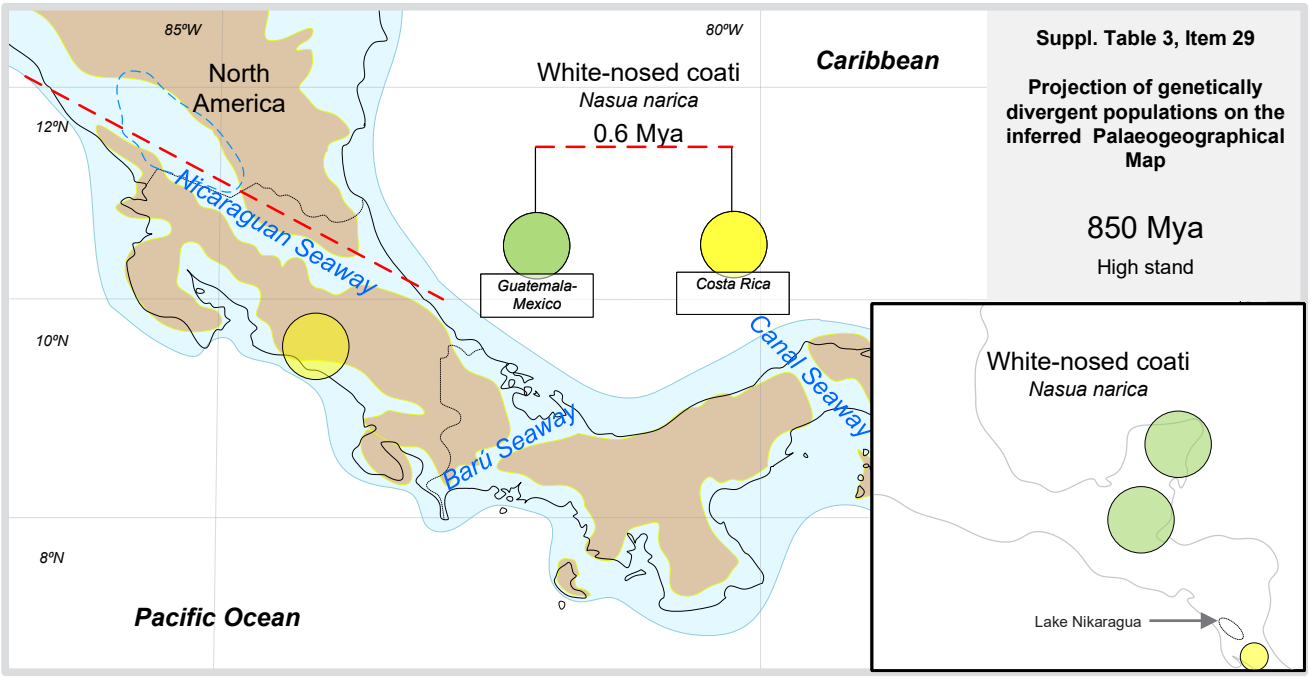

Copyright: *©2023: Leonidas Brikiatis. This is an open-access article distributed under the terms of the Creative Commons Attribution License, which permits unrestricted use, distribution, and reproduction in any medium, provided the original author and source are credited.*